JPRS-CST-92-010
22 MAY 1992

FOREIGN BROADCAST INFORMATION SERVICE

JPRS Report

Science & Technology

China

REPRODUCED BY
U.S. DEPARTMENT OF COMMERCE
NATIONAL TECHNICAL INFORMATION SERVICE
SPRINGFIELD, VA. 22161

Science & Technology
China

JPRS-CST-92-010 22 May 1992

CONTENTS

COMPUTERS

FACTORY AUTOMATION, ROBOTICS

LASERS, SENSORS, OPTICS

MICROELECTRONICS

SUPERCONDUCTIVITY

TELECOMMUNICATIONS R&D

China's Space Program by Year 2020 Outlined

92P60249 Shanghai JIEFANG RIBAO in Chinese
12 Apr 92 p 1

[Article by Li Wenqi [2621 2429 4388]: "China Plans To Send Astronauts Into Space in 8 Years, Build Space-Earth Shuttle System and Space Station by Year 2020"]

[Summary] According to the 'State Medium and Long-Term Development Program for Science and Technology' which was recently released by the State Science and Technology Commission, by the year 2000 China will build manned space vehicles and their boosters, and develop associated technologies for microgravity science application, vehicle launching and control systems, and space medicine systems. First, an unmanned test flight using a Chinese-made spacecraft is being planned before the manned mission is launched. By the year 2000, China will have a moderate-scale manned space system, will upgrade and build new launch and retrieval bases, and build a satellite-earth control network. China also plans to upgrade and build new launching facilities at the Jiuquan and Xichang launch centers to test second-generation launch vehicles, and to launch earth-synchronous and polar orbit satellites. China will have built the facilities for manned space flight by the year 2000, and by the year 2020 will finish building the technical and launch and retrieval infrastructure for a state-of-the-art space-earth transportation system. The program also calls for building an experimental space station by the year 2020, but in order to do so China will have to make breakthroughs in processing and production technologies of materials used in spacecraft manufacturing.

Blueprint For High-Tech Industrial Development

HK1605062592 Hong Kong LIAOWANG OVERSEAS EDITION in Chinese No 16, 20 Apr 92 pp 11-13

[Article by Hua Wen [5478 2429]: "Great Plans for Developing China's New, High Technology and Related Industries"]

[Text] It is necessary to "vigorously strive to use China's experimental manned spaceflight carrier to send Chinese astronauts into space" by 2000. This is one of the important messages revealed in the "National Long- and Medium-Term Scientific and Technological Development Program," which was released a few days ago.

As far as China's future development of new and high technology and related industries is concerned, the program has the following authoritative descriptions:

New- and high-tech research with the potential to make breakthroughs and with broad prospects for application will be highly stressed, and the development of new- and high-tech industries will be vigorously fostered; new- and high-tech industrial development zones will be conscientiously run, and new-and high-tech industries will be perfected to enter the international market; such programs as the "Key Task," "863 Plan," and "Torch Plan" will be actively carried out; and efforts will be made to strive to make breakthroughs in such fields as microelectronics, information, biology, new materials, aeronautics and astronautics, automation, new energy, laser technology, and oceanography, enabling China to gain some status in the global new- and high-tech realm.

New and high technology and related industries will become the key strength for international competition in the 21st Century. China's top leadership has already made policy decisions on the faster development of the country's new and high technology and related industries. As far as development focuses, strategic objectives and key links of China's new and high technology in the coming 30 years are concerned, the "National Long- and Medium-Term Scientific and Technological Development Program" and its appendices have depicted an inspiring magnificent blueprint.

Some Development Focuses and Objectives

Microelectronics technology: By 2000, the silkworm [can] integrated circuit technology will be developed, and research will be undertaken to develop one-micron very large-scale [VLSI] integrated circuits [IC's], large-scale gallium arsenide IC's, and so on; batch production of two-micron VLSI IC's will be started; and small and medium-scale gallium arsenide IC's as well as microwave monolithic IC's will be put to practical uses. Sixty percent of the large-scale IC's to be supplied to the domestic market will be home-made. By 2020, research will be undertaken to develop submicron (an equivalent of 0.8 micron) very large-scale IC technology, which will be applied to production on a trial basis, and efforts will be made to master the micron VLSI manufacturing technique and to apply it to mass production.

Computer technology: By 2000, the development of the fourth generation of computers and their application technology will be stressed; research will be undertaken to develop a new generation of computers, including non-Von Neumann, fuzzy, nonbinary, optoelectronic, biological, and superconducting computers. On the basis of the fourth generation computers, a new generation of computer and software industries will be established and developed by 2020.

Optoelectronic technology: By 2000, the design and production technology of key optoelectronic components (such as components necessary for optical communication, optical memory, and laser processing) will be mastered; devices and systems for the application of optoelectronic technology will be vigorously studied; research will be undertaken to develop the technology of vacuum and solid state video pickup, flat panel display, and high quality color display; high-power laser design and production technology will be developed; and research will be undertaken to extend the application of lasers to such fields as processing, testing, and assembly and to correspondingly develop a new generation of

lasers. By 2020, a key task will be realized in making a breakthrough in optoelectronic integration and optoelectronic IC's, ultra long wavelength and multi-wavelength optical fiber and cable, and the technology for the production and application of corresponding components.

Biotechnology: By 2000, new types of genetically engineered vaccines, monoclonal antibody diagnostic reagents, highly effective antibiotics, microbial pesticides, and dozens of modern biotechnological products will be put on the market; new varieties of top quality and highly productive animals and plants with resistance to adverse circumstances will be bred; and key aspects of conventional biotechnological industry will be transformed. By 2020, a sizable pharmaceutical industry applying modern biotechnology will be established; more biotechnological products, like various genetically engineered vaccines, DNA probes, active polypeptide medicines, new varieties of animals and plants, and secondary metabolic substances for large-scale culture of animal and plant cells will be put on the market; and protein engineering technology will be applied to such fields as medicines, food, chemical industries, and agriculture to manufacture new products.

A new generation of energy technology: By 2000, China is to complete the construction of the intermediate pilot project of 10,000 kw-class coal-fired magneto-hydrodynamic generaters; to master the pressurized water reactor nuclear power generating technology with 600,000 kw-class power plants as the main series and the advanced nuclear fuel recycling technology, to develop 900,000 and 1.2 million kw-class advanced pressurized water reactors, to conduct research in technology relating to process inherent ultimately safe [PIUS] high-temperature gas-cooled reactors and pressurized water reactors with pressure vessels, and to build a low-temperature district-heating demonstration reactor; and efforts will be made to keep track of international development of nuclear fusion technology. By 2020, as far as the development of nuclear power technology is concerned, China is to master the technology relating to PIUS reactors, master and spread the technology relating to low-temperature district-heating reactors and reactors supplying both heat and power, conduct research to master the technology relating to fast neutron breeder reactors for commercial use, modular high-temperature gas-cooled reactors, and the storage of nuclear waste and disposal of decommissioned nuclear facilities; and efforts will be made to make a breakthrough in key nuclear fission technology.

New materials technology: Research will be undertaken to develop optooelectronic material, high-performance composites, structural and functional ceramics, new metals, separation membranes, amorphous material, superconducting material, biofunctional materials, optical fiber, and other new materials. Efforts will be made to bridge the gap between China and the outside world in the development of most of the new materials, and make a technological breakthrough in exploring new frontiers in key materials. The process of applying relatively new materials to industrial production will be vigorously promoted. Apart from meeting the domestic market needs, China will promote some products to explore the international market.

Communications technology: By 2000, efforts will be focused on solving problems related to the mass production technology of a number of equipment systems, such as optical fiber communications below DS5 [565 and/or 622 Mbps], digital microwave communications below DS4 [140 Mbps], large capacity C-band and Ku-band satellite communications, and a new generation of mobile communications systems. China will also strive to develop two-way television transmission techniques combining cable with optical cable, and digital and flat panel display television technology. Moreover, research will be undertaken to develop high definition television technology, and so on. By 2020, the key tasks will be the development of large capacity and high speed optical fiber communications technology and digital satellite communications technology for integrated services.

Some Key Tasks and Objectives

In the field of spaceflight: By 2000, satellites applied to four aspects—communications and broadcasting, meteorology, land and marine resources of the Earth, and military reconnaissance and cartography, as well as their support systems—will be put into regular operation, and a small and medium launch vehicle series will be developed, and the largest payload in the geostationary orbit will reach 4.5 metric tons. Efforts will be made to develop highly functional, inexpensive, heavy launch vehicles and earth-space shuttle transport systems powered by nontoxic propellants. Research will be carried out in the field of development of experimental manned spacecraft, relevant launch vehicles, and supporting technology—unmanned test flights of experimental manned spacecraft will be conducted before a manned flight is made. China will vigorously strive to send its own astronauts into space with China's own experimental manned spacecraft.

By 2020, China will keep improving the functions of various satellites already in operation, and increasingly expand the varieties of applied satellite systems; successfully develop heavy launch vehicles and earth-space shuttle transport systems that match with spacecraft, and put them into operation. Moreover, China will construct experimental space stations with an initial operation capacity; gradually develop space stations promising initial returns; and bring space stations' applied economic, military, and social benefits into play, particularly making a breakthrough in the processing and production technology of space materials.

In the field of aviation: By 2000, China will strive to complete the production and development of 150-passenger-class mainline aircraft, and put such aircraft into active service; design and develop 75-passenger-class MD 75 aircraft through international

cooperation; complete the development of 2-metric-ton-class helicopters, increase its own production of 4-metric-ton-class helicopters, and start batch production of this type of product; and develop 8-metric-ton-class helicopters, to form China's own helicopter series. By 2020, China will develop highly efficient and energy saving civil aircraft and supersonic cruising civil aircraft and tilted rotary-wing helicopters.

In the field of high-tech shipbuilding: China will devote itself to develop freezing liquefied gas tankers, cargo ships delivering chemical products, bulk cement carriers, large container ships, large ferries carrying vehicles and passengers, non-oceangoing high speed freighters, luxury liners, 100,000-metric-ton-class freighters delivering bulk cargo and liquid products, 150,000- 300,000-metric-ton-class oil tankers, special engineering ships, fish processing ships, hydrofoils, hovercraft, wing-in-ground effect craft, jetfoils [qi yi ting], reduced bottom plating surface [xiao shui xian mian] catamarans, and high-quality luxurious yachts; develop and perfect such special technology applied to design and manufacturing of these ships; and pay attention to the application of such sophisticated and new technology as nuclear power, superconductors, and superautomation.

In the field of military materials: China will strive to complete the development of new-generation armor composites used in tanks, high-tensile and high-toughness armor and cannon steel, and shell body material with high-density and high fragment ratio, to meet the requirements of multifunctional protection and in-depth combat; complete the development of a new type of high-specific-strength and high-modulus structural material and composites for aircraft building, to further lighten structural weight; complete the development of high-temperature and titanium alloys used to build new fighter and gunship engines, to increase engine thrust-weight ratios; complete the development of high-tensile, abrasion-proof, and weldable structural and power-drive material for hulls of new-type vessels, and the development of damped oscillation reducing, noise-reducing, and sound-absorbing materials applied to ship-building, to enhance their structural strength, safety, reliability, and stealthiness, thus catering to the need for key new material for the development of the second generation of nuclear submarines and floating vessels; complete the development of spaceflight material, such as advanced heat-resistant and multifunctional composites, fire- and abrasion-proof material, sealed damping material, and high-temperature-resistant, and high-specific-strength and high-modulus structural metal and composites to meet the requirements of new-generation strategic and tactical missiles and military satellites; complete the development of antinuclear-bomb and highly efficient radiation shield material, antihydrogen-embrittlement material, and material for energy storage and other special functions to meet the requirements of new-type nuclear bomb warheads, which are small in size, have high mobility, can work safely, and produce special effects.

In the field of industrial robots: By 2000, research will be undertaken to develop robots for nuclear industries, including remote-controlled mobile robots, robots which can crawl on the wall for inspection and work under adverse circumstances, underwater robots without cables, and robots for precision assembly; and for low-price robots, assembly line robots with plane joints, large robots for casting and forging, and partially intelligent assembly line robots; meanwhile third-generation intelligence robots will be developed as well. By 2020, China will strive to develop third-generation industrial robots which will be equipped with visual and hearing sensors and natural language faculties, and to apply them to industrial production.

In the field of safety precautions: China will develop all-weather and highly reliable antiburglary and anti-intrusion comprehensive detection technology with low false alarm rates and low energy consumption as well as related alarm network technology, and go further to develop intelligent alarm technology; study and apply new and practical fingerprint, voice, and eye identification entry-control systems; study the technology of guarding against hijackers and people illegally crossing the border; study and apply the technology of detecting concealed criminal devices (for example, various explosives and weapons) and corresponding equipment series, and develop the technology to deal with problems in explosion scenes and of removing explosives with intelligent robots. By 2000, key state units, departments, and so on must be provided with multifunctional, multilevel, and comprehensive technology systems for safety precautions and alarms. A comprehensive intelligent public security defense system will be established by 2020 to foresee and follow up on developing dangerous covert criminal means, and set up corresponding detection methods and improve essential equipment.

Development Objectives of New- and High-Tech Development Areas

The establishment of new- and high-tech development areas is an important strategic plan for China to develop new- and high-tech industries. It has a great bearing on the early transformation of high-tech achievements into direct productive forces; the accelerated formation of high-tech industries in China; the accelerated transformation of conventional industries; the enhancement of Chinese products' standing and competitive power in the international market; and China's future economic, social, and scientific and technological progress.

The objectives and tasks of new- and high-tech development areas in the coming decade will be:

—Applying high-tech achievements to commodity production and industries, and introducing them into the international market. A batch of projects related to the "Torch Plan" will be launched, and efforts will be made to help 70 percent of them build up a considerable production scale and enable 30 percent to earn foreign exchange through exports. A number of large

modernized enterprises and enterprise groups with several hundred million yuan output value will be established to take part in international competition.

—Building development areas into high-tech industrial bases, to enable them to serve as the locomotives in the transformation of conventional industries with high technology, and to promote in-depth development of the reform of scientific and technological research structure, and to serve as windows open to the outside world.

—Supporting and encouraging scientific and technological personnel from scientific research institutes, post-secondary colleges, and small and medium enterprises to enter development areas to initiate various new and high-tech enterprises with collective ownership as the main form. At the same time, a number of scientific and technological entrepreneurs familiar with technical knowhow, enterprise operation, and management will be fostered.

—Developing high-tech industries emphasizing electronic information, bioengineering, new materials, aeronautics and astronautics, new energy and highly efficient energy-saving technology, ecology, oceanographic engineering, laser technology, biomedical engineering, radiation technology, and so on. Every development area will selectively develop these industries. And,

—Developing high-tech industries by introducing an open operational mechanism in which enterprises make their own management decisions, assume full responsibility for profits or losses, develop on their own initiative, and impose self-restraint.

Fire Control Computer of C601 Air-to-Ship Missile Described

92FE0365A Beijing ZHONGGUO HANGTIAN [AEROSPACE CHINA] in Chinese
No 1, Jan 92 pp 30-34

[Article by Dai Weiling [2071 1218 1545]: "Commander for China's C601 Air-to-Ship Missile"]

[Text] **Abstract:** This article gives a description of the fire control unit of the C601 air-to-ship missile. It also reviews its functions, performance, operating principle and technical characteristics.

I. Introduction

The fire control unit of the C601 air-to-ship missile is located on board the B6D bomber which carries the C601 missile. It is the computing and control center for the missile's fire control system and the automated navigation system on board the aircraft. Its main functions include the following:

1. Forming a track-while-scan (TWS) system with the search radar on board the aircraft to perform signal processing and tracking/control of targets over the ocean;

2. Solving for the missile launch parameters such as the missile range under autonomous control r_{zk}, the missile sector launch angle ψ_{0i} (i = 1 or 2 corresponds to the missile under the left wing or the right wing respectively), and loading the launch parameters onto the fire control unit and the azimuth control system of the autopilot;

3. Pre-launch inspection of the missile on the ground (with the aid of the DJ-6W ground inspection vehicle) and in the air, and controlling the launch operation based on the designated launch doctrine (single firing or dual firings);

4. Linking with the navigation equipment and the autopilot on board the aircraft to form an autonomous Doppler or inertial navigation system for controlling the aircraft trajectory.

This fire control unit has high accuracy and good performance under adverse environmental (weather, mechanical or electromagnetic) conditions; it has also proved to be highly stable and reliable. The operating temperature range is -40° to +50°C for a sealed compartment and -55° to +65°C for an unsealed compartment. The mean time between failure (MTBF) of the overall system is 200 hours or more.

The major components of the C601 fire control unit (model No. ZJ-6W) include the main module ZJ1-6W, the power supply ZJ2-6W, the control module ZJ3-6W, the onboard pre-launch inspection and launch control module ZJ4-6W, the missile junction box ZJ5-6W and the relay ZJ6-6W; there are two units each of the ZJ4-6W and ZJ5-6W for the missiles under the left and right wings. Photographs of the above modules are shown in Figure 1 [not reproduced].

The ground equipment of the system includes the DJ-6W ground inspection vehicle and the WS-6W maintenance and repair facility. The DJ-6W is used to perform pre-launch inspection of the C601 missile. The DJ1-6 pre-launch inspection console inside the vehicle and the fire control unit on board the aircraft constitutes the missile inspection system. The inspection process is displayed on the DJ1-6 panel to facilitate locating trouble spots. In addition to pre-launch inspection equipment, the vehicle also has a complete set of onboard equipment of the fire control unit as well as a power supply system, an onboard signal simulator, and a missile simulator which provide the external operating environment. The vehicle is also equipped with conventional instruments such as a computer tuning and testing station, oscilloscopes and digital voltmeters which are used to inspect and detect equipment failures; thus, it serves as a mobile maintenance and repair center. The WS-6W is the central maintenance and repair facility at the airfield; in addition to the DJ-6W equipment, it also has component test equipment, power supply test equipment and a number of regulated d.c. power supply units which can be used for the maintenance and repair of individual components of the fire control system.

The fire control unit of the C601 missile performs the following functions during an attack mission:

1. Ground preparation. This includes inspection of the onboard fire control system and use of the missile simulator inside the DJ-6 vehicle for pre-launch inspection of the aircraft. Upon completion of the inspection procedures, it proceeds to load the missile and perform pre-launch inspection of the missile on the ground.

2. After the aircraft takes off, it activates the automatic navigation unit to control the aircraft to fly along a designated flight-path toward the target zone.

3. When a target is discovered by the aircraft, it cuts off the automatic navigation unit and initiates the missile attack mode. As the double sideband system searches for and tracks the target, the fire control unit solves for the launch parameters and loads them into the missile. At the same time, pre-launch inspection of the missile is also performed on board the aircraft. Once the inspection procedure is completed, the launch parameters are loaded, and the launch conditions are satisfied, an indicator light is turned on to signal that the missiles are ready for launch (single firing or dual salvo firing).

II. Operating Principle of the Fire Control Unit

(A) System Components

The signal paths between different modules of the fire control unit, ZJ1-6W to ZJ6-6W, are shown in Figure 2. A brief description of each module is given below.

1. The Main Module (ZJ1-6W)

The main module is the nucleus of the fire control unit; it consists of the computer KS-6, the radar signal recorder LXZ, the A/D converter, the D/A converter and the D/f digital frequency converter. A system block diagram of the main module is shown in Figure 3.

(1) The Radar Signal Recorder (LXZ)

The LXZ is the signal processing and tracking/control hardware of the double sideband system; it consists of the signal detector, the tracking gate generator, and the digital circuits. A block diagram of the LXZ is shown in Figure 4. The video signal of the radar return is amplitude-detected and bandwidth-detected in the signal detector in order to preserve target information while filtering out random noise. The detected video signal is digitized in the tracking gate where a "gate image" is formed and transmitted to the computer. In the computer, the signal is further filtered using a software-generated sliding window, and the slant range R and azimuth angle q_{CL} are calculated. The fire control unit performs the functions of filtering and predicting the target parameters and transmits the tracking data to the gate generator in order to control the range/

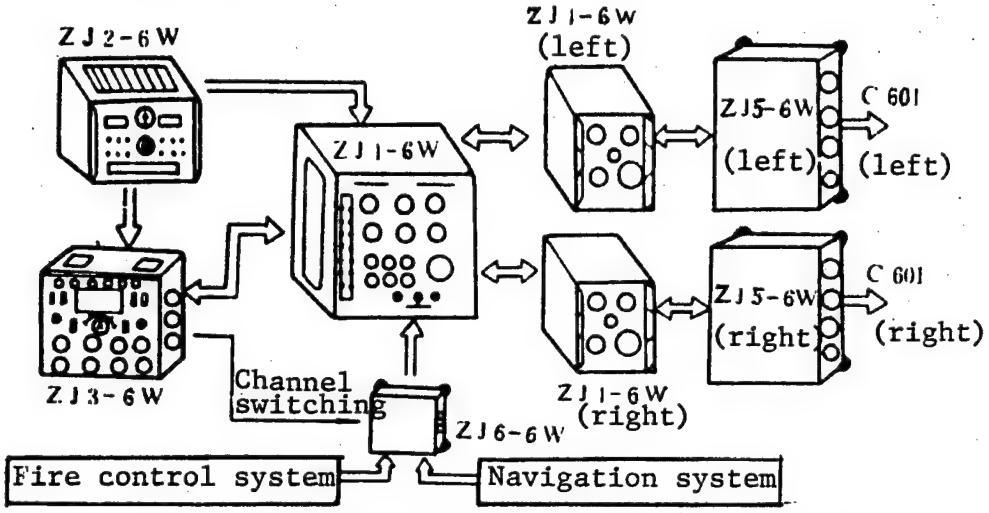

Figure 2. Components and Signal Paths of the Fire Control System

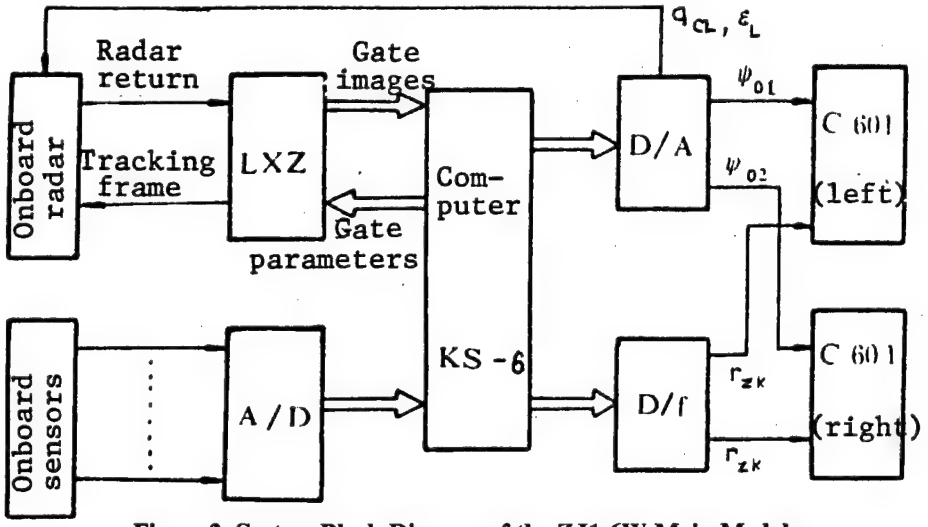

Figure 3. System Block Diagram of the ZJ1-6W Main Module

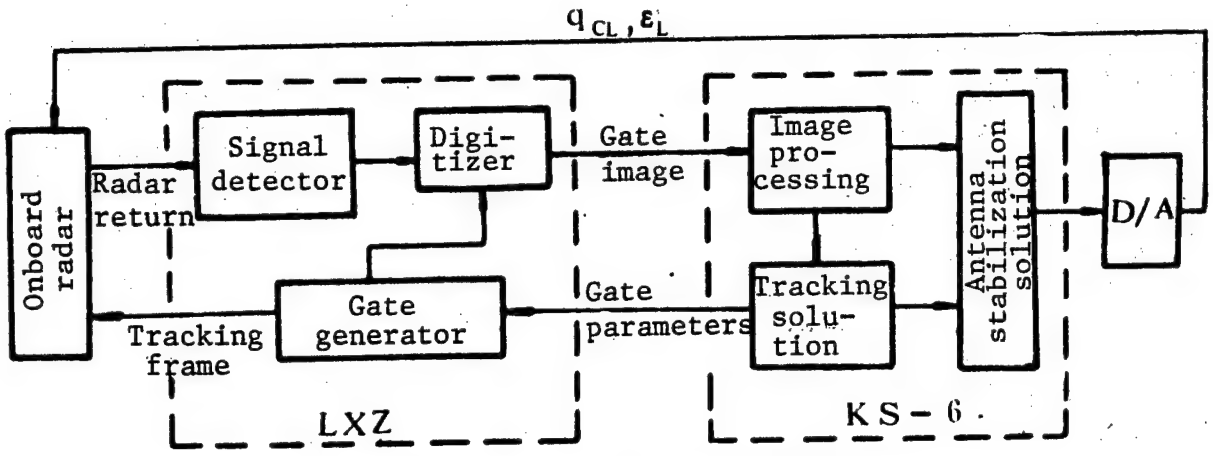

Figure 4. Block Diagram of the Double Sideband System

azimuth gates and maintain continuous track on the target. At the same time, based on the aircraft attitude signals, the computer also calculates the azimuth/pitch signals q_{CL}/ε_L, which control the tracking antenna.

(2) The KS-6 Computer

The computer is the control center of the fire control unit. The processing and control segment of the KS-6 uses standard TTL digital integrated circuits and pulse-voltage logic system; the storage unit uses CMOS random-access memory and EPROM read-only memory; the computer has a 1-MHz clock with 8-μs instruction cycle, 18-bit word length, 8K memory, and 32 basic instructions. It has a multi-stage interrupt system and uses DMA data transmission mode to provide effective real-time processing capability. Its design also incorporates a series of reliability measures to achieve a MTBF of more than 500 hours.

(3) The Converters

a) The A/D converter is designed to convert the output d.c. voltages from the onboard sensors (e.g., inertial navigation system, Doppler radar, azimuth reference gyro, gyro stabilization platform, etc.) into parallel digital code sent to the computer. The 16-channel dual-input A/D converter uses the bit-by-bit approximation code and multi-channel time-division switching technique. It has a 12-bit word-length, the input signal range is 0 to +/- 10V, the conversion accuracy is +/- 0.1 percent, and the sampling rate is 16 times per second.

b) The D/A converter is designed to convert digital data such as the sector launch angles ψ_{01}, ψ_{02}, the antenna stabilization signals q_{CL}, ε_L, and the deviation angle in the navigation state ΔK, into d.c. voltages and transmit them to the corresponding control modules. It uses a high-precision sample-and-hold circuit to achieve multi-channel time-division conversion, and has 8 output channels and a 12-bit word-length; the analog output ranges from -10V to +10V, and the conversion accuracy is +/- 0.1 percent.

c) The D/f digital frequency converter is designed to convert the missile auto-control flight range r_{zk} from parallel code to serial code so it can be received by the command computer on the missile, and to transmit a corresponding identification (including the initiation pulse, the synchronization pulse and the termination pulse). The conversion word length is 13 bits (including one parity-check bit), and the resolution is 30.77 m. The components of the D/f converter include the digital code register, the shift register and the gate control circuit; it uses a long-line drive circuit to transmit data to the onboard computer.

2. The Power Supply Module ZJ2-6W

The power supply module is designed to transform the 27-volt d.c. power source of the aircraft to the following regulated voltage sources used by the main module and the control modules: +5V, +15V, -15V, +12V, +10V, -10V. The +12V and -10V sources are the reference power supply of the A/D converter which is connected to the output potentiometer of the onboard sensors. In case a power failure occurs on the aircraft, the high-energy battery of the power supply module provides electricity to the CMOS memory to preserve information in the fire control unit. All the power supply units are designed with overload protection and are equipped with plug-in boards to facilitate maintenance.

3. The Control Module ZJ3-6W

The control module is designed to perform man-machine interactive display and control; its functions include:

(1) Selection of the following operations: real-time inspection, missile attack, navigation and non-real-time inspection. For real-time inspection, a fixed procedure is

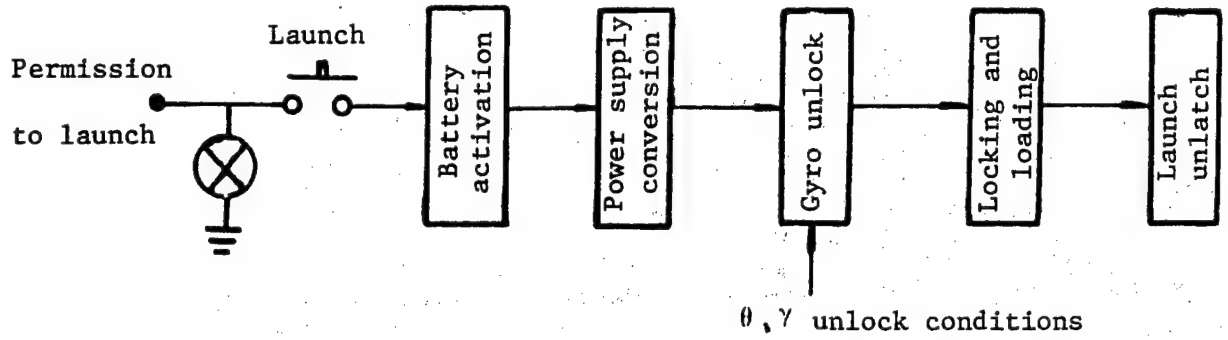

Figure 5. Missile Launch Sequence

automatically executed and the fault location is displayed. For non-real-time inspection, the operator can execute an inspection command or inspection program to perform specific diagnosis of computer faults.

(2) Loading of missile attack parameters (e.g., target mobility coefficient, automatic navigation distance, launcher correction, correction for ocean conditions, etc.) and navigation parameters (e.g., latitudes and longitudes of turning points along the flight course).

(3) Display of system operational status such as status of the power supply unit, status of missile launch inspection, status of launch readiness, and the result of self-diagnosis and the fault location.

(4) Display of the calculated results such as target parameters, A/D conversion parameters, launch parameters and the navigation states such as the current aircraft latitude, longitude, heading and remaining distance.

(5) Missile launch inspection and operation of launch control switch; the control module is composed of a control panel and six 220 x 140 mm^2 plug-in boards, and the panel is illuminated by a light board.

4. The Onboard Pre-Launch Inspection and Launch Control Module ZJ4-6W

The pre-launch missile inspection process primarily involves inspecting the initial states of the onboard equipment such as the gyro lock, the zero setting of the azimuth reference, and the safety switch of the fusing device; it also generates simulated error signals for compatibility check between the guidance radar and the autopilot. The launch control circuit of the missile is designed according to the launch sequence (see Figure 5). The launch conditions are satisfied when: (1) tracking has been initiated by the double sideband system; (2) precision calculations of the fire control unit have been completed; (3) launch parameters have been loaded; (4) the required conditions for aircraft altitude, velocity and attitude have been achieved; (5) the launch parameters are within the specified launch window; and (6) the status of all onboard equipment is normal. When all the above conditions are satisfied, then the "ready to launch" indicator light is turned on.

5. The Missile Junction Box ZJ5-6W

The function of the junction box is to control the power supply to the missile and to relay signals from the fire control unit and the missile.

6. The Relay Box ZJ6-6W

The relay box is designed to perform input-signal switching in order to expand the number of conversion channels, and to activate the power drive based on the control voltage from the computer.

(B) Mathematical Model and Computational Procedure of the Fire Control Unit

1. Trajectory of the C601 Missile

The C601 missile uses a guidance system with autonomous control plus automatic navigation; it also uses a sector launch mode. After release from the aircraft, the missile is controlled by the altimeter to activate engine ignition and to initiate level flight. The autopilot is used to control the sector angle ψ_{0i} to turn toward the combat zone and to maintain level flight. The missile velocity is integrated by the onboard command module to obtain range information; when the range is equal to the autonomous-control range r_{zk} which is loaded in the fire control unit, the missile switches into the automatic navigation mode. The trajectory of the C601 missile is shown in Figure 6.

2. Establishing Digital Platform

The xyz coordinate system shown in Figure 6 is a moving coordinate system centered at the aircraft; θ is the pitch angle, γ is the roll angle, and the XYZ is the local rectangular coordinate system. The concept of a digital platform is to convert the azimuth angle q_{CL} measured by the radar in the aircraft coordinate system into an angle q_C in the local coordinate system. This is accomplished by a matrix coordinate transformation.

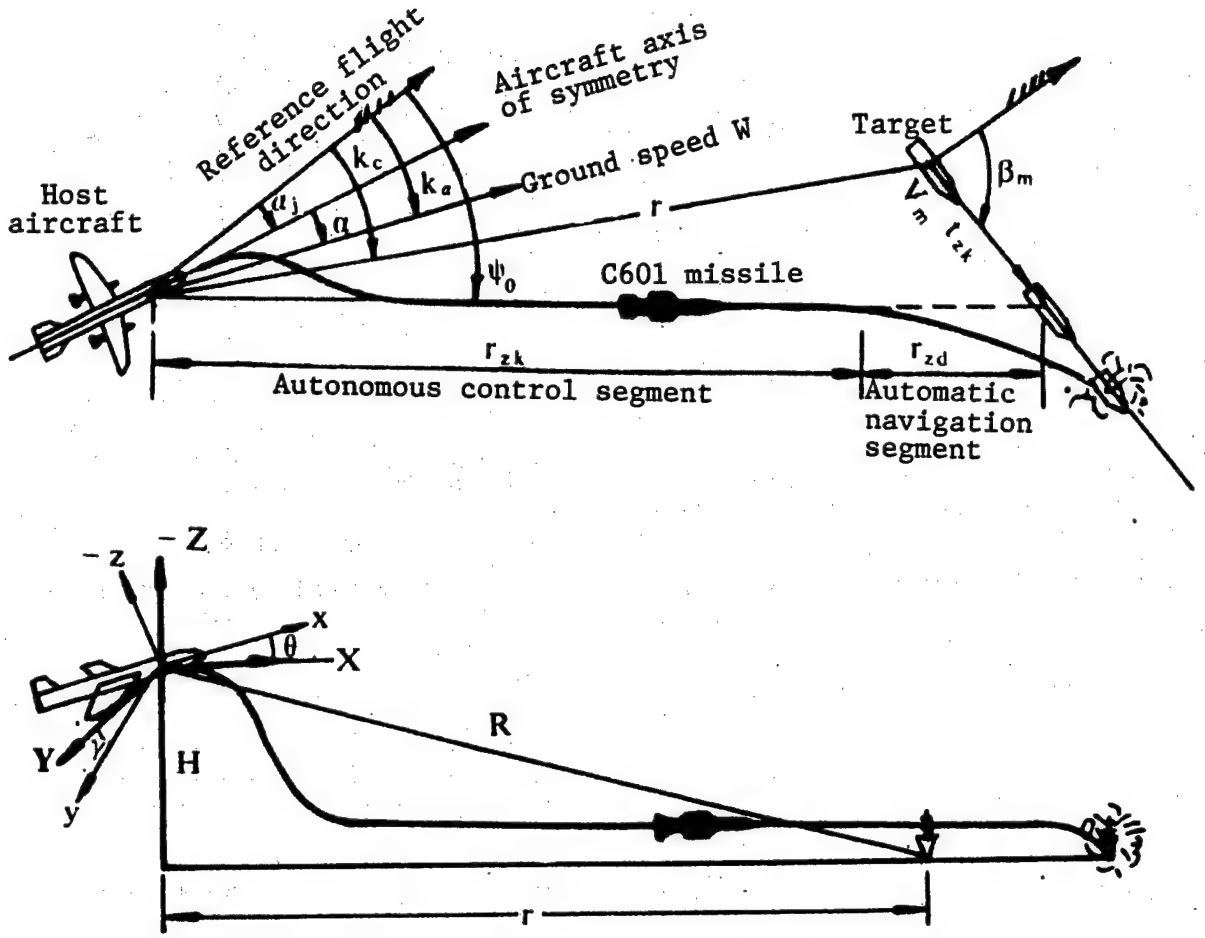

Figure 6. Trajectory of the C601 Missile

3. Establishing Azimuth Reference

In order to minimize the effect of perturbations in the flight azimuth, the missile fire control system uses the azimuth reference gyro as the azimuth reference. This gyro is activated when the double sideband system initiates the "auto-track" mode and produces in real time the subtended angle between the aircraft axis of symmetry and the azimuth direction at the time of activation, α_j, as well as the target azimuth angle q_C; the measured aircraft yaw angle α is referenced to the aircraft axis of symmetry and must be processed to determine the reference azimuth K_C and reference yaw angle K_α. Clearly, $K_C = q_C + \alpha_j$, $K_\alpha = \alpha + \alpha_j$.

4. Kalman Filter

In order to suppress measurement noise and enhance data processing accuracy, a four-state Kalman Filter whose elements are r, K_C, r[dot], K_C[dot] has been implemented in the fire control unit. The state transition matrix is derived under the assumption that both the aircraft and the target move along straight lines with uniform velocities. By establishing the state equation, the observation and the gain matrix, estimates of the state variables, r, K_C, r[dot], K_C[dot] can be obtained from the recursive Kalman Filter equations. Simulated results and flight test data have demonstrated that this filter is quite effective in smoothing out random disturbances (see Figure 7).

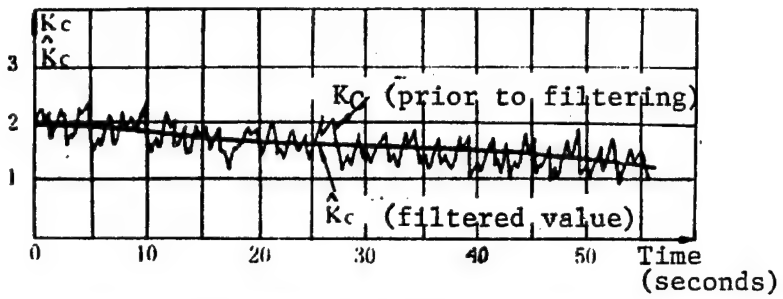

Figure 7. Performance of the Kalman Filter Against Measured Data

5. Solution of Target Velocity and Azimuth

The range and azimuth of the target relative to the aircraft (r, K_C) are measured by the onboard radar and processed by the Kalman Filter to determine the corresponding rates of change r[dot], K_C[dot]. The motion parameters of the aircraft (ground speed W, yaw angle K_a) are measured by the onboard inertial guidance system (or Doppler radar) from which the target equations of motion can be derived. The target velocity V_m and azimuth β_m can be obtained by solving the equations of motion:

$$\begin{cases} \dot{r} = V_m \cos(\beta_m - K_C) - W\cos(K_C - K_a) \\ r\dot{K}_C = V_m \sin(\beta_m - K_C) + W\sin(K_C - K_a) \end{cases}$$

6. Solution of Missile Launch Parameters (r_{zk}, ψ_{0i})

From Figure 6 one can derive the missile hit equation and solve for the autonomous-control range r_{zk} and the sector launch angle ψ_{0i}. The computational flow diagram of the fire control unit is shown in Figure 8.

III. Technical Features of the C601 Fire Control Unit

The C601 fire control unit is the control center for the missile fire control system and the aircraft navigation system. Its main features are summarized below:

—It has a double sideband system which provides control of the missile and the aircraft navigation system.

—The double sideband system uses a variety of detection techniques such as amplitude-detection, bandwidth-detection, software sliding-window detection, and applies constant false-alarm control. It has also implemented filtering/prediction techniques and adaptive tracking-control techniques to maintain target track under low signal-to-noise and fluctuating-target conditions.

—It has a good overall system design with high-performance subsystem hardware; it also incorporates technologies such as multi-channel time-division control, DMA data transmission, semiconductor storage devices, TWS system and Kalman Filter technique.

—It provides a sophisticated dynamic simulated environment by using a dynamic flight-path generator, target simulator, missile simulator, and data collection system.

—It incorporates various reliability measures and applied optimal design techniques; specifically, design requirements such as heat resistance, electromagnetic

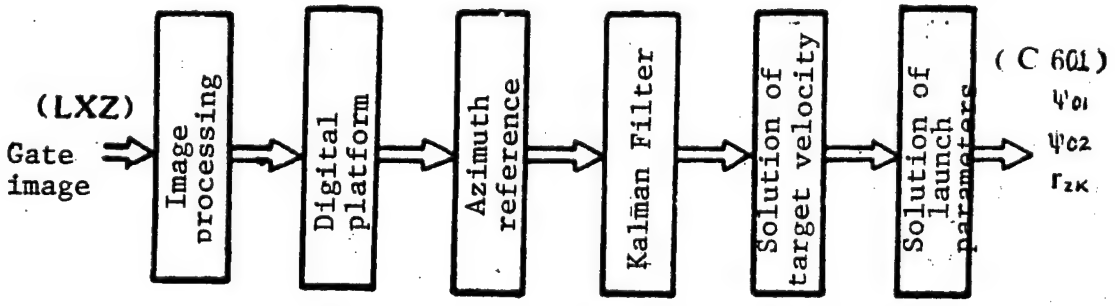

Figure 8. Computational Flow Diagram of the Fire Control Unit

tolerance and resistance against vibration and shock have been taken into consideration.

—It incorporates effective self-diagnosis and fault-location techniques and provides three levels of maintenance and repair: aircraft maintenance and repair, ground inspection vehicle, and the maintenance and repair facility.

—It has a high quality-control standard and adheres to strict quality and reliability assurance guidelines in the development process.

Panel Method for RCS Computation of Targets With Arbitrary Shapes

92FE0421A Beijing DIANZI KEXUE XUEKAN [JOURNAL OF ELECTRONICS] in Chinese Vol 14 No 1, Jan 92 pp 71-75

[Article by Zhou Jianjiang [0179 1696 3068] and Shu Yongze [5289 3057 3419] of the Nanjing Aeronautical Institute, Nanjing 210016: "Panel Method for Radar Cross Section Computation of Targets With Arbitrarily Complicated Shapes"; MS received 1 Nov 90, revised 1 Apr 91]

[Text] **Abstract:** In this article, a new method of calculating the radar cross section (RCS) of a target with arbitrary shape—the panel method—is presented. This highly efficient and robust method is based on the work of D. Klement et al. (1988). The method has been used to calculate the RCS of typical scatterers such as cones and cylinders; the calculated results are in good agreement with experimental data. The RCS of an aircraft model at different attitude angles is also calculated, and the calculated results also compare favorably with measurements.

I. Introduction

With the development of stealth technology and counter-stealth technology, the design of a new aircraft model requires accurate determination of its RCS in order to achieve an optimum configuration which minimizes the RCS within a specified angular region.

In the 1970's, Mittra[1] proposed a component synthesis technique which computes the RCS of a complex object by approximating the object by a number of simple shapes with known RCS characteristics. However, this method cannot meet today's accuracy or robustness requirements. In this article, the panel method of Ref. 2 for computing the RCS of simple shapes has been extended for calculating the RCS of complex objects; this is accomplished by taking into account the effect of diffraction of panel edges on the overall scattering field. Comparison of the calculated RCS of an aircraft model with measured data show that this method is superior to the component synthesis method.

II. Basic Methodology

The scattering object shown in Figure 1 is composed of convex and concave surfaces, cavities and edges. In practice, the characteristic dimensions of a scattering object are often much larger than the wavelength of the incident electromagnetic wave. Therefore, one can apply the Stratton-Chu integral to obtain the far-field (kR >> 1) electric field of the scattering object and to determine its monostatic RCS:[3]

$$E^s = \frac{jkZ_0}{4\pi}\frac{\exp(jkR)}{R}\int_s [\hat{R}\times(\hat{R}\times J) + Y_0\hat{R}\times M]\exp(j2k\rho\cdot\hat{R})dS \qquad (1)$$

In the above equation, J and M are respectively the surface induction current (or equivalent current) and the magnetic flux, R[caret] is the unit vector from the surface element dS to the field point, ρ is the position vector from the reference point to the surface element dS, k is the wave number, Z_0 is the free-space impedance, and $Y_0 = 1/Z_0$ is the free-space admittance.

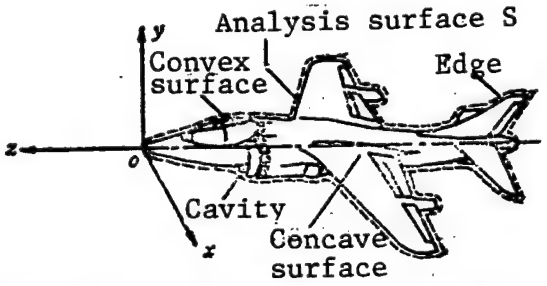

Figure 1. Schematic Diagram of the Analysis Surfaces of a Complex Object

On a smooth conducting convex surface, it is necessary to consider backscattering only, hence one can assume J(R) = 2n[caret] x H^i(R), where n[caret] is the unit normal vector pointing outward from the surface, and H^i(R) is the incident magnetic field. For a concave surface, in addition to the induced current and magnetic flux created by the incident field, it is also necessary to consider the induced current and magnetic flux created by the interaction between different surface elements of the concave surface, as well as the induced currents and magnetic flux created by other indirect incident fields. On a metallic surface, the incident magnetic flux is always zero. Inside a cavity, the scattering mechanism is rather complicated; hence the simple methods for analyzing convex or concave surfaces are no longer applicable. In this article, an equivalent method is developed to determine the contribution of the cavity on the overall scattering field. Specifically, by choosing the aperture surface of the cavity as the analysis surface and analyzing

the transmission characteristics of electromagnetic waves inside the cavity, the field distribution over the analysis surface is first determined; then the equivalent current and the magnetic flux over the analysis surface can be readily obtained.[4]

The contribution of the edge diffraction field to the overall scattering field is determined using the physical theory of diffraction (PTD); the edge diffraction field is:

$$E^{s_u} = \frac{jkZ_0}{4\pi}\frac{\exp(jkR)}{R}\int_l [\hat{R}\times(\hat{R}\times I_u\hat{l}) + Y_0\hat{R}\times M_u\hat{l}]\exp(jk\rho\cdot\hat{R})dl \qquad (2)$$

where l[caret] is the tangential unit vector along the edge segment dl; the other parameters in the equation have the same meaning as those in equation (1). I_u, M_u are respectively the edge (Wu-fei-cai-fu) induced current and magnetic flux:

$$I_u = -Y_0\sqrt{8\pi/(jk)}(1/\sin\beta)D_s^u[E^i(R)\cdot\hat{l}] \quad (3)$$

$$M_u = -Z_0\sqrt{8\pi/(jk)}(1/\sin\beta)D_h^u[H^i(R)\cdot\hat{l}] \quad (4)$$

In the above two equations, β is the subtended angle between the incident ray and the edge tangential vector l[caret]; D^u_s, D^u_h are respectively the (Wu-fei-cai-fu) electrically polarized and magnetically polarized diffraction coefficients.

In general, analytical expressions for the integrals in equations (1) and (2) are not obtainable; the integrals must be carried out numerically on a computer. To simplify the computation, the surface of integration in equation (1) can be divided into small panel elements (hence the name panel method), where the maximum error between each panel and the actual surface of the object is limited to 1/16 of the wavelength of the incident electromagnetic wave.[2] Thus, the three-dimensional vector integral of equation (1) is converted into the sum of two-dimensional vector integrals over each panel element. In the special case of a metallic surface, the value of the surface current over each panel is equal to the value at the tangent point between the panel and the curved surface, and the magnetic flux is zero, hence an analytical expression of the integral can be derived. Application of this method to the calculation of cavity RCS is given in Refs. 4 and 5. An analytical expression of the integral in equation (2) can be derived using a similar procedure where the curved edges are approximated by piece-wise linear segments.

III. Application of the Panel Method

In this section, RCS calculations for a cone, a cylinder and an aircraft model are carried out using the above method, and the calculated results are compared with measured data.

1. Cone

As shown in Figure 2, the electrical field vector of the incident wave is said to be horizontally polarized when it is parallel to the θ[caret] vector of the corresponding spherical coordinates and vertically polarized when it is parallel to the φ[caret] vector. The cone parameters used in the calculation are as follows: radius of the base circle—8.03 cm, height—40.17 cm, cone angle—11.3°; the cone surface is divided into 24 panels. The wavelength of the incident wave is 5 cm. Comparison between the calculated results and measured results under the conditions of horizontal polarization and a single station are shown in Figure 3.[6]

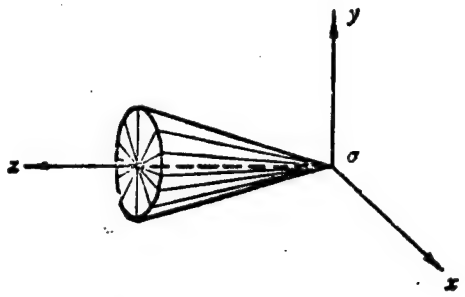

Figure 2. Cone

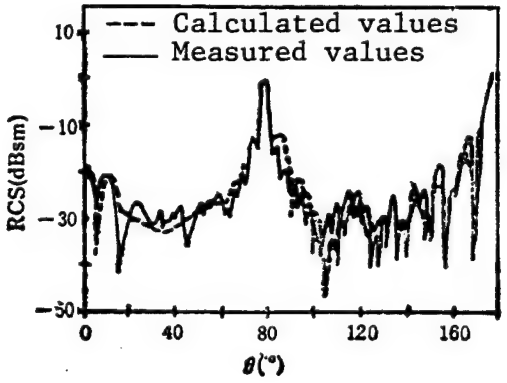

Figure 3. Radar Cross Section of a Cone (horizontal polarization, monostatic setup)

2. Cylinder

As shown in Figure 4, the dimensions of the cylinder are: radius of the base circle—9.53 cm, height—43.84 cm; the surface is divided into 45 panels. The wavelength of the incident wave is 5 cm. Comparisons between the calculated and measured results under the conditions of vertical polarization and horizontal polarization are shown in Figure 5 and Figure 6, respectively.

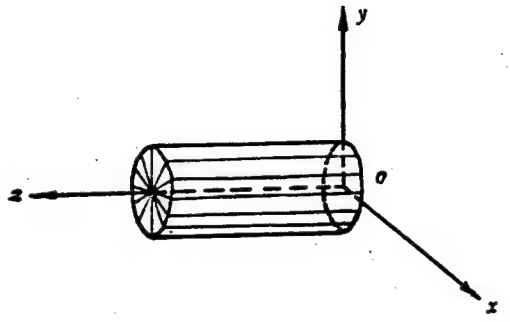

Figure 4. Cylinder

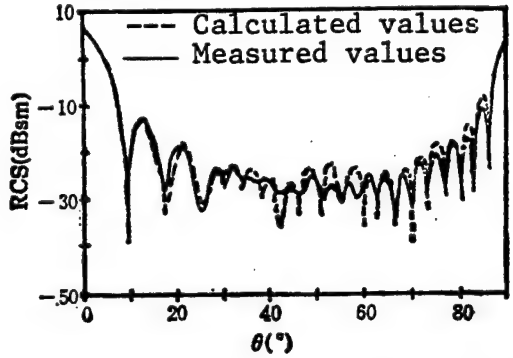

Figure 5. Radar Cross Section of a Cylinder (vertical polarization, monostatic setup)

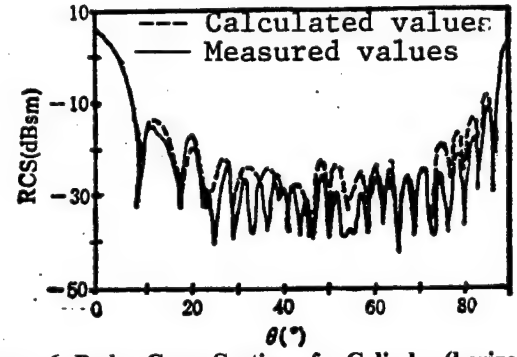

Figure 6. Radar Cross Section of a Cylinder (horizontal polarization, monostatic setup)

3. Aircraft Model

A schematic diagram of the aircraft model is shown in Figure 1; the attitude of the aircraft in a rectangular coordinate system is expressed in terms of the pitch angle α (see Figure 7 (a)) and the roll angle β (see Figure 7 (b)). The aircraft model is 1.4 m long and has a wing span of 0.88 m; the model surface is divided into 2,043 panels, and the wavelength of the incident wave is 3 cm. Under the conditions α = 0, β = 0 (horizontal flight), the panel data of the aircraft surface are generated directly using CAD; for α not = 0 or β not = 0, the panel data for different aircraft attitudes can be obtained through a simple coordinate transformation:

For $\alpha \neq 0, \beta = 0$:

$$\left.\begin{aligned} x' &= x \\ y' &= z\sin\alpha + y\cos\alpha \\ z' &= z\cos\alpha - y\sin\alpha \end{aligned}\right\} \quad (5)$$

For $\beta \neq 0, \alpha = 0$:

$$\left.\begin{aligned} x'' &= x\cos\beta - y\sin\beta \\ y'' &= x\sin\beta + y\cos\beta \\ z'' &= z \end{aligned}\right\} \quad (6)$$

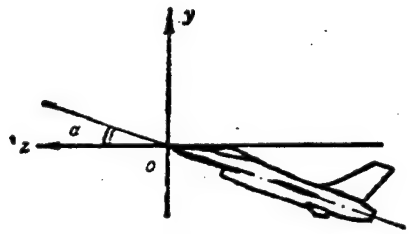

(a)

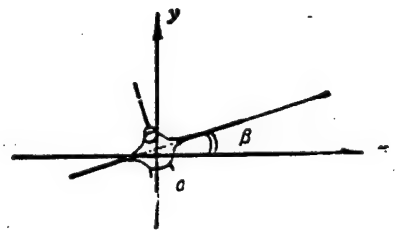

(b)

Figure 7

By dividing the aircraft surface into small panels and applying the method proposed in this article, one can compute the RCS of the entire aircraft model and generate curves of RCS distribution for different attitude angles. A selected number of the calculated values and the corresponding measured results are shown in Figure 8 and Figure 9. As indicated in these figures, the rather large errors in the vicinity of θ = 30° are attributed to the fact that in the calculations, the air inlet of the aircraft model is approximated by a rectangular pipe with a constant cross-sectional area equal to the lip area, whereas the actual air inlet has an elliptical lip and an s-shaped inside channel with variable cross sections. In processing the data, both the measured values and the calculated values (in units of square meters) at one per degree are smoothed using a 5° window and a 5° threshold value.

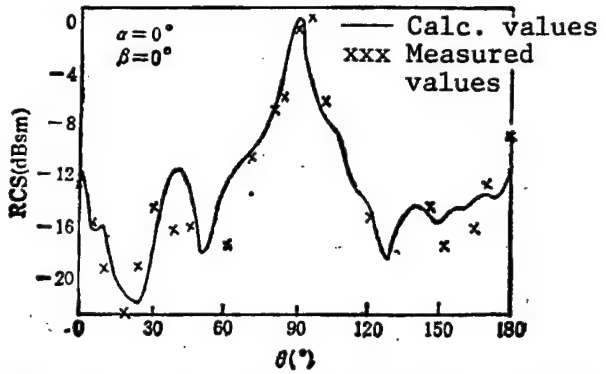

Figure 8. Radar Cross Section of Aircraft Model (horizontal polarization, monostatic setup)

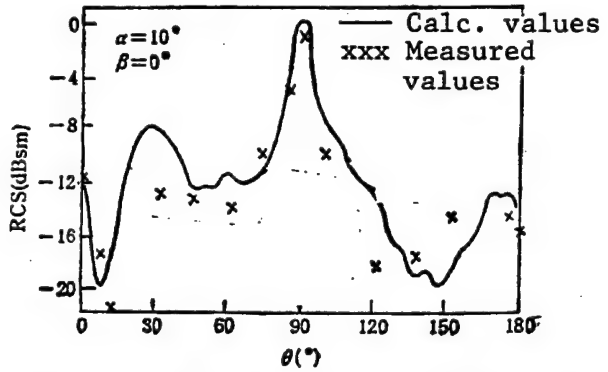

Figure 9. Radar Cross Section of Aircraft Model (vertical polarization, monostatic setup)

A computer program which implements the panel method on an IBM 4381 computer requires 4 min of CPU time to calculate the RCS of the above aircraft model at 181 points for one attitude (including the RCS of the air inlet pipe and the tail nozzle). While the computation time of the panel method is somewhat longer than that for the Mittra method, it carries out the RCS computation based on an accurate representation of the object configuration, whereas the Mittra method can only perform RCS computation by using simple shapes to emulate a complex object. The panel method can also be used to perform sensitivity analysis of RCS variations with respect to changes in the target configuration. Clearly, the panel method is more accurate than the Mittra method.[7]

IV. Concluding Remarks

To satisfy the requirements of efficiency and robustness, this article has proposed the panel method for RCS computation. Sample calculations have shown that this method is more accurate than the component synthesis method proposed by Mittra, and can be used for computing the RCS of an arbitrarily complex object.

References

1. R. Mittra, S. W. Lee, C. A. Chuang, "Analytical Modeling of the Radar Scattering Characteristics of Aircraft," AD-773685 (1974).

2. D. Klement, J. Preissner, V. Stein, IEEE TRANS. ON AP, AP-36 (1988), 2, 228-237.

3. E. F. Knott et al., "Radar Cross Section: Estimation, Measurement, Reduction" (Trans. into Chinese), Electronics Industry Publ. House, Beijing, 1987.

4. C-C. Huang, P. H. Pathak, "Ray Analysis of EM Backscatter From a Cavity Configuration," AD-A133262 (1982).

5. H. R. Witt, E. L. Price, PROC. IEE, 115 (1968), 1, 94-100.

6. Li Zhuzhen, editor, "Commonly Used Methods for RCS Computation (special issue)," Target Characteristics Research and Editorial Department, 1981.

7. Zhou Jianjiang, Li Jian, Shu Yongze, "Panel Method and Component Synthesis Method for Computing the RCS of Complex Targets," Ministry of Aerospace Industry, Institute of Science and Technology, Internal Report, 1990.

Main Details of FY-2 Meteorological Satellite's Remote Sensor Released

92P60242A Beijing ZHONGGUO HANGTIAN [AEROSPACE CHINA] in Chinese, Special issue, Dec 91 pp 45-49

[Article by Ma Henian [7456 7729 1628], vice director of the State Meteorological Administration: "Present Applications, Future Development of China's Meteorological Satellites"]

[Excerpt] [Passage omitted] Satellite meteorology activities are just beginning to unfold. Based on the polar-orbit meteorology of the already successfully launched FY-1 and FY-1A [satellites], experiments are being conducted to continually improve and perfect the system, and a polar-orbit metsat series providing multifunctional services is in the initial stages of development. Simultaneously, measures are being taken to develop a geostationary meteorological satellite, the FY-2; the main characteristics of the FY-2's basic onboard remote sensing detector are given in Table 4 below.

Table 4. Main Parameters of the FY-2 Onboard Remote Sensing Detector

Channel	Spectral range (μm)	Instantaneous FOV (μrad)	Sub-satellite-point resolution (km)	Spin rate (cycles/min)	Scan time per picture (min)
Visible	0.55-1.05	35	1.25	100	25
IR	10.5-12.5	140	5	100	25
Water vapor	5.7-7.1	140	5	100	25

China Plans To Send Man Into Space

40100033A Beijing CHINA DAILY in English
11 Apr 92 p 1

[Article by Zhou Jie, staff reporter]

[Text] China plans to send its first man into space eight years from now, according to a State report on scientific development strategy.

"An unmanned spacecraft will be launched before the year 2000, to be followed by the first manned space flight in China's history," said the report.

An experimental space station, which can be used for economic, military and social purposes, is expected to be launched before 2020, according to the report approved by the State Council and released on April 7.

The manned space mission is one of the most urgent targets in China's space programme for the remaining years of this century, the report said.

This is the first time China has officially revealed its plans to send a man into space.

In the next 30 years, the report said, China plans to build a reusable transport system linking space and earth—probably some type of space shuttle or similar spacecraft.

A medium-sized compound dedicated to manned space flight will be set up before 2000. It will include sections devoted to technology, launching and retrieval of spacecraft. The country will meanwhile prepare to build a sophisticated space transportation terminal, incorporating those sections and astronaut quarters. The terminal is scheduled for completion before 2020. A permanent command centre for manned space flights will be set up simultaneously.

The report said that China will build new launching and recovery bases and satellite monitoring networks as the programme develops.

The space blueprint indicated that China will continue to develop its launch rockets, including the large carriers necessary for manned space flight. The new rockets are expected to be in service before 2020.

Development of key technology for the manned space programme is one of the most important tasks now facing China's space scientists. Such technology will include a life-support system and environmental controls within the spacecraft; an emergency monitoring and rescue system; return and retrieval technology; the selection and training of astronauts; space nutrition and medical care.

Other technology must also be worked out: Joining, supplying, repairing and assembling of spacecraft; designing an energy supply system and an on-land training simulator; preparing medical experiments to be carried out in space and developing the technology for sustaining a permanent space station.

It is believed that a manned space mission has long been in China's plans, but the goal has so far been hampered by a shortage of funds.

Surface Mount Technology, Other Defense-Electronics Achievements of Institute 2 Certified

92P60217A Beijing ZHONGGUO DIANZI BAO [CHINA ELECTRONICS NEWS] in Chinese 23 Mar 92 p 3

[Article by Jin Jianzhong [6855 1696 0022]: "Technology Institute Unveils Five New Technology Achievements"]

[Summary] In order to improve the quality and reliability of the nation's defense electronics products, MMEI's Institute 2 (the Technology Institute) has carried out intense research into new fabrication technologies. On 7 March, five Institute 2 achievements—new electromachining technology, an SMT [surface mount technology] laser soft borer/soldering apparatus and fabrication research, the SMT-89PL-A automatic platform-style chip adhesive mounting machine, research on an integrated precision machining technology, and research on a technology for testing solderability of chip-type components—passed technical appraisal in Taiyuan.

The new electromachining technology is oriented toward precision line-cutter machine tools, and will permit the first domestic implementation of 16-bit computer control units for CNC machine tools. With this new technology, machining accuracy can be raised to 0.008 mm, and machining surface roughness Ra is less than 0.8 micron. The SMT laser soft borer/solderer, jointly developed with Harbin Institute of Technology, is the first such domestically developed unit to be used for fabrication of 100-pin flat package ICs with a 0.65-mm-precision lead spacing. The SMT-89PL-A automatic platform-style chip adhesive mounting machine has a speed of 1,800 chips/hour and an accuracy of 0.2 mm. The integrated precision machining technology is oriented toward metal forming, tool and die design and manufacturing, and machining of precision machinery, and includes development of the SR-C three-level guide way and turnover inner guide, which turns the workpiece into any of seven positions (0°, +/-45°, +/-90°, and +/-105°). Finally, the technology for testing solderability of chip-type components is designed for further expanding applications of SMT.

Transformation Induced Superplasticity in 18Ni Maraging Steel

40100034A Beijing JINSHU XUEBAO [ACTA METALLURGICA SINICA] in Chinese
Vol 28 No 2, Feb 92 pp A57-A61

[Article by Yin Zhongda, professor, Faculty of Metal Heat Treatment, Harbin Institute of Technology and Zhou Yongkang of the Shanghai Centrifugal Machinery Research Institute (MS received 21 Jan 91; revised 4 Jul 91)]

[Abstract] After exploring the influence of stress, cold-rolling reduction and cooling rate on transformation-induced strain, a transformation-induced superplasticity forming technique for 18Ni maraging steel (2450MPa) was developed. Through 14 times γ to α (and vice versa) cyclic transformation, limited elongation of 320 percent can be obtained in 60 percent cold-rolled specimen. TEM observation reveals that the morphology of stress-induced martensite is massive.

Zhejiang University Deposits Diamond Thin Film on C_{70} Film

92P60233A Beijing GUANGMING RIBAO in Chinese
3 Apr 92 p 2

[Articlke by Yuan Xiang [5913 4382]: "China Grows Diamond Thin Film on Carbon-70 Film"]

[Summary] On 14 March, Zhejiang University researchers for the first time domestically succeeded in growing diamond thin films on a C_{70} film, which in turn was grown on a silicon substrate—a major advance in the nation's research and development of C_{60} materials. The Zhejiang research group, led by Prof. Li Wenzhu [2621 2429 6999], grew the C_{70} film via ion bombardment; using this C_{70} film as the core material, the group then employed rf plasma chemical vapor deposition to grow the diamond thin films. C_{70} is a variant of C_{60}, the recently discovered (1985) third allotype of carbon—after graphite and diamond.

Doped Strontium Barium Niobate Conjugate-Effect Crystal Certified

92P60218A Beijing ZHONGGUO KEXUE BAO [CHINESE SCIENCE NEWS] in Chinese
24 Mar 92 p 2

[Article by Li Shuben [2621 2885 2609]: "Doped Strontium Barium Niobate Conjugate-Effect Crystal Developed"]

[Summary] The "doped strontium barium niobate (SBN) conjugate-effect crystal material" jointly developed by the Heilongjiang Province Institute of Technical Physics and Harbin Institute of Technology as a key province S&T project recently passed expert appraisal. Doped SBN crystal, which has excellent phase-conjugate effects, is a critical material in the fabrication of electro-optic modulators and infrared detectors. It can be used in many new high-tech areas, such as moving-target direction finding and tracking, image processing, optical computing, interferometry, metrology, and fiber optic gyro systems, and hopefully will replace the now prohibitively expensive and difficult to grow barium titanate crystal.

Production of Purified Human Leukointerferon Approved

92P60260A Beijing KEJI RIBAO [SCIENCE AND TECHNOLOGY DAILY] in Chinese 13 Mar 92 p 1

[Article by Li Mingqi [2621 2494 0796] and Yin Hongqu [1438 1347 5028]]

[Summary] A purified human leukointerferon, developed by the Institute of Microbiology and Epidemiology, Academy of Military Medical Sciences, has been approved by the Ministry of Public Health for scale production. In 1969, the institute started its research on technology to produce highly-active interferon by inducing it from extracorporeal circulation blood and normal spleen. Advanced technologies involved in preparing this product in vitro are the specific antibody affinity chromatography and the ultrafiltration-condensation technique. Clinically, the product has been tested and found effective in treating various viral diseases, inhibiting growth and spread of tumor cells, and enhancing immunity and body strength. To meet the requirements of large-scale production, a modern production line has been established by the Beijing Sihuan (Four Ring) Biological and Biochemical Products Incorporation, a plant affiliated with the Academy of Military Medical Sciences.

Microvector System Encephalitis B Vaccine Developed

92P60260B Beijing KEJI RIBAO [SCIENCE AND TECHNOLOGY DAILY] in Chinese 13 Mar 92 p 1

[Article by Yang Guangming [2799 0342 2494] and Jin Haiying [6855 3189 5391]]

[Summary] An encephalitis B vaccine using a Chinese-made microvector system has been jointly developed by the Shanghai Institute of Biological Products, Ministry of Public Health, and the East China Institute of Chemical Engineering. The microvector-bioreactor system contains a bioreactor filled with a suspension of microspherical vectors for mass production of animal cells by absorption. Unlike the complex, animal source-restricted conventional hamster-kidney-protocyte method, the microvector system can easily produce large quantity of animal cells without any restriction. By using the microvector system, the institute was able to produce the purified encephalitis B vaccine from large-scale monkey kidney cell cultures.

New Drug for Substance Addiction Treatment

92P60260C Beijing GUANGMING RIBAO in Chinese 18 Apr 92 p 1

[Article by Ye Hui [0673 6540]]

[Summary] A new drug "Anlisu" [1344 0448 5685], developed by Yang Guodong [2799 0948 2767], director of Ningbo Microcirculation and Henbane Drugs Research Institute, has been successfully used in treating drug addiction. The recovery rate of Anlisu is said to be 100 percent after being tested on 2,000 drug abusers across the nation, and Anlisu is also said to cure 12 drug addicts in Yunnan in 10 days. Anlisu contains primarily the Chinese herbal medicine "henbane" (Hyoscyamus niger), which is normally used as an anodyne or sedative. Yang Guodong has also made achievements in using henbane to treat aplastic anemia, coronary heart disease, hyperlipemia, epilepsy and tetrodontoxism (puffer fish poisoning).

Hepatitis C Virus Genomic Library Established

92P60260D Shanghai WEN HUI BAO in Chinese 3 Apr 92 p 3

[Article by Jiang Heping [5592 0735 1627]]

[Summary] The first hepatitis C virus (HCV) genomic library specific for Chinese has been established in Shanghai by the Microbiology Research Laboratory of the Second Military University, the third one in the world (the others being in the United States and Japan). In 1988, Associate Professor and Chairman of the Microbiology Research Laboratory Qi Zhongtian [2058 0022 3944] started his HCV research with the collection of infected sera and plasma specimens of high-incidence population in Shanghai, Jiangsu, Hebei, Shandong, and Henan, and conducted tests including in vitro bacteriophage coating, plaque immunoassay, and subcloning techniques in order to establish an HCV genomic sequences specific to Chinese. His work has laid foundation for developing specific hepatitis C screening and diagnostic systems, and for producing hepatitis C vaccine. The laboratory is now conducting research on HCV antigen-antibody screening kits based on the newly established HCV genomic sequence.

Genetic Recombination and *Fib* Genes Transfer of the Plasmid of *E. herbicola* CSH 1065

40091014A Beijing YICHUAN XUEBAO [ACTA GENETICA SINICA] in Chinese Vol 19 No 1, Feb 92 pp 76-85

[English abstract of article by Zhao Yang [6392 2254] of the Kunming Institute of Botany, the Academy of Science of China, Kunming]

[Text] We inserted kanamycin resistance (*Km*) gene and mobilized function (*Mob*) gene on the plasmid of *E. herbicola* CSH1065 by using DNA molecular cloning and genetic recombination techniques. Therefore, the plasmid of *E. herbicola* CSH1065 to *E. coli* HB101 could be transferred by conjugation. The expression of those genes concerning fungi inhibition function (*Fib*) of *E. herbicola* CSH1065 in *E. coli* HB101 was observed. This result confirmed again the fungi inhibition genes of *E. herbicola* CSH1065 is only related to its plasmid genome not to its chromosome genome. Meanwhile those yellow pigment genes located on the plasmid don't involve the

antifungi function of *E. herbicola* CSH1065. All those results were convinced by DNA molecu lar hybridizations.

Multi-Origin Usage for Chromosome Replication of Suppressive Integration Strain of *dna*A46 Mutant of Escherichia Coli Integrated with R6K

40091014B Beijing YICHUAN XUEBAO [ACTA GENETICA SINICA] in Chinese Vol 19 No 1, Feb 92 pp 86-92

[English abstract of article by Lu Jianwei [4151 6015 1792], Mao Yumin [3029 5940 3046], et al., of the Institute of Genetics, Fudan University, Shanghai; the project supported by the National Natural Science Foundation of China (3870279)]

[Text] The chromosome of temperature sensitive initiation mutant *dna*A46 of *Escherichia* coli K-12 fails to replicate at 42°C. Suppressive integration (Sin) strain integrated with the R6K plasmid was screened at 42°C. Marker frequency determination of the Sin strain reveals that replication was initiated at the normal site of initiation at 30°C, while at three different sites at 42°C. Two of the sites have been reported in the stable DNA replication mutant, one of them is a noval site. Inhibition of chromosome replication was not observed for the *recA* derivative of Sin initiated at two of the initiation sites close to the nor mal initiation site. Inhibition was observed for chromosome replication initiated near the site where chromosome replication normally terminates. It indicates that chromosome replication initiated at sites close to the terminus is *recA* gene dependent.

Synthesis, Cloning and Sequencing of the Major Out Capsid Protein in Rice Dwarf Virus

40091014C Beijing WEISHENGWU XUEBAO [ACTA MICROBIOLOGICA SINICA] in Chinese Vol 32 No 1, Feb 92 pp 72-74

[English abstract of article by Ye Yin [0673 1377], Zhao Feng [6392 0023], et al., of the Institute of Microbiology, Academia Sinica, Beijing]

[Text] Rice dwarf virus (RDV) is a major problem in rice production in China. Its genome contains 12 segments of dsRNA while segment 8 encodes the major out capsid protein. Viral dsRNA was separated from purified RDV of a Chinese isolate. The two first strands of cDNA of segment 8 were synthesized with two primer s: 3' terminal primer, 5'-ATGTCACGCCA GATCTGGTT-3' and 5' terminal primer, 5'-ATGTC ACGCCAGATCTG-GTT-3', and the gene was amplified by PCR. Complete nucleotide sequence demonstrated that the major out capsid protein gene consists of 1256 base pairs, with 65 bases difference from the result of Japan. Protein sequence of 420 amino acids was deduced, with 10 amino acids differing from that of Japanes isolate.

Breakthroughs Made in Using Gene To Treat Hemophilia B

40101016A Beijing XINHUA in English 1416 GMT 8 Apr 92

[Text] Shanghai, April 8 (XINHUA)—Chinese scientists have made breakthroughs in using gene [as received] to treat Hemophilia B.

Patients with hemophilia, a hereditary disease, suffer from excessive bleeding caused by an inborn deficiency in the substance necessary for blood clotting. Hemophilia B is caused by a deficiency of plasma thromboplastin component (PTC), or the IX Factor.

Scientists from the Genetics Institute of Fudan University carried out experiments by first introducing the IX Factor of human beings into the cells of rabbit skins and then transplanting the genetically processed cells into the abdominal cavity of rabbits.

Clinical analysis revealed that over the past 10 months the rabbits have produced a high proportion of IX Factor in their blood.

"The experiments are the most advanced of their kind in the world," according to Xue Jinglun, vice director of the institute who is also in charge of the experiment program.

Large-Scale Production of Genetic Interferon Set To Begin

40101016B Beijing XINHUA in English 0259 GMT 26 Apr 92

[Text] Shanghai, April 26 (XINHUA)—The Alpha 1 type genetic engineering interferon, a kind of high-tech biological internal therapeutic medicine developed by Chinese scientists will be put into large-scale production.

It is said to be the first high-tech biological product put into industrialized production in China, which indicates that China's development capacity of high-tech products is approaching the world's advanced level.

The Alpha 1 type genetic engineering interferon is said to be able to be used in treating over 30 kinds of diseases and malignant tumors.

The interferon was successfully developed by scientists of the Chinese Academy of Preventive Medicine through genetic engineering in 1984.

The scale production of this kind of interferon will be undertaken by the Shanghai Institute of Biologicals which belongs to the state Ministry of Public Health.

According to the report of the ministerial appraisal led by famous scientist Tan Jiazen, techniques in the production including large scale fermentation, dissociation, extraction, and purification as well as the production line, have reached international standards for medicine production.

According to experts, as of now, the same of interferon has not yet been produced in other countries. Clinical reports on 387 cases from over 20 hospitals show that the interferon can effectively cure chronic hepatitis B, hairy cell leukemia, hepatitis C and tumors.

Compared with similar medicines, the Alpha 1 genetic engineering interferon has noticeable advantages of low side reactions and causing no antibody reaction in the human body.

Experts say that the medicine has provided an important therapeutic method for some high incidence diseases which lack efficient treating therapies.

Cloning of Midecamycin 4"-acyltransferase and Its Expression in Spiramycin Producing Strains

40091013A Beijing SHENGWU GONGCHENG XUEBAO [CHINESE JOURNAL OF BIOTECHNOLOGY] in Chinese Vol 8 No 1, Feb 92 pp 1-14

[English abstract of article by Wang Yiguang [3076 0110 0342], Jin Lianfang [6855 5571 5302], et al. of the Institute of Medicinal Biotechnology, Chinese Academy of Medical Sciences, Beijing]

[Text] A midecamycin 4"-acyltransferase gene was discovered from primary clone pCN_6C_5 (48.5 kb), containing midecamycin biosynthetic gene.[1] Subcloning of pCN_6C_5 DNA into plasmid vector pIJ_{680} BamHI site resulted in obtaining of recombinant plasmid $p_{66}B$. Transformation of $p_{66}B$ DNA into spiramycin producing strains resulted in direct production of 4"-isovalerylspiramycin. In order to identify the completeness of cloned midecamycin 4"-isovaleryltransferase gene on plasmid $p_{66}B$ from pCN_6C_5 DNA and the possible existence of other 4"-acyltransferase gene in the midecamycin producing strain *S. mycarofaciens 1748 genome. Colony hybridization of genomic library of S. mycarofaciens* 1748 was performed by using the BamHI-BamHI 2.3 kb insert on $p_{66}B$ DNA as probe. Another positive clone $pCN_{10}F_5$ was obtained. A BamHI-BamHI 8.0 kb homologous region on $pCN_{10}F_5$ was determined by Southern hybridization and was subcloned into plasmid $pWHM_3$ as well as pIJ_{680}. Recombinant plasmids pWF_5 and p_6F_5 were obtained. Transformation of these plasmids into spiramycin producing strains resulted in production of two major acylspiramycin components. Based on their physiochemical properties and spectral evidences, component I has been identified as 4"-propionylspiramycin III, component II as 4"-propionylspiramycinll. Southern hybridization confirmed that the BamHI-BamHI 8.0 kb fragment was cloned in the spiramycin producing strain. Only $pCN_{10}F_5$ clone was identified from genomic library of *S. mycarofaciens* 1748 when the 4"-isovaleryltransferase gene of carbomycin producing strain *S. thermotolerans* was used as a probe in colony hybridization, that suggested there is a difference between the 4"-acyltransferase genes in the pCN_6C_5 and in $pCN_{10}F_5$ clones.

Reverse DNA Sequencing by Using the Heat-Stable Bst Polymerase System

40091013B Beijing SHENGWU GONGCHENG XUEBAO [CHINESE JOURNAL OF BIOTECHNOLOGY] in Chinese Vol 8 No 1, Feb 92 pp 28-33

[English abstract of article by Lu Youyi [0712 1635 0308], Ye Shengyu [0673 4141 6877], et al. of the Shanghai Institute of Biochemistry, Shanghai]

[Text] Reverse DNA sequencing was a simple and rapid method to check the available DNA data by sequencing the original DNA in the opposite orientation. Because this method has the double stranded sequencing nature, high background, extra bands occurred not infrequently on the autoradiographs. These short comings have now been overcome by using the heat stable Bst polymerase system developed in this lab. The reverse DNA sequence patterns obtained by using this system were now fully comparable with those patterns generated on the single-stranded DNA template.

High Level Expression of *Escherichia coli* β-galactosidase in *Heliothis armigera* Cells by Using a Baculovirus Vector

40091013C Beijing SHENGWU GONGCHENG XUEBAO [CHINESE JOURNAL OF BIOTECHNOLOGY] in Chinese Vol 8 No 1, Feb 92 pp 34-39

[English abstract of article by Zhu Guokai [2612 0948 0418], Tu Yizeng [1458 4135 1073], et al. of the Shanghai Institute of Entomology, Academia Sinica, Shanghai]

[Text] The *E. coli* β-galactosidase gene carried by a baculovirus vector pAc360-β-gal was transferred into the AcNPV genome by cotransfection of *S. frugiperda* cells. A recombinant baculovirus, AcNPV-β-gal was obtained by means of X-gal selection and plaque purification. This recombinant baculovirus could effectively infect established *H. armigera* cell line and express the biologically active β-galactosidase under the control of the baculoviral polyhedrin promotor. More than 80 percent the β-galactosidase was secreted from infected *H. armigera* cells and over 50,000u/ml of activity, equal to calculate 170 μg/ml of protein was detected in infected cells medium. Separation with SDS-PAGE and detection of β-galactosidase activity directly on gels showed that the products of the foreign gene expressed in *H. armigera* cells infected with AcNPV-β-gal existed in the forms of five active polymers or complexes. By comparison of abilities of the β-galactosidase expression with wildly used *S. frugiperda* cells, we think *H. armigera* cells might

be developed as an alternative to *S. frugiperda* cells and the *H. armigera* cells—AcNPV might become a new insect cells—baculovirus expression system.

Construction of a Secretion-Expression Vector of *Bacillus*

40091013D Beijing SHENGWU GONGCHENG XUEBAO [CHINESE JOURNAL OF BIOTECHNOLOGY] in Chinese Vol 8 No 1, Feb 92 pp 40-47

[English abstract of article by Xin Feng [6580 0023] and Jiang Ruzhang [5592 1172 3864] of the Department of Biology, Nankai University, Tianjin]

[Text] A *Bacillus* protein secretion-expression vector $pAMY_{403}$ has been constructed based on the promoter and signal sequence coding region of α-amylase gene from *Bacillus licheniformis.* It possesses a polylinker with the restriction sites of PstI-HheI-SmaI-BamHI-SalI after signal peptide coding region. The α-amylase gene carried by plasmid $pAMY_{403}$ in *B. subtilis* can be expressed and secreted as its parental plasmid $pAMY_{413}$. When β-lactomase gene from *B. licheniformis* is cloned at SmaI sites of $pAMY_{403}$, it can express and secret normally.

Polylinkers of plasmid $pAMY_{403}$ provide cloning sites both for inserting heterogenes to produce non-fusion protein (e.g., insert at NheI or PstI site) and for protein fusion in different reading frames at other restriction sites. Therefore plasmid $pAMY_{403}$ can adapt to any project of construction chimeric secretion plasmid in *B. subtilis.*

Construction of Slow-Secreting Mutant Gene and Its Application

40091013E Beijing SHENGWU GONGCHENG XUEBAO [CHINESE JOURNAL OF BIOTECHNOLOGY] in Chinese Vol 8 No 1, Feb 92 pp 48-53

[English abstract of article by Qi Beijing [2058 5563 7234], Wu Zirong [0702 5261 2837], et al. of the Molecular Biology Laboratory, Department of Biology, East China Normal University, Shanghai]

[Text] A 300 bp human cDNA sequence was introduced through in-frame insertion into the pro-peptide coding region of the *Bacillus subtilis* extracellular neutral protease gene (nprE). The inserted sequence had no significant effect on the translation, processing and folding of the gene product, but reduced the rate of secretion more than ten fold. The "slow-secreting" phenotype of the mutant gene and the easy detection of the indicating enzyme has opened up a new direction for us to study protein secretion in *B. subtilis.* Also reported in this communication is the preliminary characterization of two temperature sensitive mutants affecting the neutral protease production, which were isolated using the newly constructed slow-secreting mutant gene.

Stability Improvement of Plasmid Harboured in Genetically Engineered Strain and Production of Phenylalanine

40091013F Beijing SHENGWU GONGCHENG XUEBAO [CHINESE JOURNAL OF BIOTECHNOLOGY] in Chinese Vol 8 No 1, Feb 92 pp 54-59

[English abstract of article by Liang Shizhong [2733 0013 0022] of the Institute of Biotechnology, South China University of Technology, Guangzhou and Gao Heyong [7559 3109 3144], et al. of the IC Biotech., Faculty of Engineering, Osaka University, Japan]

[Text] In this study, a new plasmid $pSY_{200\text{-}14}$ was constructed by gene-recombination technology, which has a genetic system of phenylalanine production, by using plasmid $pSY_{130\text{-}14}$ and pSY_{16}. The $pSY_{130\text{-}14}$ contains $pheA^{FR}$ and $aroF^{FR}$, the feedback inhibition resistant phenylalanine-production genes, and a temperature-sensitive repressor cI_{857}, whereas pSY_{16} possesses a partition system and is a low copy plasmid. Subsequent experiments have shown that the recombinant AT_{2471}/$pSY_{200\text{-}14}$ constructed is more stable than original strain AT_{2471}/$pSY_{130\text{-}14}$, in other words, the former kept the stability as high as 100 percent under selective pressure in 30-42°C. In a 2.5L jar fermentor, the production of phenylalanine after 48h cultivation reached 14.2g/L that was 11.8 percent higher than old strain under the conditions of impeller speed 850 rpm, aeration rate 1.0 vvm, temperature 38.5°C and pH7.0.

Production of Monoclonal Antibody in Hollow Fiber Culture System With Serum-Free Medium

40091013G Beijing SHENGWU GONGCHENG XUEBAO [CHINESE JOURNAL OF BIOTECHNOLOGY] in Chinese Vol 8 No 1, Feb 92 pp 70-76

[English abstract of article by Zhou Weisong [0719 4850 2646] and Cai Shaohua [5591 1421 5478] of the Biotechnology Research Center, Chinese Academy of Agricultural Science, Beijing]

[Text] Hybridoma 7E8 cells, which produced IgG_{2a} against potato virus X, were cultured in VF-2 hollow fiber cell culture system with 1640 SFM serum-free medium. The maximam viable cell density was 2.34 x 10^6 cells/ml that was 3.7 times and 2.2 times of the maximam viable cell density achieved in spinner flask culture system and in static flask culture system, respectively. 10,000 ml cell cultural supernatant had been collected in 42 days cultural period. The ELISA titer of monoclonal antibody (McAb) in the supernatant was about 1:20000 that was 25 times of the titers attained in spinner flask culture system and in static flask culture system. From 1000ml cell cultural supernatant, an amount of 51.2 mg 7E8 McAb IgG had been purified by 50 percent saturated ammonium sulfate precipitation and Sephadex G-200 chromatography. The average yield of McAb in the hollow fiber cell culture system was 12.3

mg/d. The results of the study suggest that it is hopeful fol hybridoma cell culture in the hollow fiber cell culture system with serum-free medium for McAb production on larger-scale.

Production of 6-amino Penicillanic Acid in Immobilized Cell Membrane Bioreactor

40091013H Beijing SHENGWU GONGCHENG XUEBAO [CHINESE JOURNAL OF BIOTECHNOLOGY] in Chinese Vol 8 No 1, Feb 92 pp 77-81

[English abstract of article by Ma Shihong [7456 1102 3163], Du Jiangying [6757 4829 3841], et al. of the Institute of Chemical Physics, Academia Sinica, Dalian and Wu Ruping [0702 3067 1627], Feng Yimin [7458 0001 3046], et al. of the Institute of Pharmacy, Academia Sinica, Shanghai]

[Text] 6-Amino penicillanic acid has been produced in an immobilized cell membrane bioreactor, which was constructed with hollow fiber or flat membrane and operated in the backflush mode. The cell containing penicillin acylase was immobilized on the surface of membrane by cross-linking and intercepting, the loading of cells was high, and enzyme activity per unit volume of the reactor was also high. The penicillin of high concentration can be converted completely within 2 h. After 50 runs, the activity remained in the reactor was about 87 percent of the initial one, the average yield of 6-APA was 90.1 percent with the purity of 98.68 percent.

Selection of D-xylose and Cellobiose-Fermenting and Ethanol-Producing Strains by Electric Field-induced Protoplast Fusion

40091013I Beijing SHENGWU GONGCHENG XUEBAO [CHINESE JOURNAL OF BIOTECHNOLOGY] in Chinese Vol 8 No 1, Feb 92 pp 82-86

[English abstract of article by Wang Yuewu [3769 1471 0063], Song Linsheng [1345 2651 3932], et al. of the Department of Biology, National University, Tianjin]

[Text] The protoplast fusion between *Candida guilliermondii* S208 (Arg^-) and *Saccharomyces cerevisiae* 314 was induced with the model GH-401 Electric Induced Gene Transfer/Cell Fusion System by three pulses (18kV/cm, 10 μs duration) applied at an interval of 1s. The frequency of appearance of prototrophic hybrids was 3.6×10^{-3}.

Stable fusion products were obtained after continual subculture on selected and unselected medium more than 20 times. The results of comparative studies showed that the fusion products were real hybrids of both parents. Two fustants, F-106 and F-308, could ferment both D-xylose (2 percent) and cellobiose (2 percent) to ethanol. The ethanol production of F-106 were 3.1 g/l and 1.05 g/l respectively, F-308 were 0.2 g/l and 2.8 g/l respectively.

Technology Investigation of Separating Magnetic Immobilized Enzyme by High Gradient Magnetic Field

40091013J Beijing SHENGWU GONGCHENG XUEBAO [CHINESE JOURNAL OF BIOTECHNOLOGY] in Chinese Vol 8 No 1, Feb 92 pp 99-101

[English abstract of article by Zhang Zhaoqing [1728 0340 1987], Guan Chengxin [7070 2052 0207], et al. of the Institute of Applied Physics, Henan Academy of Sciences, Zhengzhou and An Zhifa [1344 3112 3127] of the Institute of Biology, Henan Academy of Sciences, Zhengzhou]

[Text] New developments in magnetic labeling techniques for cells and microspheres have extended the useful range of high gradient magnetic separations (HGMS) into many important areas of biotechnology. We use the superparamagnetic powder to put magnetic labels on the α-amylase, glucoamylase, glucoseisomerase and proteinase, then separate them by HGMS. At least the separate efficiency can be more than 95 percent, the activity of the magnetic immobilized enzyme are better, for the industrial application in the future we offer an initial imagination.

The Preparation and Stability of Liposome-Encapsulated Ara-A

40091013L Beijing YAOXUE XUEBAO [ACTA PHARMACEUTICA SINICA] in Chinese Vol 27 No 1, Jan 92 pp 74-80

[English abstract of article by Xue Yuying [5641 3768 5391] and Weng Guoying [5040 1613 5391] of the Nanjing Institute of Materia Medica, Nanjing]

[Text] This paper uses several preparation methods, such as thin-film, reverse-phase evaporation and freeze-thawing methods, and also compares encapsulation percentage of Ara-A (Vidarabine) in liposome (EN%) of these methods. The best operational conditions of preparing liposome-encapsulated Ara-A are explored. A higher EN%, about 50%, which is 10 times that reported in foreign literature, is obtained by using improved freeze-thawing method, and this method is easy to operate and repeatable. At the same time, the physical and chemical stabilities of the liposome-encapsulated Ara-A were observed. The result shows that there are no distinct changes in shape, size distribution of liposome, and EN% as well as Ara-A contained in liposome by means of sterilization at 100°C for 30 minutes. Accelerating test at a constant temperature indicates that liposome-entrapped Ara-A has certain chemical stability.

Preparation and *in vitro* Antiviral Activity of Liposomes of Lipophilic Esters of Acyclovir

40091013K Beijing YAOXUE XUEBAO [ACTA PHARMACEUTICA SINICA] in Chinese Vol 27 No 1, Jan 92 pp 15-21

[English abstract of article by Tong Ping [4547 1627], Shao Sen [6730 2773], et al., of the 302 Hospital of Infectious Diseases, Beijing; Hou Xinpu [0186 2450 2613] of the Department of Physiochemistry; Zhang Yingmei [1728 4481 1188], Zhang Chenhui [1728 2525 2547] of the Department of Microbiology, Beijing Medical University, Beijing]

[Text] The long chain acyclovir such as the acyclovir laurate and acyclovir palmitate were prepared directly from acyclovir by application of the usual esterification methods with appropriate acyl chlorides. The lipophilic prodrugs were found to be retained easier by liposomes whereas acyclovir escaped readily from liposomes. When assayed in African green monkey cell cultures against herpes simplex virus type I strain, the acyclovir palmitate liposomes proved to be more active compared with the parent drug and its liposome, suggesting an enhanced compatibility between the ester and liposomal lipids and an increased uptake of encapsulated prodrug by infected cells.

Preparation and Application of Monoclonal Antibody Against Schistosoma Gut Associated Cathodic Antigen

40091013M Shanghai ZHONGHUA CHUANRANBING ZAZHI [CHINESE JOURNAL OF INFECTIOUS DISEASES] in Chinese Vol 10 No 1, Feb 92 pp 10-13

[English abstract of article by Yan Zizhu [0917 5261 0504], Lu Zaiying [0712 0375 1305], et al. of the Institute of Parasitic Diseases, Shanghai Chinese Academy of Preventive Medicine]

[Text] Monocolonal antibody 3D8A against schistosoma japonicum was obtained by cells hybridoma technique. Its isotype is IgM, and target antigen is the gut of adult worm and egg of schistosoma. It moved to cathode in immunoelectrophoresis, and was shown to be a glycoprotein. 3D8A, after purified and labeled with fluorescence isothiocyanate, was used in direct IFA, microamount of antigen in liver tissues of mice infected with schistosoma could be found. The serum circulating antigen in patients from Anhui and Hubei could be detected by direct dot-ELISA with McAb 3D3A labeled with peroxidase. The positive rate was 82.5 percent, and none was positive in normal individuals.

Experimental Studies on Specific Transfer Factor and Its Augment Component of Japanese Encephalitis Virus

40091013N Shanghai ZHONGHUA CHUANRANBING ZAZHI [CHINESE JOURNAL OF INFECTIOUS DISEASES] in Chinese Vol 10 No 1, Feb 92 pp 33-36

[English abstract of article by Song Changzheng [1345 7022 1767], Li Baolin [2621 1405 2651], et al. of the Laboratory of Electron Microscopy, Shandong Academy of Medical Sciences, Shandong]

[Text] Specific transfer factor (STF) of Japanese encephalitis virus (JEV) was prepared from splenic leukocytes of live JEV-immunized goat. JEV-Ab_2 was used as a specific ligand for isolating STFac (augment component) from STF. The potency and specificity of STF and STFac were evaluated by leukocyte adherence inhibition microtest and footpad swelling assay. It was found that STF and STFac had the function of transferring JEV specific cellular immunity in vivo and in vitro. In comparison with STF and NTF (non-immunized transfer factor), STFac could significantly protect mice from lethal challenge with JEV.

First Strain of HIV Isolated From a Chinese AIDS Patient

40091012A Beijing ZHONGHUA WEISHENGWUXUE HE MIANYIXUE ZAZHI [CHINESE JOURNAL OF MICROBIOLOGY AND IMMUNOLOGY] in Chinese Vol 12 No 1, Feb 92 pp 1-4

[English abstract of article by Sun Zhonghe [1327 0022 0735], Xu Wanping [6079 8001 1627], et al., of the Institute of Microbiology and Epidemiology, Academy of Military Medical Sciences, Beijing]

[Text] We have isolated the first strain of HIV with cocultivation of the blood specimen of a Chinese AIDS patient and the PHA-actived PBMC. This virus could induce obvious CPE: syncytium formation and balloon-like cells in the culture of PBMC, MT_4 and C_{8166} cells and was identified as HIV with neutralization test, enzyme-labeled antibody staining, electron microscopy, western blot and PCR. The CPE and protein composition of this strain, as compared with the standard strain, appeared some difference, its significance may be elucidated in the further research.

Cloning and Expression of a Segment of HIV-1 Gag Gene in *E. coli*

40091012B Beijing ZHONGHUA WEISHENGWUXUE HE MIANYIXUE ZAZHI [CHINESE JOURNAL OF MICROBIOLOGY AND IMMUNOLOGY] in Chinese Vol 12 No 1, Feb 92 pp 5-8

[English abstract of article by Wu Weixing [0702 5898 2502], Wang Hongyan [3076 7703 7159], et al., of the Institute of Basic Medicine, Academy of Military Medical Sciences, Beijing]

[Text] HIV-1 gag antigens can be used in diagnosing AIDS and in monitoring progress of HIV-1 infections. A segment of HIV-1 gag gene (encoding 207th to 331st residues of gag protein) was amplified by PCR method in vitro, and cloned into the *E. coli* expressive vector pEx31. The insert resulted in high level expression of the recombinant gag containing protein, MS2-gag2. This product could be partially purified to 85 percent by simple inclusion bodies centrifugation. ELISA indicated that the expressive MS2-gag2 protein could be recognized by the specific antibody in AIDS patients' serum.

A Core Gene of Hepatitis C Virus Expressed in *E. coli*

40091012C Beijing ZHONGHUA WEISHENGWUXUE HE MIANYIXUE ZAZHI [CHINESE JOURNAL OF MICROBIOLOGY AND IMMUNOLOGY] in Chinese Vol 12 No 1, Feb 92 pp 9-11

[English abstract of article by Wang Yu [3076 1342], Tao Qinin [7118 0366 2404], et al., of the Institute of Hepatology, People's Hospital, Beijing Medical University]

[Text] The putative core gene of hepatitis C virus was expressed in *E. Coli.* A fusion polypeptide of phage T_7 gene 10 leader peptidecore peptide of HCV was shown to be expected size, 48kD. Western blotting with the *E. coli* lysate showed strong reaction with HCV positive sera. Thus, this fusion protein should be useful in an enzyme-immunoassay for anti-HCV.

Study of AHC Viruses on Pathogenicity in Suckling Mice and Cellular Sensitivity

40091012D Beijing ZHONGHUA WEISHENGWUXUE HE MIANYIXUE ZAZHI [CHINESE JOURNAL OF MICROBIOLOGY AND IMMUNOLOGY] in Chinese Vol 12 No 1, Feb 92 pp 12-15

[English abstract of article by Li Lina [2621 7787 1226], Mu Guifan [3092 2710 5672], et al., of the Department of Microbiology and Immunology, Institute of Basic Medical Sciences, Chinese Academy of Medical Sciences]

[Text] The pathogenicity in suckling mice, replication at 33°C and cellular sensitivity of AHC (acute hemorrhagic conjunctivitis) viruses were studied. The results showed 1) CA_{24v} could be divided into two subtypes, 70 morbid and non-morbid to suckling mice, and all of E_{v70} were non-morbid. 2) Both E_v and CA_{24v} could grow well at 33°C. 3) E_{v70} could replicate in non-primate cells; on the other hand, CA_{24v} was first discovered to replicate in some non-primate cells and to produce CPE. Variation of E_{v70} and CA_{24v} in antigenicity as well as in tissue tropism were discussed. It is suggested that the alteration of tissue tropism of AHC viruses may play a role, in course of these two viruses different in origin, antigenicity and genome, causing the clinical identity—AHC.

Effects of Epidemic Hemorrhagic Fever Virus on the Chemiluminescence of Human Mononuclear Leukocytes and Polymorphonuclear Leukocytes

40091012E Beijing ZHONGHUA WEISHENGWUXUE HE MIANYIXUE ZAZHI [CHINESE JOURNAL OF MICROBIOLOGY AND IMMUNOLOGY] in Chinese Vol 12 No 1, Feb 92 pp 16-19

[English abstract of article by Zhang Xuejun [1728 1331 6511] of the Department of Microbiology, Anhui Medical University, Hefei]

[Text] Luminol-dependent cellular chemiluminescence responses were measured after the interactions of the epidemic hemorrhagic fever virus (EHFV) with normal human mononuclear leukocytes (MNL) and polymorphonuclear leukocytes (PMN). The results showed that EHFV alone induced mononuclear leukocytes chemiluminescence (MNL-CL), but failed to induce polymorphonuclear leukocytes chemiluminescence (PMN-CL). It was considered that human MNL might possess cell membrane receptors for EHFV. After EHFV or inactivated EHFV were incubated with human MNL and PMN for 25 minutes, EHFV depressed the Con A-induced MNL-CL and opsonized zymosan-induced PMN-CL, while inactivated EHFV also depressed opsonized zymosan-induced PMN-CL but failed to inhibit Con A-induced MNL-CL. It is suggested that after the interactions between EHFV and MNL or PMN, EHFV inhibited or impaired the activity of oxidative metabolism and generation of oxygen radicals in human MNL and PMN.

Preliminary Research on the Shigella Flexneri 2a Membrane Antigens Purified by Affinity Chromatography With Monoclonal Antibodies

40091012F Beijing ZHONGHUA WEISHENGWUXUE HE MIANYIXUE ZAZHI [CHINESE JOURNAL OF MICROBIOLOGY AND IMMUNOLOGY] in Chinese Vol 12 No 1, Feb 92 pp 20-24

[English abstract of article by Li Hong [2621 4767], Zhou Jiamin [0719 0163 2404], et al., of the Institute of Microbiology and Epidemiology, Academy of Military Medical Sciences, Beijing]

[Text] It was reported that the membrane antigens of Shigella flexneri 2a were purified by affinity chromatography with monoclonal antibodies (2E6 and 4F1). The results indicated that the purified antigens eluted from McAb 2E6 and 4F1 affinity columns were lipopolysaccharide-protein complexes, in which the molecular weights of three main proteins were 67k, 51k and 22k, respectively. Mouse active immunoprotection tests

showed that the lipopolysaccharides in the purified antigens played a key role in protecting mice from challenge with homologous virulent bacterial strain.

Extracting and Characterizing Luciferase From Photobacterium Phosphoreum (T_3)

40091012G Beijing ZHONGHUA WEISHENGWUXUE HE MIANYIXUE ZAZHI [CHINESE JOURNAL OF MICROBIOLOGY AND IMMUNOLOGY] in Chinese Vol 12 No 1, Feb 92 pp 25-28

[English abstract of article by Luo Jianhui [5012 1696 6540], Chen Tianshou [7115 1131 1108], et al., of the National Institute for the Control of Pharmaceutical and Biological Products]

[Text] Photobacterium phosphoreum (T_3) is chosen as the strain for extracting luciferase. Roughly extracted luciferase is obtained by removing debris of broken-down cell after centrifugation. Luciferase is partly purified through DEAE-cellulose DE_{52} and DEAE-sephadex A_{50} chromatography. In the experiment, luciferase recovery rate is 30.8 percent, luciferase specific activity is 293582 counts/s/mg, which increases 35.2 folds comparing with stable at 1°C -18°C, decreases activity when temperature is above 18°C. Luminescent spectrum analysis shows that the in vitro photospectrum induced by extracted luciferase is the same as that of the living photobacterium phosphoreum.

Study on the Binding Characteristics of the Neurotoxins From *Ophiophagus hannah* Venom to the Nicotinic Acetylcholine Receptor

40091012H Shanghai SHENGWUHUXUE YU SHENGWUWULI XUEBAO [ACTA BIOCHIMICA et BIOPHYSICA SINICA] in Chinese Vol 24 No 1, Jan 92 pp 14-21

[English abstract of article by Liu Jingfang [0491 7234 5364] and Chen Lijun [7115 7787 4596] of the Shanghai Institute of Physiology, Academia Sinica]

[Text] Four neurotoxins, i.e. *O. hannah* neurotoxins V, VII, VIII and X, were isolated and purified from the venom of *O. hannah.* All the neurotoxins showed a single band on polyacrylamide gel electrophoresis (PAGE). The molecular weights of *O. hannah* neurotoxins V, VII, VIII and X were estimated to be 7800, 6700, 8400 and 8000 respectively by SDS-PAGE. The four were identified to be postsynaptic neurotoxins by blocking the transmission in chick biventer cervicis nerve-muscle preparation.

The binding characteristics of *O. hannah* neurotoxins VII and VIII to nicotinic acetylcholine receptor (nAChR) from the electric organ of *Narcine maculata* were studied by competitive inhibition experiment. The result showed that both *O. hannah* neurotoxins VII and VIII competed for the same binding site on the nAChR with cobrotoxin. Equilibrium inhibition constants (K_1) of *O. hannah* neurotoxins VII and VIII were separately 3.5×10^{-7} M and 2.1×10^{-7} M. The affinities of *O. hannah* neurotoxins VII, VIII and cobrotoxin to the nAChR were the same.

Studies on Tissue Schizonticide of Malaria Parasite: Synthesis of 2-Substituted Benzyloxy (or Methoxy)-5-Substituted Phenoxy Analogues of Primaquine

40091012I Beijing YAOXUE XUEBAO [ACTA PHARMACEUTICA SINICA] in Chinese Vol 26 No 12, Dec 91 pp 895-901

[English abstract of article by Zheng Xianyu [6774 6343 5148], Chen Chang [7115 2490], et al., of the Institute of Parasitic Diseases, Chinese Academy of Preventive Medicine, Shanghai 200025]

[Text] 2-Chloro-6-methoxy-8-nitroquinoline was reacted with substituted benzyl alcohols (or sodium methanol) and then brominated to give 2-substituted benzyloxy-6-methoxy- and 2,6-dimethoxy-5-bromo-8-nitroquinolines (compounds 5-8 in Table 1). These products were condensed with substituted phenols to form corresponding 5-substituted phenoxy compounds (9-19 in Tables 1 and 2) which were subsequently reduced to afford 2-substituted benzyloxy-6-methoxy- and 2,6-dimethoxy-5-substituted phenoxy-8-aminoquinolines (20-28, 47 and 48 in Tables 3 and 6). Condensation with 4-bromophthalimidopentane yielded corresponding 8-(4-phthalimido-1-methylbutyl)aminoquinolines (29-37, 49 and 50 in Tables 4 and 6) which were subsequently treated with hydrazine hydrate to give 2-substituted benzyloxy-6-methoxy- and 2,6-dimethoxy-5-substituted phenoxy-8-(4-amino-1-methylbutyl)amino-quinolines, compounds III and IV (38-46, 51 and 52 in Tables 5 and 6), the analogues of primaquine.

Compounds III and IV were tested against *Plasmodium yoenii* in mice infected with sporozoites. The parasitaemia of 80 percent and 90 percent of tested mice was negative at an oral single dose of 100 mg/kg of compounds 39 and 45, respectively. The results of further studies on compound 45 showed that the parasitaemia of 80 percent of mice was negative at a single dose of 20 mg/kg, and the acute toxicity in mice was less than that of primaquine.

Synthesis and Analgesic Activity of Analogs of U-50488, an Opiate Kappa-Agonist

40091012J Beijing YAOXUE XUEBAO [ACTA PHARMACEUTICA SINICA] in Chinese Vol 26 No 12, Dec 91 pp 902-905

[English abstract of article by Ma Sicai [7456 2448 2088] and Yang Yulong [2799 3768 7893] of the Institute of Materia Medical of General Hospital of Nanjing 210002; and Yuan Xiaomei [5913 1420 1188] of the Institute of Medicinal Chemistry, PLA]

[Text] This paper reports the synthesis and analgesic activities in mouse hot plate test and writhing test of

some analogs of U-50488, a *K*-agonist. Results showed that compounds in which the amino group was pyrrolinyl had higher *K*-agonist activity and the substitution of two chlorine atoms in 3 and 4-positions of the benzene nucleus was very important to *K*-activity. Furthermore, all of compounds in which the amino group was piperidyl, piperazinyl or morpholinyl exhibited very weak *K*-agonist activity.

Neural Network Research, Applications Reported

Speech Recognition Studied

92P60267A Beijing JISUANJI SHIJIE [CHINA COMPUTERWORLD] in Chinese No 13, 1 Apr 92 pp 7,9

[Article by Wu Wenhu [0702 2429 5706] of the Computer Department, Qinghua University: "Present State, Future of Chinese Speech Recognition"]

[Excerpt] [Passage omitted] A weak point of neural network models is sequential differences. Using neural networks to build sequentially strong speech-signal recognition models can be quite troublesome. Some researchers have proposed the time delay neural network (TDNN), which cannot make up for all [sequential] differences. The highest degrees of accuracy in domestic application of TDNN models are over 90 percent for initial consonant recognition, 95 percent for vowel recognition (including recognition of vowel syllables ending in n and ng), 98 percent for recognition of the four tones, and 98 percent for recognition of short word lists and individual words. [passage omitted]

Two New Simulation Systems Developed

92P60267B Beijing ZHONGGUO DIANZI BAO [CHINA ELECTRONICS NEWS] in Chinese 15 Apr 92 p 1

[Article by Tan Guoping [6151 0948 1627]: "New Achievements in Nation's Research on Intelligent Computers: China University of Science & Technology's 'General-Purpose Parallel Neural-Network Simulation System' and 'Special-Purpose-Processor-Based Neural-Network Simulation System' Projects Pass State Appraisal"]

[Summary] A State 863 Plan priority research Project assigned to China University of Science & Technology (CUST) and entitled "System Structure for Neural Information Processing Support, Its Software Support Environment" passed the formal appraisal organized by the State S&T Commission in Hefei on 8 April. CUST, one of the first domestic institutions to study neural networks, accepted the 863 Plan task in July 1990, and had already made certain breakthroughs before the project was completed. The now-completed project includes development of two new neural-net simulation systems: the "general-purpose parallel neural-network simulation system (GP2N2S2)" perfected by researchers in CUST's Computer Department and the "special-purpose-processor-based neural-network simulation system (SP2N2S2)" perfected by researchers in CUST's Electronic Technology Section. GP2N2S2, designed to provide a research environment and applications tool, has up to 12,000 simulation nodes permitting over 300,000 connections and a connection update speed of 100,000 IPS [instructions per second]. SP2N2S2, tracking the worldwide state-of-the-art, consists of hardware based on special-purpose processors (DSP chips) and a corresponding software support environment.

Radar Multitarget Tracking Studied

92P60267C Beijing DIANZI XUEBAO [ACTA ELECTRONICA SINICA] in Chinese Vol 20 No 4, Apr 92 pp 45-49

[Article by Yu Shaobo [0151 1421 3134] and Liu Mengren [0491 1322 0088] of the Department of Computer Science, Naval Academy of Engineering, Wuhan 430033, and Hu Shouren [5170 1343 0088] of the Department of Computer Science, National Defense University of Science & Technology (Changsha Institute of Technology), Changsha 410073: "Neural-Network Approach for Radar Multitarget Tracking"; MS received Mar 90, revised Apr 91]

[Abstract] A neural-network method for radar multitarget tracking is proposed and simulation results given. Advantages and disadvantages of the new approach are considered.

The method is based on an Interpolative Probability Field (IPF) network, which is an organic synthesis of Grossberg's Boundary Contour System (BCS)[5] and descriptive target probabilistic dynamic characteristics (i.e. information describing the possibility of target motion). The BCS model uses a competitive learning algorithm and can use differential equations for description. The competitive learning algorithm essentially suppresses the number of adjacent processing elements (PEs) until only one PE is left active; this PE represents the current target track point. The BCS model is shown schematically in Figure 2 below, while Figure 1 depicts the probabilistic distribution of target motion.

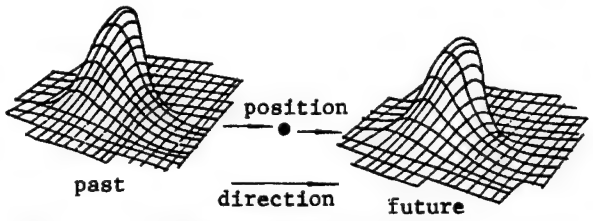

Figure 1. Probabilistic Distribution of Target Motion

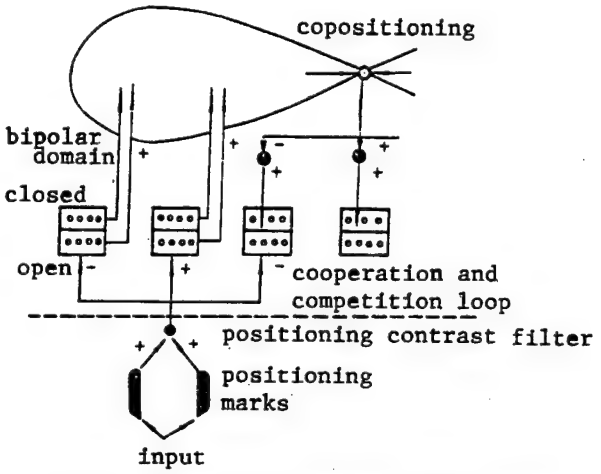

Figure 2. Hierarchial Structure of BCS Model

Figure 3 shows results of a simulated IPF network applied to simultaneous tracking of two targets; after 120 samples, the target track is clearly displayed. Figure 4 shows results of such a simulation with 15 simultaneous targets and 16, 40, 80, and 200 time samples. Figure 5 reveals one of the problems with the method. If the number of time samples is insufficiently large, a false track can be generated; the bottom left part shows a 100-sample recursive plot, incorrectly suggesting two semicircular tracks, while the bottom right part shows a 200-sample recursive plot, correctly suggesting two mutually perpendicular tracks.

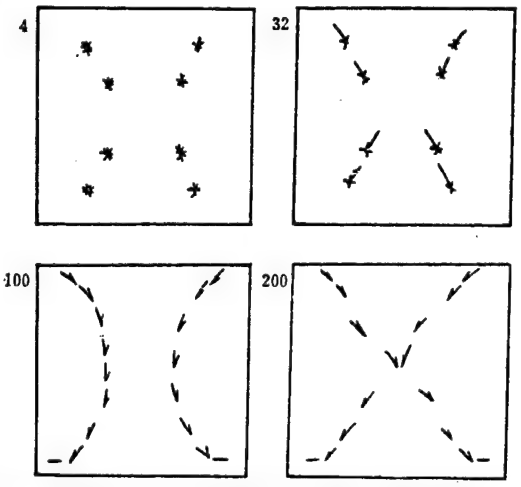

Figure 5. Processing of Delayed Data (Two Targets)

One of the major problems with implementing a neural-net-based radar multitarget tracking system is the huge number of PEs required. This number is based on the tracking accuracy required and the size of the spatial volume to be covered. Table 1 gives examples for two spatial volumes, each with five degrees of accuracy. If volume is reduced to 20 km x 40 km x 20 km (final figure represents altitude here and in table), the number of PEs required varies from 8.2×10^6 to 4096×10^6. A further implementation problem is operating speed: to develop a real-time system with so many PEs would be very difficult with current software simulation technology; it would be preferable to employ neural-net chips or optical neurocomputer technology. Related to this second problem is insufficient knowledge of the higher-layer characteristics of

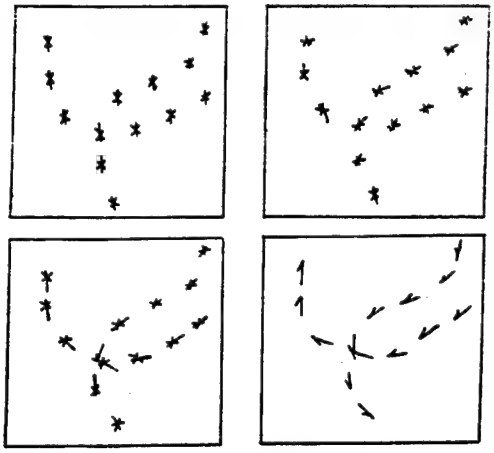

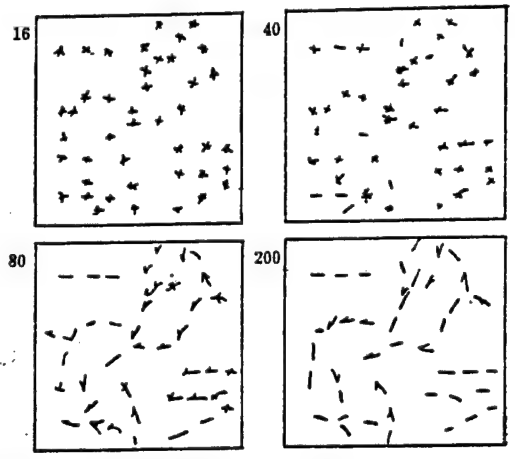

Figure 3. (left) Track of Two Targets; Figure 4. (right) Track of 15 Targets

generic systems combining modules common to both the IPF network and other neural-net models. Such a general scheme is presented in Figure 6 below, in which MP is a monocular preprocessor, FCS is a feature contour system, and ORS is an object recognition system. A third major problem is the inherent characteristics of the IPF network, such as anti-jamming ability and redundancy/fault-tolerance, subjects which require more research.

Table 1. Volume of Coverage, Accuracy, and Neural-Net Scale

Volume of coverage (km)	Accuracy (m)	No. of PEs	Volume of coverage (km)	Accuracy (m)	No. of PEs
40 x 40 x 20	$(100)^3$	$32 \times 32 \times 10^6$	80 x 80 x 20	$(100)^3$	$128 \times 32 \times 10^6$
	$(200)^3$	$4 \times 32 \times 10^6$		$(200)^3$	$128 \times 4 \times 10^6$
	$(300)^3$	$1.18 \times 32 \times 10^6$		$(300)^3$	$128 \times 1.18 \times 10^6$
	$(400)^3$	$0.5 \times 32 \times 10^6$		$(400)^3$	$128 \times 0.5 \times 10^6$
	$(500)^3$	8.2×10^6		$(500)^3$	$1.02 \times 32 \times 10^6$

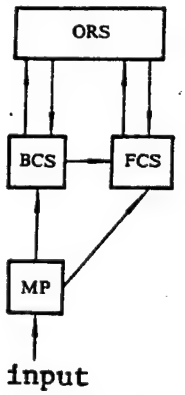

Figure 6. Expansion of IPF Network

References

[1] Hu Shouren and Yu Shaobo: "Guide to Neural Network Systems," National Defense University of S&T Publishing House, 1990, Changsha.

[2] Yu Shaobo and Liu Mengren: "Applications of Neural Networks," HAIGONG XUEBAO [JOURNAL OF THE NAVAL ACADEMY OF ENGINEERING], Vol 13 No 2, pp 47-51, 1990, 2.

[3] Yu Shaobo and Hu Shouren: "Capabilities of Neural Networks," HAIGONG XUEBAO, Vol 13 No 1, pp 34-37, 1990,3.

[4] Hu Shouren and Yu Shaobo: "Artificial Intelligence and Neural Networks," JISUANJI KEXUE [COMPUTER SCIENCE], Vol 14 No 2, pp 51-53, 1990, 4.

[5] Grossberg, S. and Mingolla, E.: "Neural Dynamics of Surface Perception: Boundary Webs, Illuminants, and Shape-from-Shading," COMPUTER VISION, GRAPHICS, AND IMAGE PROCESSING, 37, pp 116-165, 1987.

[6] DARPA Neural Network Study, Final Report, 1989, 3, 22.

Five Firms in Sino-U.S.-Hong Kong Workstation Joint Venture

92P60236A Beijing JISUANJI SHIJIE [CHINA COMPUTERWORLD] in Chinese No 14, 8 Apr 92 p 3

[Article by Yu Shusen [0060 2885 2773]: "Five Chinese, U.S., Hong Kong Firms Form Huaqi Corp."]

[Summary] Yunnan Electronic Equipment Plant, the U.S. firm SGI [Silicon Graphics] Electronic Computer Corp., the Hong Kong firm Tiangao [1131 7559] International Ltd., Asia Simulation Systems Control Ltd., and the Nanshan Investment Management Co. (subordinate to the Shenzhen Nanshan district government) have jointly founded the Huaqi [5478 1142] Corporation, the Letter of Intent for which was signed on 8 March in Kunming. SGI will provide a complete set of new-technology equipment for producing its IRIS Indigo vision processing workstation, Yunnan Electronic Equipment Plant will be responsible for manufacturing and sales, Tiangao International Ltd. will be responsible for software support, and Asia Simulation Systems Control Ltd. will provide marketing support for the new joint venture, to be located in Nanshan district. Gross investment for the Huaqi Corp.—a five-way joint-venture high-tech enterprise economic entity with excellent complementary strengths—is US$3.28 million, of which Nantian [as published; probably typo for Nanshan] will put up 48 percent.

The IRIS Indigo workstation, which has a 133 Mbytes/s data transmission rate and a high-speed CPU, is ideal for three-dimensional graphics processing—especially visual simulation—in a variety of fields, such as machinery design, geographical information, urban planning, architecture, artistic graphics, earth sciences, flow dynamics, and industrial control. After the joint venture is implemented, its products will be sold on the domestic and international markets.

Automatic Handwritten-Chinese-Character Recognition System on Market

92P60219B Beijing ZHONGGUO DIANZI BAO [CHINA ELECTRONICS NEWS] in Chinese 18 Mar 92 p 2

[Article by Zhang Jingan [1728 2417 1344]: "Automatic Handwritten-Chinese-Character Recognition System Put on Market"]

[Summary] The Beijing University Computer Institute recently decided to formally market the automatic handwritten-Chinese-character recognition system developed by a research team led by institute professor Gu Xiaofeng [7357 1420 7685]. The institute began its research on automatic handwritten-Chinese-character recognition technology in 1986, and a prototype system passed ministry-level appraisal in July 1990. This earlier system's recognition accuracy (via computer learning) was about 80 percent, accuracy without learning was about 70 percent, and recognition speed was about 1.67 seconds/character. Now, after a year and a half spent on improving the prototype, the system's recognition speed has been improved by over 100 percent—to 0.8 second/character (or about 2,000 characters per half hour, including computer learning), and average recognition accuracy has been improved 10 percentage points. Tested at the institute with characters written by institute personnel, the system demonstrated a 97.5 percent accuracy including computer learning. Tested with characters written by this reporter, the system had a first-time accuracy (not including computer learning) of 63 percent. The system runs on an IBM PC or compatible microcomputer (MSDOS or PCDOS3.0 operating system) and requires a scanner.

Domestically Developed Switchable Packet Assembler/Disassembler Certified

92P60219E Beijing JISUANJI SHIJIE [CHINA COMPUTERWORLD] in Chinese No 13, 1 Apr 92 p 2

[Article by Xiao Yan [2556 3601]: "China's Independently Developed Switchable PAD To Be Widely Used in Packet Switching Networks"]

[Summary] The switchable packet assembler/disassembler (SPAD) developed by MPT's Data Communications Technology Institute recently passed the technical appraisal held by a number of organizations. The SPAD is one of the primary pieces of equipment used in the nation's public packet switching network, and is designed to assemble data packets received from a certain number of asynchronous terminals. It uses the internationally known X.25 protocol via one or more synchronous interfaces to send these packets out into the packet switching network. Also, it disassembles the data packets received from the packet switching network and sends them to the proper asynchronous user terminals. The SPAD can be used in provincial packet switching networks and private networks as well as in the public network, and can replace imported equipment. It is understood that foreign PADs have 8-16 ports, but this independently developed SPAD has 24 ports, and has switching functions as well. Such a product cannot be found overseas. Even comparing it to non-switching foreign-made PADs, it has a superior performance-to-cost ratio: each of the SPAD ports has a price only one-seventh that of a foreign-made PAD port. In terms of performance, the experts agreed that this SPAD meets late-eighties international standards.

Military Electronics Chassis/Rack-and-Panel CAD System Developed

92P60219C Beijing ZHONGGUO DIANZI BAO [CHINA ELECTRONICS NEWS] in Chinese 20 Mar 92 p 3

[Article by Jin [6855]: "Military Electronics Chassis, Rack-and-Panel CAD System Developed"]

[Summary] In order to raise design standards for chassis and rack-and-panel equipment in the nation's electronics industry, MMEI's Technology Institute [i.e., Institute 2] has developed a military electronics chassis/rack-and-panel CAD system, which was formally certified on 7 March in Taiyuan. Functionally, this software has four subsystems: general-purpose chassis design, special-purpose chassis design, front panel design, and color design. Software design technology works under the AUTOCAD10.0 graphics environment, with FORTRAN, TURBO-Pascal, and AUTOLISP languages accepted. A 286, 386, or 486 microcomputer is the system's operating environment.

Military Electronics Overall System CAD Technology Certified

92P60219F Beijing ZHONGGUO DIANZI BAO [CHINA ELECTRONICS NEWS] in Chinese 3 Apr 92 p 3

[Article by Ke Ren [0668 0086]: "Overall Structure CAD Technology Research Passes Appraisal"]

[Summary] The "military electronics overall system CAD technology research" joint project of MMEI's Institute 14 and Xidian University passed the technical appraisal held a few days ago in Nanjing. This 3-year project has resulted in the development of the EMS CAD software system, which runs UNIX on an SGI or Apollo workstation, and is oriented to overall electromechanical system design of three-dimensional structures—especially of military equipment such as radar antenna structures, chassis and racks and panels, and antenna mountings. The appraisal experts noted that the system meets 1980's international standards.

Jiangnan Plant To Invest 40 Million Yuan in Disk-Drive Production Technology

92P60219A Beijing JISUANJI SHIJIE [CHINA COMPUTERWORLD] in Chinese No 11, 18 Mar 92 p 1

[Article by Zhou Shuaixiang [0719 1596 3276]: "40 Million Yuan Invested To Accelerate Disk-Drive Production Technology Transformation"]

[Summary] In order to adapt to market changes, the state-run Jiangnan (JN) Machinery Plant during the Eighth 5-Year Plan will invest over 40 million RMB in new production-line equipment for manufacture of disk drives. The new equipment will permit JN to increase its annual capacity to 500,000 3.5-inch floppy disk drives and 50,000 3.5-inch Winchester disk drives, which should meet the demand for such disk drives in microcomputers. JN's present annual capacity, based on production lines imported from France, Japan, and the United States, is 50,000 drives, and its domestic market share is 60 percent. JN will combine a State Technology Transformation special-project loan with self-raised funds to cover the investment. In addition to this investment in 3.5-inch disk-drive production technology, JN is also considering plans to develop even smaller new products: a 2-inch floppy disk drive and a 2.5-inch Winchester disk drive.

Domestically Developed 130-mm Winchester Disk Drive, Controller Design Finalized

92P60219D Beijing JISUANJI SHIJIE [CHINA COMPUTERWORLD] in Chinese No 13, 1 Apr 92 p 1

[Article by Wan Qi [8001 3823]: "Domestic 130-mm Winchester Disk Drive and Controller Pass Design Finalization"]

[Summary] The "ZPC-30 Winchester disk drive (WDD) and KWT-521 ESDI [enhanced small device interface] interface Winchester disk controller development and domestic manufacturing technology" key State Seventh 5-Year Plan S&T project passed the design finalization conducted a few days ago in Hangzhou by MMEI's Computer Department. Jointly developed by MMEI's Hangzhou Institute 52 and State-Run Plant 4509, the model ZPC-30 130-mm half-height WDD, with a non-formatted capacity of 106 MB, has an ESDI, a data transmission rate of 10 Mbps, an average track access time of 19 ms, and a 3,600 rpm rotation speed, meeting mid-to-late-eighties international standards. The ZPC-30 is an ideal external storage device for a 386-class microcomputer or workstation. Much independent work went into the overall system design, including design of the ASICs, application of surface mount technology, and development of the ESDI technology. The model KWT-521 ESDI Winchester disk controller in a microcomputer with an AT-BUS (ISA) bus can connect two high-bit-rate (10-15 Mbps) ESDI high-capacity (up to 670 MB non-formatted) WDDs.

State-of-the-Art Intelligent Programmable Regulator Unveiled

92P60234A Beijing ZHONGGUO DIANZI BAO [CHINA ELECTRONICS NEWS] in Chinese 6 Apr 92 p 3

[Article by Hu Hanjun [5170 3352 6511]: "Domestic Human-Like Intelligent Programmable Regulator at Advanced World Level"]

[Summary] The joint development of the FZK human-like intelligent programmable regulator by Qinghua University's Department of Automation and Hubei Province's Yichang [1355 2490] Municipal Radio Plant indicates that the nation's artificial intelligence and control research has reached a world-class level. This regulator, whose development was initiated in July 1988 out of environmental protection requirements, is used in a cyclic vulcanization bed [xunhuan liuhua chuang] boiler, incorporates the MCS-51-series single-chip computers, and has a modularized (40 different modules) design. The FZK regulator can be used for automated control of industrial processes in a variety of fields—such as machinery, chemical engineering, metallurgy, electric power, food products, and defense—and has a price only one-third that of the advanced KMM imported instrument. Recently, representatives of the U.S. firm Systems Control Co. expressed to the Yichang plant an interest in jointly utilizing this advanced equipment in industrial control systems.

Hybrid Electro-Optical Real-Time Pattern Recognition System Tested

92FE0388A Shanghai HONGWAI YU HAOMIBO XUEBAO [JOURNAL OF INFRARED AND MILLIMETER WAVES] in Chinese Vol 10 No 6, Dec 91 pp 465-473

[Article by Wang Ruli [3769 3067 4567] and Hua Tiejun [5478 6993 0971] of the Shanghai Institute of Technical Physics, Chinese Academy of Sciences, Shanghai 200083: "Hybrid Electro-Optical Real-Time Pattern Recognition"; MS received 6 Sep 91]

[Text] **Abstract**

In this article, a hybrid electro-optical real-time pattern recognition system is introduced. Preliminary experimental results show that this system can perform the functions of high-speed automatic target classification, model discrimination and rotation-invariant pattern recognition.

1. Introduction

The last decade of the 20th Century will be an era of high-level artificial intelligence information systems; current research in computers which emulate the activities of the human brain such as learning, self-organization, and self-association is expected to accelerate the arrival of a global technological revolution. Typical examples of this research include optical computers and neural-network computers.

The technologies of optical computing and artificial neural-network computing have the capabilities of real-time parallel processing of two-dimensional information and fuzzy information. However, various technical difficulties still exist with these technologies; they are not ready for practical implementation. Recently, a technological breakthrough has been made to use hybrid electro-optical techniques for real-time pattern recognition and for processing fuzzy or distorted information. This breakthrough has attracted worldwide attention because of its far-reaching effect on the modernization of military and space technologies and its important role in the development of one of the artificial-intelligence products—artificial vision.

In recent years, China has also been actively engaged in the study of this advanced topic of information science, and has obtained some preliminary results. For example, a prototype of a hybrid electro-optical pattern recognizer has been successfully developed and laboratory tests of automatic target discrimination techniques have been conducted. This article gives a description of the structural design of this system and of the optical correlator, and presents the test results of certain applications of the system.

2. Structural Design of the System

2.1 System Block Diagram

As shown in Figure 1, the hybrid electro-optical real-time pattern recognition system consists of three major segments: the image generation and data collection segment, the optical image processing and computer discrimination segment, and the display segment.

The operating procedure of the system is as follows: first, a CCD camera is used to obtain binary images or image data streams (which may be collected by visible or infrared sensors, radars, lasers or sonars); the image data are transmitted via the CRT-LCLV (liquid-crystal light valve) to the optical correlator, where target discrimination is performed using the optical 4f correlation system; the correlation peak, which is the output of the target

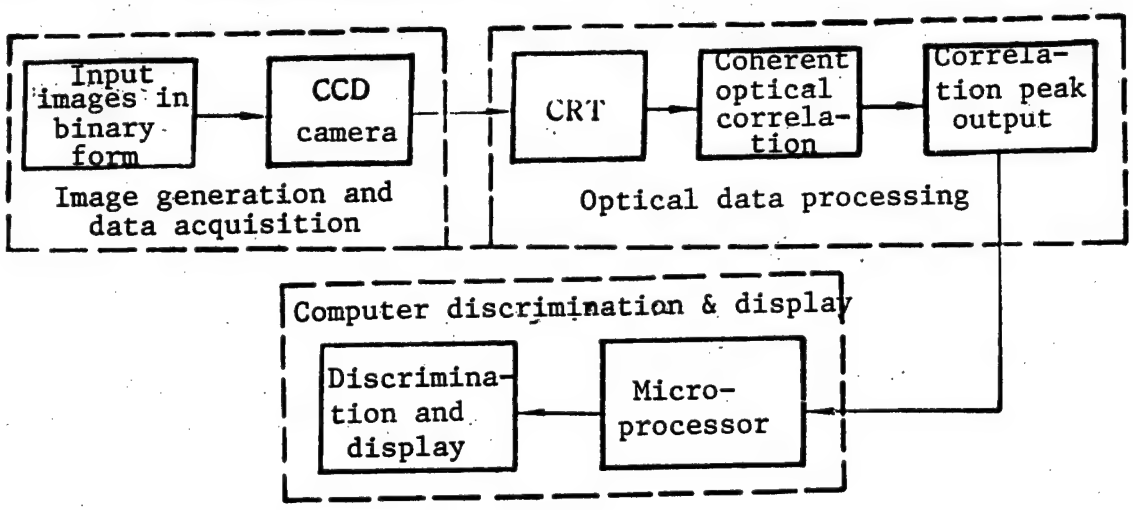

Figure 1. System Block Diagram of a Hybrid Electro-Optical Processing System Capable of Real-Time Target Discrimination

discriminator, is captured by another small CCD camera, and is transmitted to a microprocessor (PC 386) via a video acquisition circuit; finally, the microprocessor produces a real-time display of the target and the associated information such as its configuration, name and the distribution of correlation peaks.

2.2 Key Technologies and Technical Performance

Figure 2 [not reproduced] shows a photograph of the hybrid electro-optical real-time pattern recognition system; the arrow in the photograph points to the coherent optical correlator. The system has incorporated the following key technologies:

(1) Development of a three-dimensional distortion-free phase-only hologram matched filter based on the theory of geometric three-dimensional model (GTDM) pattern-recognition method.

(2) Establishment of a new hybrid technical approach based on digital computer simulation and quasi-physical simulation; this new approach reduces the development cycle of the matched filter and improves the accuracy of pattern recognition.

(3) Application of new techniques in optical electronics and artificial neural networks for the development of components and devices such as the silicon-base liquid crystal light valve (Si-LCLV) and the electronic artificial neural-network angular discriminator.

The technical performance parameters of the hybrid electro-optical real-time pattern recognition system are given in Table 1.

Table 1. Technical Performance Parameters of the Hybrid Electro-Optical Real-Time Pattern Recognition System

Dimensions of optical correlator (cm^3)	76 x 31 x 33
Spatial light modulator (SLM)	Liquid-crystal light valve (LCLV)
Response time (ms)	Si-LCLV: about 30 Cds-LCLV: about 100
Matched filter	Multiple phase-only matched filters, rotation-invariant matched filter, GTDM filter
Number of discriminated targets (single matched filter)	8

3. Optical Correlator

3.1 Basic Principle

This article will discuss only the problem of signal processing in the frequency domain under coherent-light illumination. The coherent optical processing system shown in Figure 3 has a linear amplitude response; hence one can write:

$$I(x_3, y_3) = K\left|\int_{-\infty}^{+\infty} g(\xi, \eta)h(x_3-\xi, y_3-\eta)\,d\xi\,d\eta\right|^2; \quad (1)$$

where I is the light intensity distribution, g is the input function, and h is the artificial impulse function.

The computational procedure is as follows: first, the monochromatic light generated by the laser passes through the spatial filter/beam spreader and the collimation lens (L_1) to form a parallel light beam which illuminates the input object plane (P_1); by placing the image to be processed in the P_1 plane and passing the light beam through the Fourier transform lens L_2, an amplitude distribution function $K_1G(x_2/\lambda f, y_2/\lambda f)$ is formed on the spectral plane (P_2). Clearly, G is the Fourier transform or the frequency spectrum of g. K_1 is a complex constant which can be realized by a filter in the P_2 plane to change the amplitude and phase of the spectrum G.

Let H be the Fourier transform of h, then the amplitude transmissivity of the filter in the spectral plane is

$$t(x_2, y_2) = K_2H(x_2/\lambda f, y_2/\lambda f). \quad (2)$$

Thus, the amplitude distribution behind the filter is proportional to GH and can therefore be transformed into the intensity distribution $I(x_3, y_3)$ on the P_3 plane by an inverse Fourier transform lens (L_3).

In the practical application of optical pattern-recognition systems, generally only the existence and the location of the detected signals are of interest; the fidelity

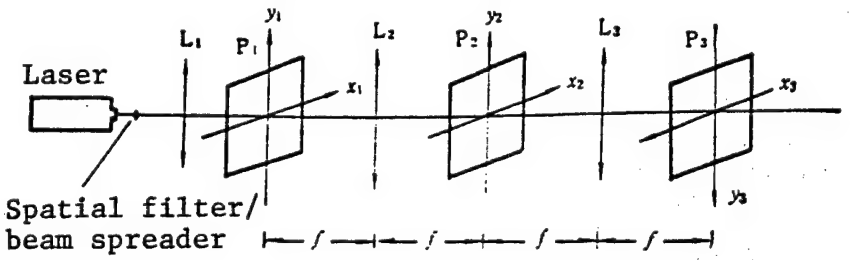

Figure 3. Schematic Diagram of the 4f Coherent Optical Processing System

of the image is of less importance. Therefore, most problems in practice can be solved by using a phase-only matched filter.

Consider a specific signal s(x, y), and consider the impulse response h(x, y) as a spatial-invariant linear filter. If we let

$$h(x, y) = S^*(-x, -y) \qquad (3)$$

then this filter is matched with the signal s(x, y). If a filter matched with s(x, y) is applied to the input image g(x, y), then the output V(x, y) can be written in the form:

$$V(x, y) = \int_{-\infty}^{+\infty}\int g(\xi, \eta)h(x-\xi, y-\eta)d\xi\, d\eta$$

$$= \int_{-\infty}^{+\infty}\int g(\xi, \eta)S^*(\xi-x, \eta-y)d\xi\, d\eta \,. \qquad (4)$$

Clearly, V(x, y) is the cross-correlation function between the input image g(x, y) and the signal s(x, y). When g(x, y) = s(x, y), then V(x, y) proportional to SS^* becomes the autocorrelation function, which will be displayed as a bright spot on the focal plane P_3 behind the lens L_3. Here S = unordered set: s, and the superscript * indicates the complex conjugate.

3.2 Optical Configuration Design and Key Device Functions

3.2.1 Optical Configuration Design

From the point of view of practical considerations, we have chosen a folded optical configuration for the prototype design (see Figure 4). Most of the components, e.g., the He-Ne laser and the CCD camera, are commercially available.

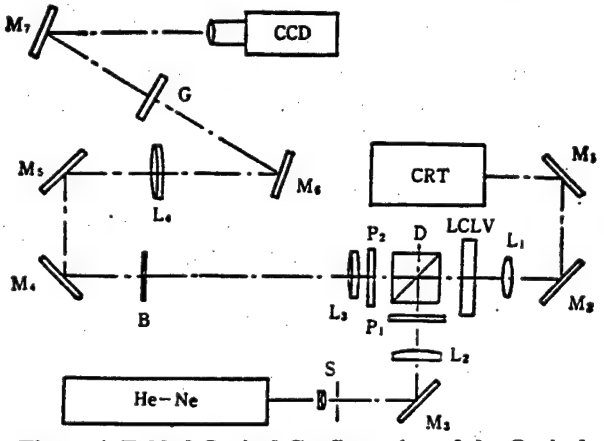

Figure 4. Folded Optical Configuration of the Optical Correlator

M_1-M_7: plane mirrors; L_1: imaging lens group; L_2: collimation lens; L_3, L_4: Fourier transform lenses; S_1: spatial filter/beam spreader; P_1, P_2: polarizers; D: beam splitter; B: matched filter; G: projection screen

3.2.2 Fourier Transform Lens

In this experiment, we use the domestically made Model 300 Fourier lens; its technical specifications are listed in Table 2.

Table 2. Technical Specifications of the Fourier Lens

Focal length (mm)	301.85
Relative aperture	1/10
Maximum diameter of processing area (mm)	30
Maximum diameter of spectral area (mm)	30
Maximum spatial frequency (lp/mm)	78

The point spread function and the MTF [modulation transfer function] curve of this Fourier lens are shown in Figure 5 and Figure 6, respectively.

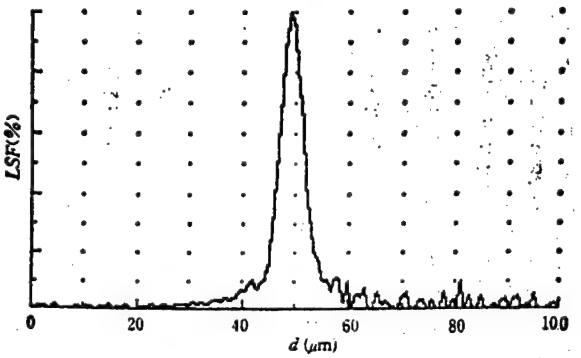

Figure 5. Point Spread Function of Lens

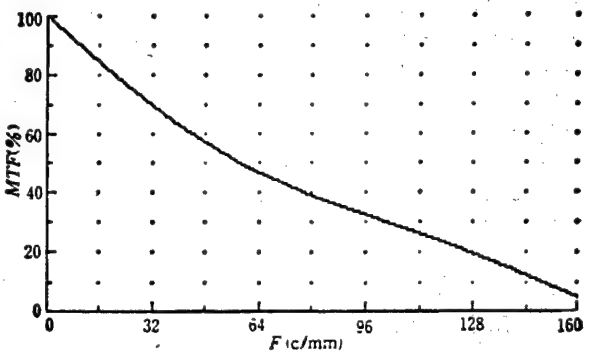

Figure 6. MTF Curve of Lens

3.2.3 Spatial Light Modulator—Liquid Crystal Light Valve (LCLV)

The SLM is an important optical information processing device which converts non-coherent light into coherent light. The devices which are commercially available on the market today such as CdS-LCLV and CdSe-LCLV generally have a response time of approximately 80-100

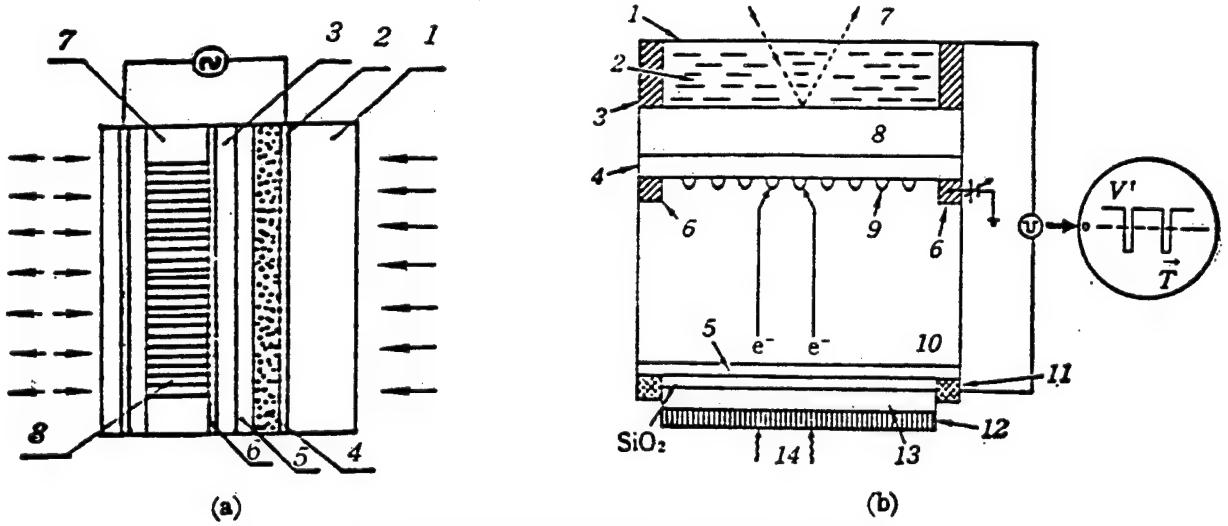

Figure 7. Structure of the Liquid Crystal Light Valve

(a) CdS-LCLV: 1. Glass plate; 2. Transparent electrode; 3. Dielectric mirror; 4. CdS light-sensitive layer; 5. CdTe light-resistant layer; 6. Directional membrane; 7. Spacer; 8. Liquid crystal layer.

(b) Si-LCLV: 1. Transparent electrode; 2. Liquid crystal electro-optical layer; 3. Insulation layer; 4. SiO_2 gate insulator; 5. Thin P^{++} back contact; 6. N rings; 7. Output light beam; 8. Si/SiO dielectric mirror; 9. N micro diodes; 10. π silicon; 11. Aluminum-base thermal contact; 12. Fiber-optic plate; 13. Optical glue; 14. Input light beam.

ms. We have developed two LCLVs, i.e., the CdS-LCLV and the Si-LCLV, whose structures are shown in Figure 7(a) and Figure 7(b) respectively.

3.2.4 Spatial Matched Filter

In 1964, Vander Lugt succeeded in developing an optical spatial matched filter using holographic principles; this new technology contributed to the subsequent rapid development in optical information processing. However, this filter is difficult to realize in practice because of its large search space and its hardware-dependent implementation. Today computer holographic techniques can be used to realize a variety of effective matched filters such as the amplitude-and-phase matched filter, the amplitude-only matched filter and the phase-only matched filter.

In our system, we have used a phase-only composite filter design and a GTDM phase-only filter design. These designs can accommodate 64 matched filters within an area of 1 cm^2; each filter can store nine images, hence 1 cm^2 contains 576 images (see Figure 8).

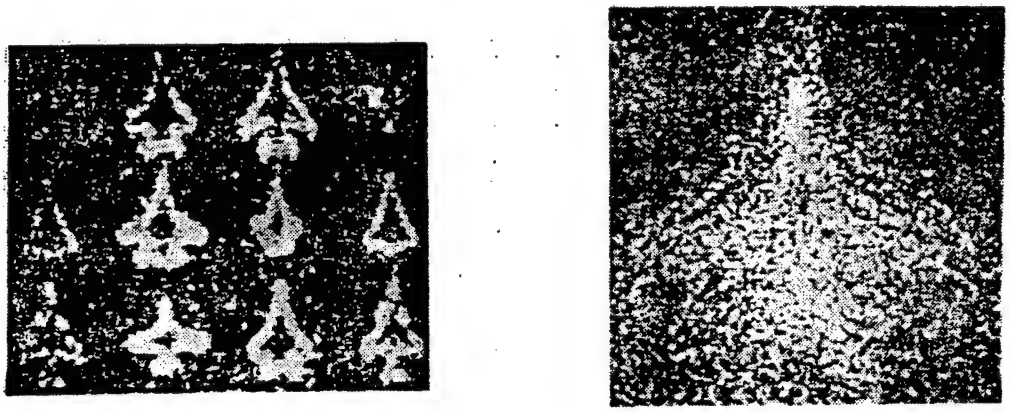

(a) Images produced by using reference-light illumination

(b) Image obtained by phase-only composite filter

Figure 8. Phase-Only Matched Filter for Nine Different Aircraft Models

4. Test Results

4.1 Target Classification

This prototype system can perform real-time discrimination of fighter aircraft, commercial airplanes and missiles (see Figure 9 and Figure 10 [not reproduced]).

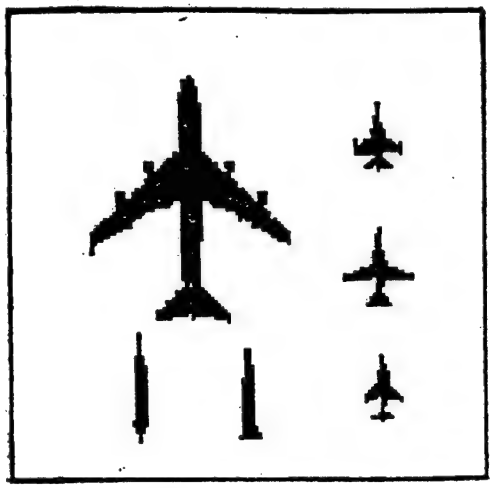

Figure 9. Input Images of a Boeing 747 Airplane, Two Missiles and Three Fighter Aircraft

4.2 Target Model Identification

Figure 11 shows 16 different models of fighter aircraft to be identified; Figure 12 [not reproduced] shows the cross-correlation peaks using a composite phase-only matched filter for automatic identification.

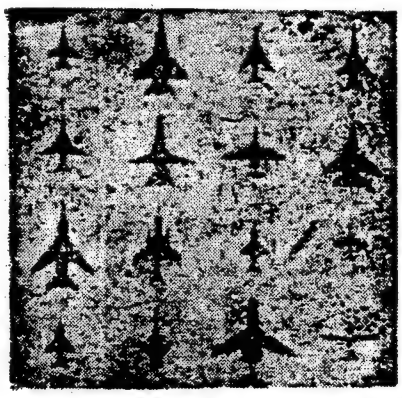

Figure 11. Input Target Signals of 16 Different Fighter Models

4.3 Rotation-Invariant Target Recognition

Because the attitude of an aircraft is subject to instantaneous change with six degrees of freedom, it is important to develop a rotation-invariant matched filter for target recognition. Figure 13 illustrates the correct identification of an F-16C fighter aircraft rotating from 0° to 90° using a GTDM matched filter.

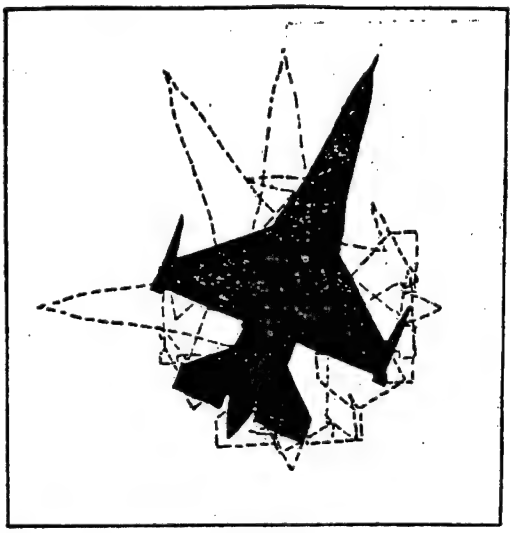

Figure 13. Correct Identification of an F-16C Fighter Aircraft Rotating From 0° to 90° in Two-Dimensional Space

The same GTDM filter can also be used to recognize the target as it rotates from the top view to the side view (see Figure 14). We have also used computer simulation to demonstrate the feasibility of a multi-target rotation-invariant GTDM matched filter.

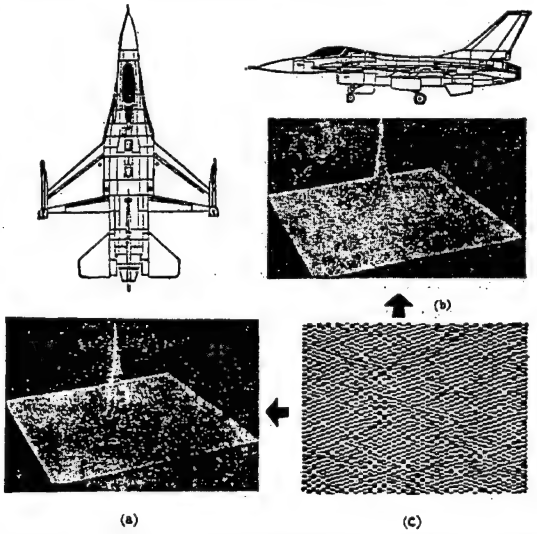

Figure 14. Use of GTDM Filter To Obtain Distinct Correlation Peaks as the Aircraft Rotates From Top View to Side View

(a) Target in top view and correlation peak; (b) Target in side view and correlation peak; (c) Use of GTDM filter to identify target at different rotation angles

5. Conclusion

A hybrid electro-optical real-time pattern recognition system has great potential in automatic target recognition because it combines the advantages of both optics technology and computer technology.

The primary areas of future research will be in system miniaturization, component integration, and improvement in the reliability and fault tolerance of the overall system. In closing, it should be remarked that application of hybrid electro-optical pattern recognition systems can be expanded into other scientific disciplines such as biology and psychology, etc. Such efforts will promote new developments in materials, components and systems.

Domestic Development of IR Devices Analyzed

92P60214A Beijing ZHONGGUO HANGTIAN [AEROSPACE CHINA] in Chinese No 3, Mar 92 pp 41-45

[Article by Liu Jintian [0491 6930 3240] of the Beijing Institute of Remote Sensing Equipment: "Worldwide Infrared Device Development Trends"]

[Excerpts] Abstract: The role and position of infrared (IR) devices in weapon systems is outlined and the worldwide development status of IR technology is detailed. [Passage omitted]

III. Status of IR Devices

1. Domestic Status

Domestic development of IR devices has a 30-year history: from the early 1960s to the present. Over this period, the power of the technology has gradually increased, and a number of varieties of detectors have been developed and manufactured. In East China, the Shanghai Institute of Technical Physics (SITP) has acted as a driver, spurring on thermal device development at several plants, institutes, and universities. Their products include thermoelectric detectors (TGS) [expansion uncertain]; lithium tantalate, lithium niobate, and macromolecular compounds (such as PVF_2); and intrinsic quantum detectors such as lead sulfide (PbS), lead selenide (PbSe), indium antimonide (InSb), and mercury cadmium telluride (HgCdTe). In the area of 8-14-micron-wavelength HgCdTe devices, SITP has made breakthroughs, including development of a 60-element photoconductive detector with a detectivity (D* value) of 2×10^{10} cm-$Hz^{1/2}$/W and excellent homogeneity (see Figure 1).

In the north, the North China Optoelectronics Institute (NCOI) has developed an 8-12-micron-band 32-element photovoltaic HgCdTe device and a 32 x 32-element InSb charge injection device. The Beijing Institute of Remote Sensing Equipment has developed large-area multi-element PbS detectors with performance and uniformity meeting utilitarian requirements, and the institute's multi-element linear-array InSb photovoltaic device [see Figure 2] is available for trial use in complete [detector] systems; also, the institute has developed a 233K photoconductive InSb detector with low vibration noise.

In the southwest, the Kunming Institute of Physics (KIP) is currently developing a scanning integrating (SPRITE) [signal processing right in the element] device; and the Chongqing Optoelectronics Institute has developed a 128 x 128-element PtSi [focal] plane array device.

Two-color devices have excellent anti-jamming characteristics. The Shanghai Xinyue [2450 6460] Instruments Plant has developed UV and mid-IR-band two-color devices; and NCOI, SITP, and KIP have developed mid- and long-wavelength two-color devices. [Passage omitted]

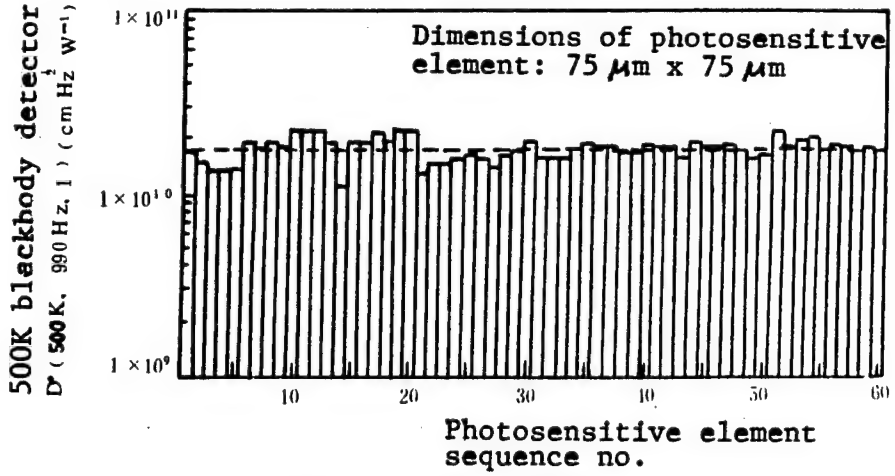

Figure 1. Plot of Distribution of D* Value for 60-Element Monolithic Detector

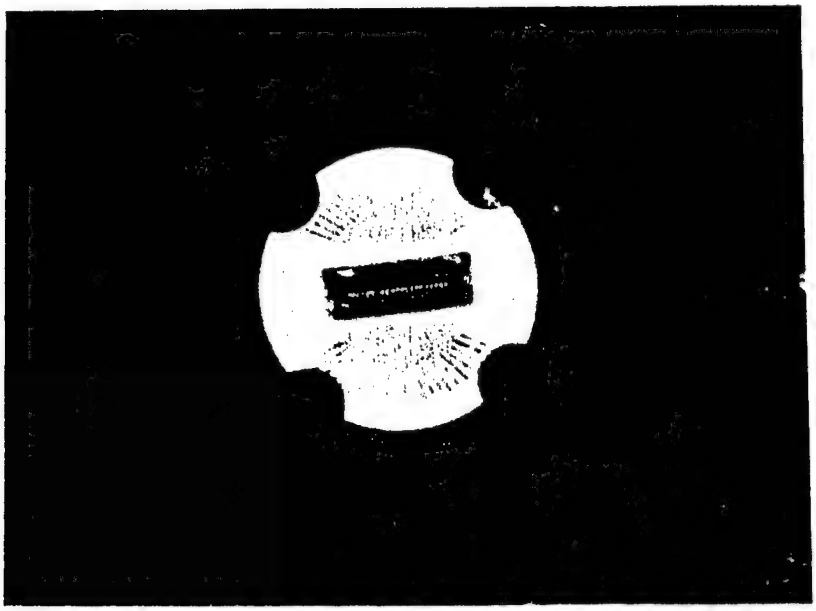

Figure 2. 40-Element Photovoltaic Detector Developed by Beijing Institute of Remote Sensing Equipment

256 x 256-Pixel Platinum Silicide IR Focal Plane Array Developed

92P60220C Beijing ZHONGGUO DIANZI BAO [CHINA ELECTRONICS NEWS] in Chinese 27 Mar 92 p 3

[Article by Yu Ruming [0151 3067 2494]: "Institute 44 Develops 60,000-Pixel Detector"]

[Summary] A 256 x 256-element platinum silicide (PtSi) Schottky barrier IR focal plane array (FPA)—the largest such domestic FPA in surface area—has been developed by MMEI's Institute 44 in a project successfully culminating on 16 March 1992. This IR detector has a backlit optimized thin PtSi optical cavity structure, with vertical and horizontal shift registers in a four-phase interline transfer buried-channel architecture. With a total pixel count of 65,336, this late-eighties-level device uses a standard TV format with interlaced scanning, and puts out clear room-temperature target images in the 1-5-micron mid-to-short IR band. This type of FPA has numerous applications in areas such as tactical seekers (homers), forward-looking IR systems, satellite remote sensing, night vision, security, resources exploration, transportation monitoring, medical treatment, and industrial measurement. The same institute had earlier developed a 128 x 128-pixel PtSi IR FPA, which was certified in January 1992 [see JPRS-CST-92-007, 16 Apr 92 p 28].

New Advances in HgCdTe Liquid Phase Epitaxy Technique

92P60220B Beijing ZHONGGUO DIANZI BAO [CHINA ELECTRONICS NEWS] in Chinese 20 Mar 92 p 3

[Article by Li Qiongrui [2621 8825 3843]: "New Advances in Research on Mercury Cadmium Telluride Liquid Phase Epitaxy Techniques"]

[Summary] In order to promote development of thin-film-type mercury cadmium telluride (HgCdTe) detectors—the primary devices used for detection in the 8-14-micron infrared band—MMEI's Institute 11 conducted a long, in-depth study of HgCdTe liquid phase epitaxy (LPE) techniques. Recently, institute scientists reported new advances in their research: epitaxial thin films grown via LPE meet mid-to-late-eighties international standards in terms of uniformity, primary-state thin-film optical qualities, and electrical characteristics. Breakthroughs were made in a number of critical technologies, including self-balancing, mother-liquid in-situ synthesis, partially saturated mercury-vapor pressure control, specific graphite-boat design, and specialized absorption blocks. These advances will greatly quicken the pace of domestic development of large-area IR focal plane arrays and CCDs.

Domestic Satellite Laser Range Finding Technology at State-of-the-Art

92P60220A Urumqi XINJIANG RIBAO in Chinese 21 Feb 92 p 3

[Unattributed article: "Nation's Satellite Range Finding Technology at Advanced International Level"]

[Summary] Shanghai, 20 Feb (XINHUA)—The dual-wavelength (1,064 nm/532 nm) high-power mode locked laser system for China's first third-generation artificial satellite laser range finder passed CAS-level technical appraisal a few days ago in Shanghai. The experts judged this system as being at the international state-of-the-art.

Tested for 6 years (over a million times per year) at the Shanghai Observatory in a variety of conditions—including recent successful tests at dawn and dusk, and in dim moonlight and daylight—and for 4 years at the Wuhan Seismological Institute, the system has demonstrated a ranging accuracy of 2-3 cm. Developed by the CAS Shanghai Institute of Optics and Fine Mechanics (SIOFM) and first installed at the Shanghai Observatory in 1986, this system generates a picosecond pulse. With this extremely short pulse length, it is ideal for measuring ultrafast processes. There are numerous applications in physics, chemistry, biology, optoelectronics, lasers (e.g., in a picosecond-level synchronously pumped tunable dye laser), and nonlinear optics (e.g., in a broad-tunable picosecond-level parametric laser). SIOFM has used such a laser to study nonlinear crystals and organic nonlinear materials, and has developed certain materials with a conversion efficiency exceeding that reported by a number of foreign commercial producers.

Spatial Filter Preprocessing Method, Its Application to Single Snapshot Array Processing

92P60251A Beijing DIANZI KEXUE XUEKAN [JOURNAL OF ELECTRONICS] in Chinese Vol 14 No 2, Mar 92 pp 120-126

[Article by Zhang Ming [1728 6900] of Department 4, Nanjing Aeronautical Institute, Nanjing 210016, and Yang Wanlin [2799 8001 7792] and Li Lemin [2621 2867 3046] of the University of Electronic Science and Technology, Chengdu 610054: "Spatial Filter Preprocessing Method and Its Application to Single Snapshot Array Processing"; MS received 17 Nov 90, revised 9 Sep 91]

[Abstract] A new method for resolving multiple signal sources in passive sensor arrays (such as are used in radar, sonar, radioastronomy, and seismology) is proposed. The new method, based on spatial filter preprocessing, yields resolution enhanced over that of existing spectral estimation algorithms, such as Schmidt's MUSIC [multiple signal characterization],[2] Kumaresan and Tufts' minimum range number method,[3] Shan's spatial smoothed MUSIC method,[4] Williams' modified spatial smoothed MUSIC (MSSM) method,[5] Tufts and Kumaresan's modified forward-backward linear prediction (MFBLP) method,[6] and Cadzow's signal enhancement method,[7] all of which rely instead on SVD (singular value decomposition) for preprocessing of the measured data. Specifically, the new method yields a significantly improved effective signal-to-noise ratio (SNR) and a more accurate autocorrelation estimation. The new method combines spatial filter preprocessing[8] with follow-up processing using a simple projection (PROJ) algorithm previously published by one of the authors.[11]

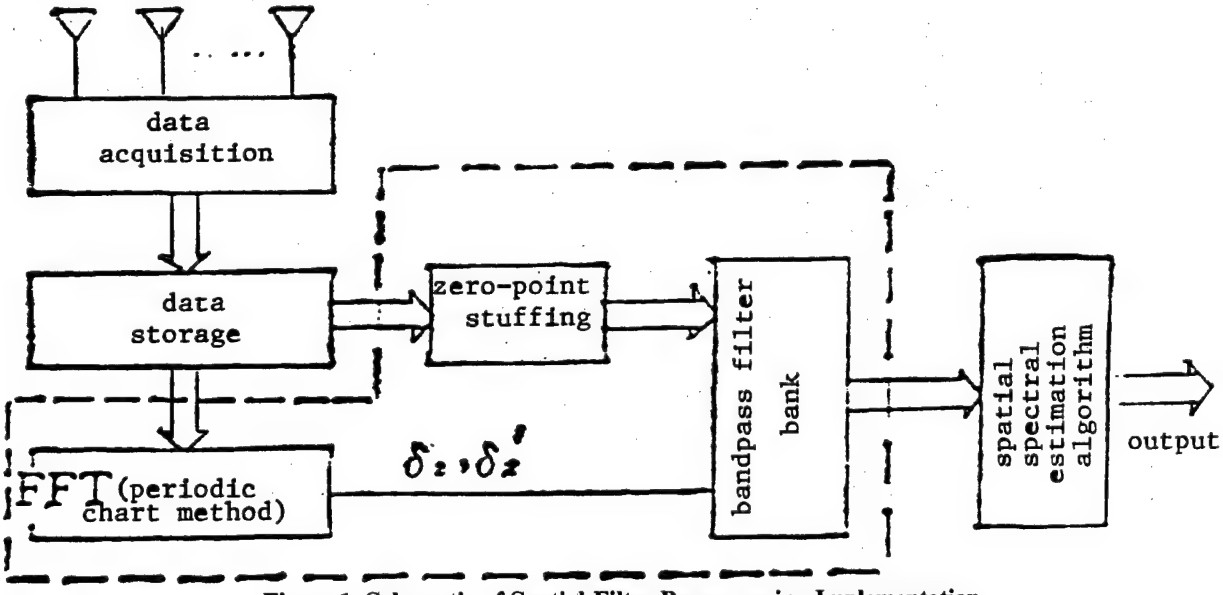

Figure 1. Schematic of Spatial Filter Preprocessing Implementation

A schematic of the spatial filter preprocessing implementation is shown below in Figure 1. Results of a simulation for a system with 17 array elements, two signal sources, a single snapshot, and a signal with a complex amplitude defined by a_1=1 and $a_2 = \exp(j\varphi)$ are given in Figures 2-6 below (in which θ represents the incident angle of the signal to the array broadside). As can be seen from the figures, the newly presented method can resolve the two sources—and in some cases up to four sources (see Figure 6).

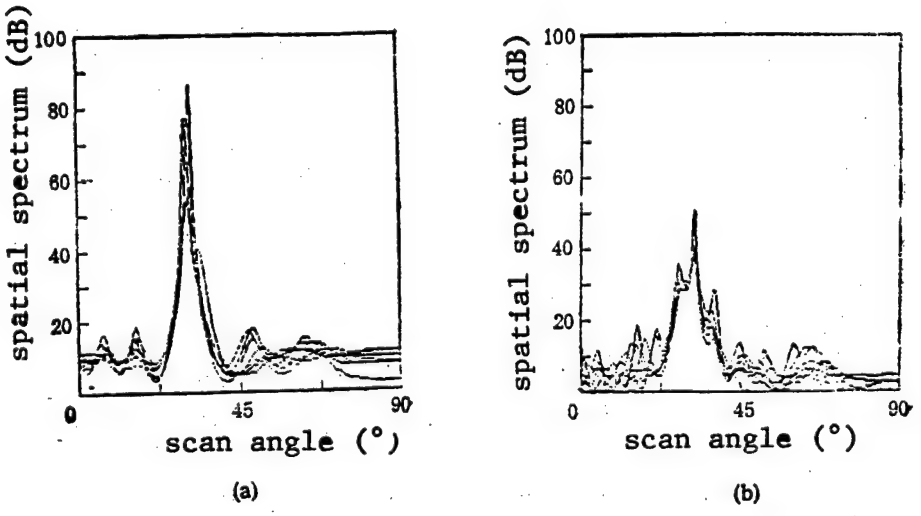

Figure 2
(a) MFBLP Method (b) MSSM Method
(SNR = 10dB, $\theta_1 = 30°$, $\theta_2 = 32°$, $\phi = 45°$)

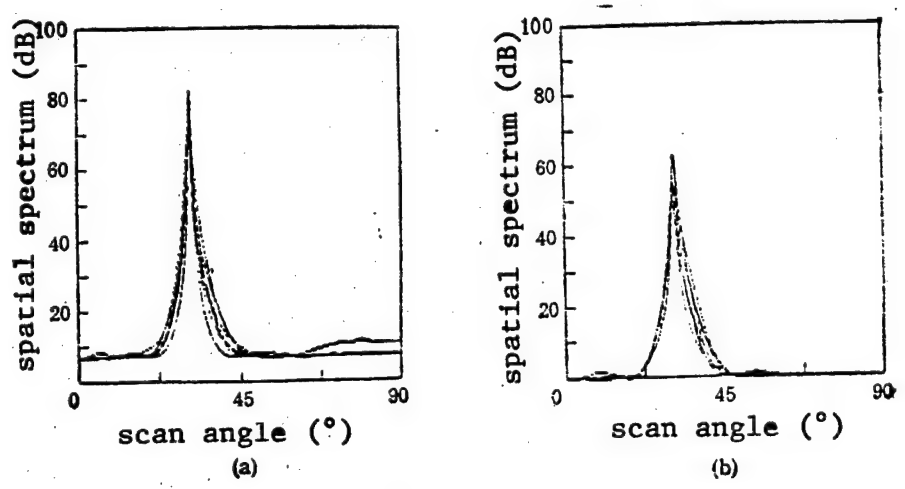

Figure 3
(a) PROJ alg. (b) PROJ algorithm after interpolation
(Same conditions as Figure 2)

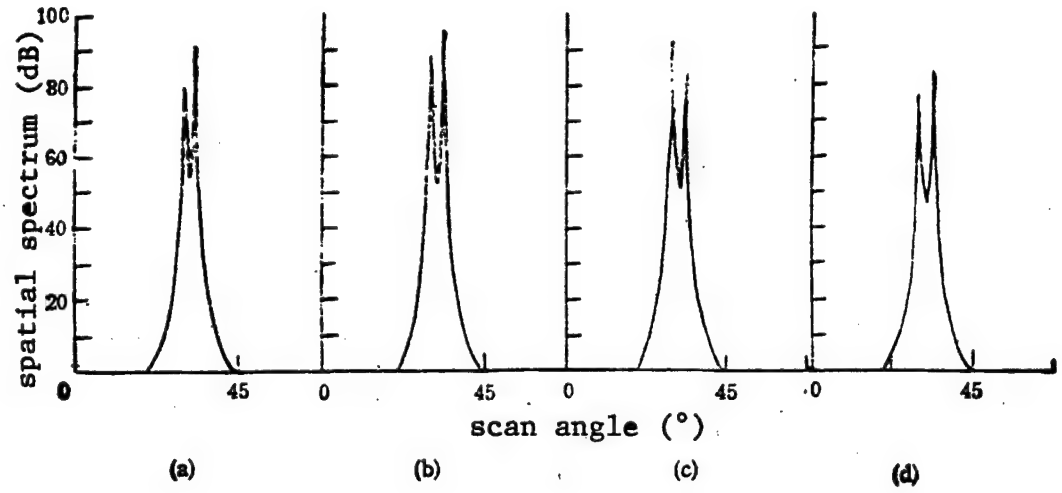

Figure 4
New Method; Except for ϕ, Same Conditions as in Figure 2
(a) $\phi = 0°$ (b) $\phi = 45°$ (c) $\phi = 90°$ (d) $\phi = 180°$

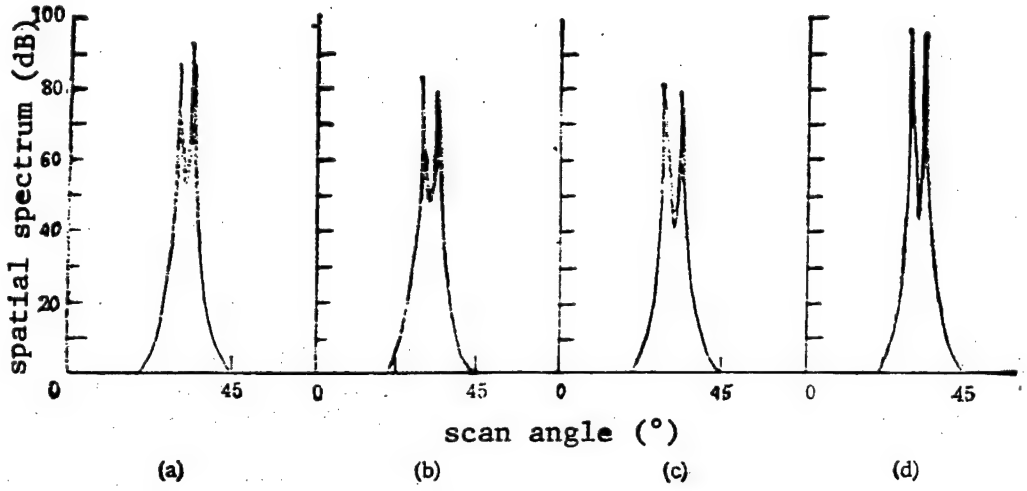

Figure 5
New Method; Except for SNR, Same Conditions as in Figure 2
(a) SNR = 20dB (b) SNR = 5dB (c) SNR = 0dB (d) SNR = −5dB

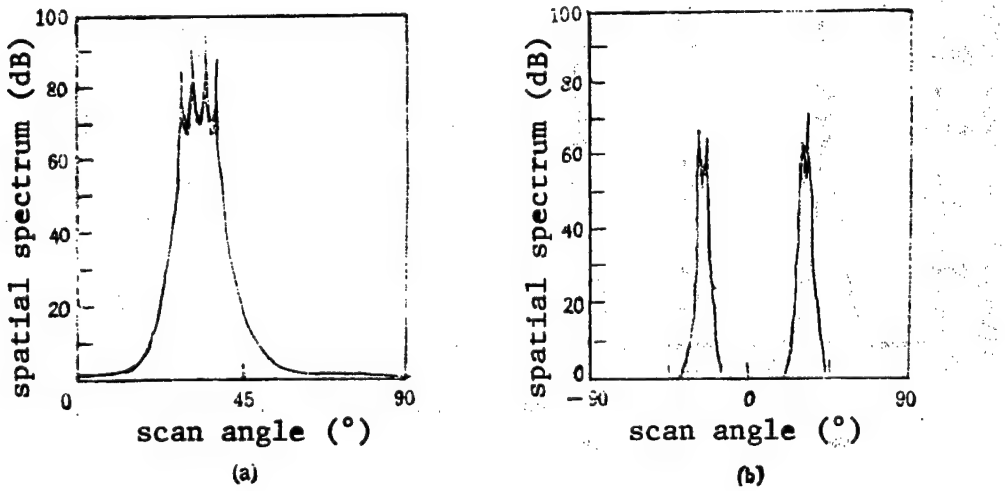

Figure 6

(a) New Method, SNR = 10 dB, $\theta_1 = 30°$, $\theta_2 = 32°$, $\theta_3 = 34°$, $\theta_4 = 36°$, $\varphi_1 = 0°$, $\varphi_2 = 90°$, $\varphi_3 = 180°$; (b) New Method, $\theta_1 = -27°$, $\theta_2 = -25°$, $\theta_3 = 30°$, $\theta_4 = 32°$, Other Conditions Same as in Figure 6(a)

References

1. W. F. Gabriel, PROC. IEEE, 68 (1980) 6, 645-666.

2. R. O. Schmidt, IEEE TRANS. ON AP, AP-34 (1986) 3, 276-280.

3. R. Kumaresan, D. W. Tufts, IEEE TRANS. ON AES, AES-19 (1983) 1, 134-139.

4. T. J. Shan et al., IEEE TRANS. ON ASSP, ASSP-33 (1985) 8, 806-811.

5. R. T. Williams et al., IEEE TRANS. ON ASSP, ASSP-36 (1988) 4, 425-432.

6. D. W. Tufts, R. Kumaresan, PROC. IEEE, 70 (1982) 9, 975-989.

7. J. A. Cadzow, IEEE TRANS. ON ASSP, ASSP-35 (1988) 1, 49-62.

8. S. M. Kay, IEEE TRANS. ON ASSP, ASSP-29 (1981) 8, 859-867.

9. R. W. Schafer, L. R. Rabiner, PROC. IEEE, 61 (1973) 5, 692-702.

10. R. E. Crochiere, L. R. Rabiner, IEEE TRANS. ON ASSP, ASSP-23 (1975) 3, 444-454.

11. M. Zhang et al., IEE PROC-F, 138 (1991) 5, 407-410.

S-Band 20W Pulse Gunn Oscillator Developed

92P60251B Beijing DIANZI KEXUE XUEKAN [JOURNAL OF ELECTRONICS] in Chinese
Vol 14 No 2, Mar 92 pp 208-211

[Article by Xie Jiade [6200 1367 1795], Xu Yinsheng [1776 1377 3932], and Di Haiying [1646 3189 5391] of the Yaguang Electronic Engineering Plant, Chengdu 610051: "S-Band 20W Pulse Gunn Oscillator"; MS received 17 Dec 90, revised 23 Apr 91]

[Abstract] With advantages such as long life, high reliability, small volume, and light weight, pulse Gunn oscillators have proven to be quite useful in all-solid-state long-range radar systems, pulse target signal simulators, satellite-borne and missile-borne responders, and electronic countermeasures systems. The structure (see Figure 1 below) and design principles of a pulse Gunn diode, microwave circuitry, and pulse modulator (see Figure 2 below) are described. The main parameters of such a Gunn oscillator developed by the author and tested in a pulse radar target signal simulator are as follows: in the 3-4 GHz frequency range, maximum pulse power is 20W, maximum efficiency is 5 percent, and operating ratio is less than or equal to 1 percent. The pulse modulator provides an adjustable rectangular pulse voltage with an amplitude of 15-65 V, a width of 0.8-5 μs, a repetition rate of 500-2,000 Hz, and a current capacity of 15 A. Three other figures (not reproduced) show graphs of frequency and power characteristics of the oscillator at varying bias voltage, oscillator power at varying frequency, and the modulator pulse voltage and oscillator video pulse waveforms.

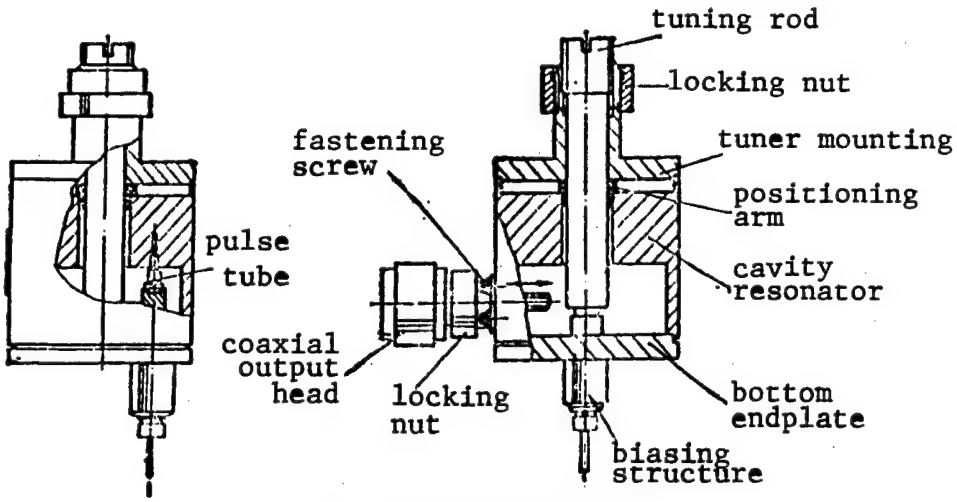

Figure 1. Oscillator Structure

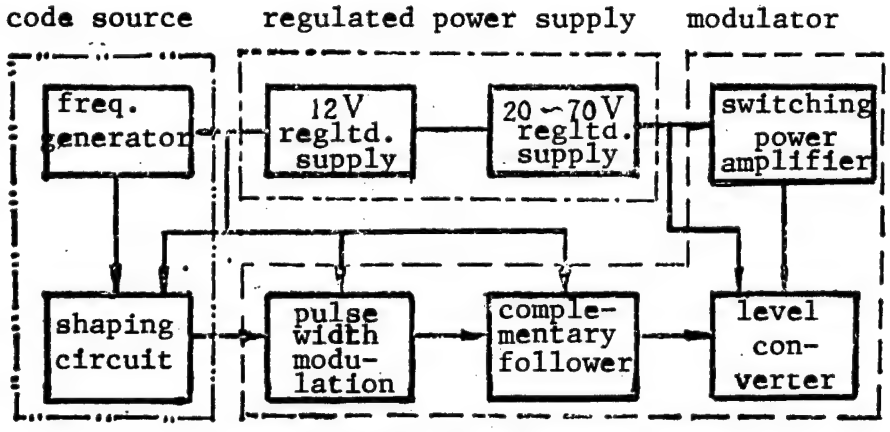

Figure 2. Schematic of Pulse Modulator Circuit

References

1. Xie Jiade, WEIBO [MICROWAVES], 1987, No 3, pp 35-43.

2. Ibid., DIANZI XUEBAO [ACTA ELECTRONICA SINICA], 1988, No 4, pp 118-119.

Application of Transient Electromagnetic Pulse in Detecting Subsurface Targets

92P60251C Beijing DIANZI KEXUE XUEKAN [JOURNAL OF ELECTRONICS] in Chinese Vol 14 No 2, Mar 92 pp 212-216

[Article by Wang Baoyi [3769 0202 5030], Xu Runmin [1776 3387 3046], Deng Yangjian [6772 2254 0256], and Yu Huiqing [0151 1920 0615] of the Department of Radio, Sichuan University, Chengdu 610064, and Long Xianhui [7893 2009 1920] and Wang Yongde [3769 3057 1795] of the Institute of Electronic Technology, Chengdu 610036: "Application of Transient Electromagnetic Pulse in Detection of Subsurface Targets"; MS received 7 Jan 91, revised 6 May 91]

[Abstract] In the past 20 years, the use of carrier-free electromagnetic narrow-pulse detection for underground targets has seen rapid advancement.[1-7] This kind of radar, also known as impulse radar, has higher range resolution and other advantages over the other types of ground-probe (i.e., underground) radar. In 1986, Japanese scholars reported development of an experimental underground target-detection computerized imaging system able to provide a picture of a buried four-element pipeline mesh with an element horizontal spacing of 50 cm and an element vertical spacing of 20 cm.[6] Chinese researchers have also reported experimental systems for detection of underground pipeline,[4,7,8] but the recordings of the reflected waveforms from the target were difficult to interpret. An improved system, based on a

nanosecond EM pulse and a specially developed high-quality traveling-wave three-layer sector antenna, has been developed and is described. Terminal processing includes a fast, high-resolution graphics display. With the new system, 100-mm-diameter metal pipes buried about 1 m below the surface can be clearly detected and displayed.

The system, shown schematically in Figure 1 below, has a horizontal resolution of 50 cm, a vertical resolution of 20 cm, a small antenna (70 cm long, see Figure 3), and requires about 3 minutes on an Apple II microcomputer to calculate and print out the curves and target gray levels. The nanosecond Gaussian pulse has an amplitude of 100 V, a half-power-point width of 2.5 ns, a rise time of 1-1.2 ns, and a variable EMP repetition rate (50 kHz, 100 kHz, and 200 kHz). Figures 5, 6, and 7 below show gray-level plots of a single target pipe, a double target, and a three-pipe target, respectively. Two other figures (not reproduced) show the continuous resistance loaded cylindrical antenna schematic and a schematic of the on-site buried pipeline configuration.

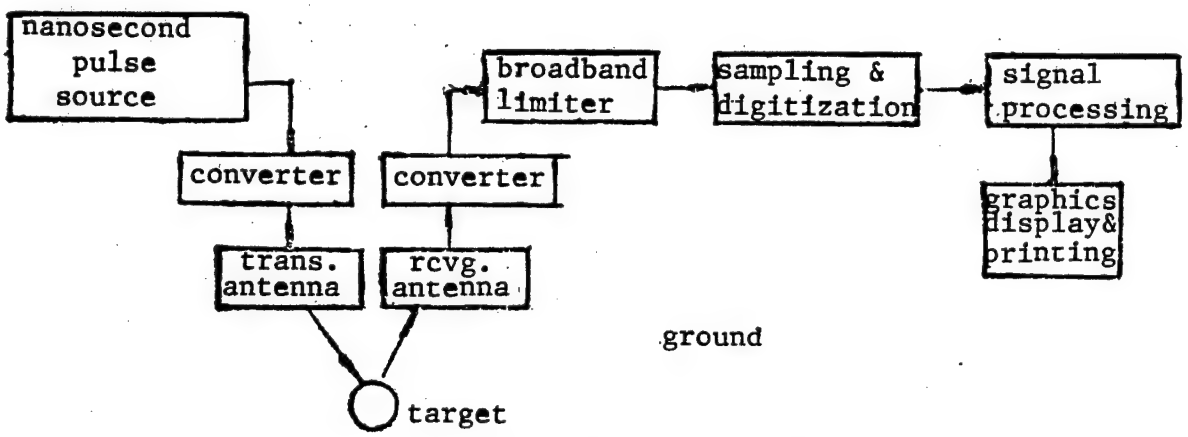

Figure 1. Schematic of System Principle

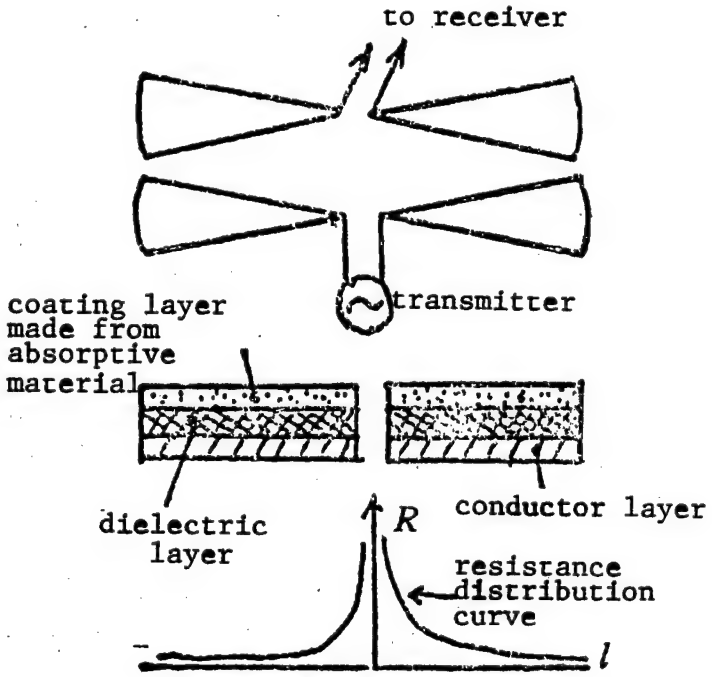

Figure 3. Antenna Schematic

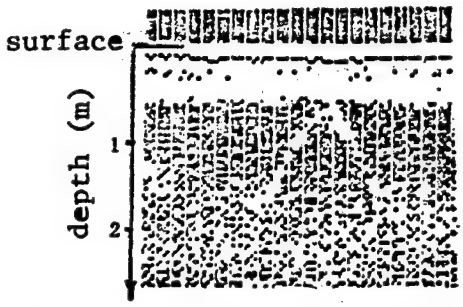

Figure 5. Single-Target Test

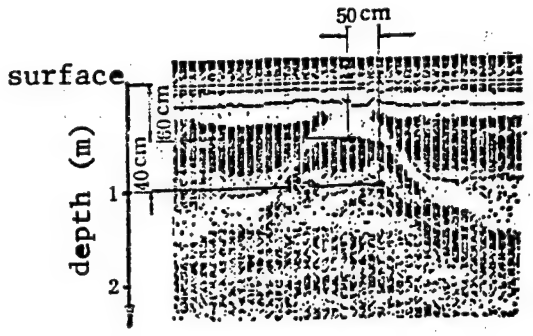

Figure 6. Double-Target Test

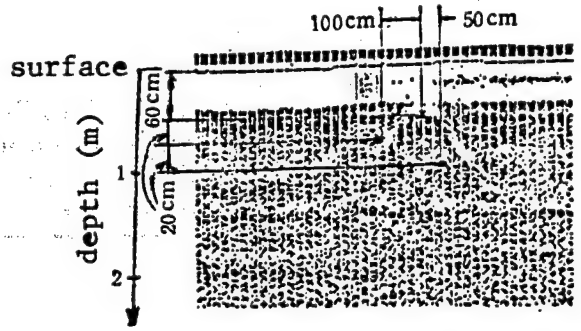

Figure 7. Three-Target Test

References

1. D. J. Daniels et al., "Introduction to Subsurface Radar," IEE PROC.-F, August 1988, Special Issue on Subsurface Radar, 278-320.

2. J. D. Young, R. Caldecott, "Underground Pipe Detector," U.S. Patent 4062010 (1977).

3. L. C. Chan, D. L. Moffatt, L. Peter, PROC. IEEE, 67 (1979) 7, 991-1000.

4. Pan Zhongying et al., DIANBO KEXUE XUEBAO [JOURNAL OF ELECTROMAGNETIC WAVE SCIENCE], 3 (1988) 3/4, 68-76.

5. Keiichi Ueno et al., "An Underground Object Imaging System With Computerized Reconstruction," NTT Elec. Com. Lab., 9-11, Midori-Cho, 3-Chome Musashino-shi Tokyo 180 Japan (1986).

6. Teruo Usami et al., "Detection of Underground Pipes by Synthetic Aperture Techniques," THE TRANS. OF THE IECE OF JAPAN, 69E (1986) 4, 491-493.

7. Liao Chunlin and Zhang Xiyuan, "Implementation of, Experiment With Carrier-Free Pulse Underground Target Detection System," Proc. of the 1986 Annual National Conference on Electromagnetic Waves, Beijing, pp 351-353.

8. Nie Zaiping and Xie Jun, "Use of Transient Electromagnetic Pulse for Detection of Underground Targets," Technical Report of the University of Electronic Science and Technology, Chengdu, December 1985.

9. T. T. Wu, R. W. P. King, IEEE TRANS. ON AP, AP-12 (1965) 5, 369-374.

Effects of Deformable-Mirror/COAT-System Finite Subaperture Size on Compensation Efficiency

92P60256A Shanghai ZHONGGUO JIGUANG [CHINESE JOURNAL OF LASERS] in Chinese Vol 19 No 2, Feb 92 pp 127-131

[Article by Feng Yuezhong [7458 1471 1813], Gong Zhiben [7895 4249 2609], and Song Zhengfang [1345 2973 2455] of the CAS Anhui Institute of Optics and Fine Mechanics, Hefei 230031: "Effects of COAT-System Finite Subaperture on Compensation Efficiency"; MS received 24 Jul 90, revised 24 Dec 90]

[Abstract] Residual phase error after deformable-mirror correction of atmospheric-turbulence-induced laser

beam wavefront phase distortion is analyzed. Deformable mirrors used as spatial filters and coherent adaptive optical technique (COAT) systems have been studied by the authors previously,[1] but an infinitely small subaperture size was assumed. Since practical systems have finite subaperture size, it is worthwhile to consider the effects of this finite size on Strehl's ratio (SR, a measure of beam quality, = I/I_0) and—since a high SR value does not in itself indicate that the system's compensation ability is good—on compensation efficiency as well. Compensation efficiency (R) is a new parameter proposed by the authors, and is defined as follows:

R = SR after compensation/SR before compensation

Although SR increases as subaperture size decreases, the former decreases very slowly when the latter is small. Based on the authors' theories, optimal size can be easily determined for high performance-to-cost ratio. Calculations reveal that R is low for weak turbulence, increases for a while as turbulence grows, and then rapidly decreases after reaching its maximum value.

The deformable-mirror subaperture element arrangement and element spacing (a) are shown in Figure 1 below. Figure 2 below shows a plot of SR vs a for three different values of the turbulence parameter r_{ot} (where r_{ot} is defined as the atmospheric coherent length of 0.6328-μm-wavelength visible light transmitted over 10 km, and is therefore representative of turbulence intensity); λ is the laser wavelength, D is the effective transmission aperture, and L is the transmission range. Calculations show, for example, that with weak turbulence (r_{ot} = 15 cm), 4,921 elements are required to yield a post-compensation SR of 0.9; with medium turbulence (r_{ot} = 1 cm), 12,061 elements are required to yield an SR of 0.5; and in strong turbulence (r_{ot} = 0.1 cm), 120,000 elements are required to yield an SR of 0.5. Figure 3 below shows a plot of R vs r_{ot} for four different values of a.

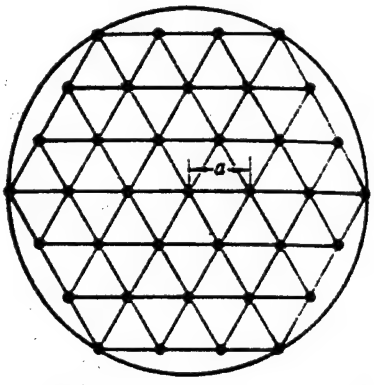

Figure 1. Distribution of Subaperture Elements

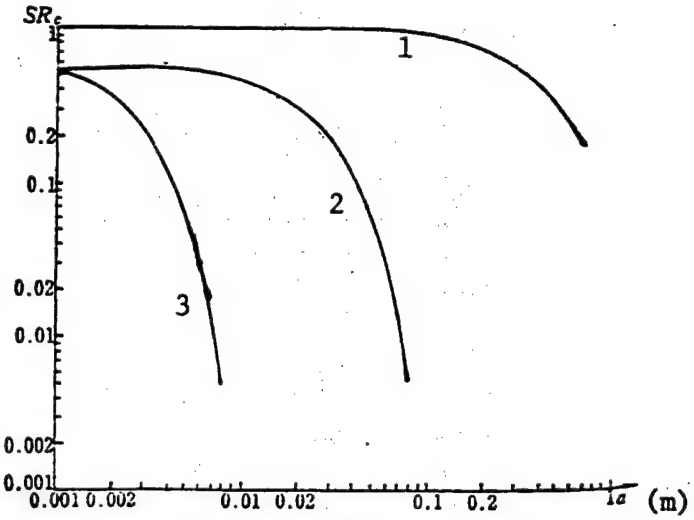

Figure 2. Strehl's Ratio vs a for Different Turbulence

λ = 1 μm; D = 4 m; L = 10 km; 1—r_{ot} = 15 cm; 2—r_{ot} = 1 cm; 3—r_{ot} = 0.1 cm

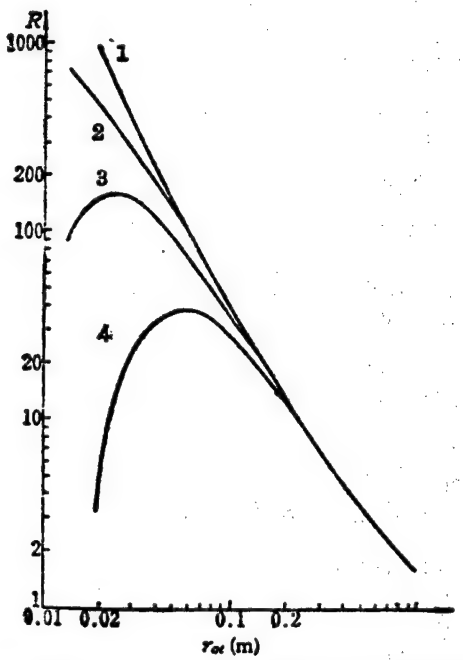

Figure 3. Compensation Efficiency vs Turbulence for Different Subaperture Size

D = 1 m, L = 10 km, λ = 1.06 μm; 1—a = 0.01 m; 2—a = 0.05 m; 3—a = 0.1 m; 4—a = 0.2 m

References

1. Feng Yuezhong et al., GUANGXUE XUEBAO [ACTA OPTICA SINICA], 11, 1010 (1991).

2. J. E. Harvey, G. M. Callahan, PROC. OF SPIE, 141, 50 (1978).

3. V. I. Tatarski, "Theory of Wave Transmission in Turbulent Atmosphere," trans. into Chinese, Science Publishing House, 1978.

4. R. F. Lutomirski et al., APPL. OPT., 10, 1652 (1971).

Ar-Ion-Laser-Pumped CW Ti-Gem Laser Developed

92P60255A Shanghai ZHONGGUO JIGUANG [CHINESE JOURNAL OF LASERS] in Chinese Vol 19 No 2, Feb 92 p 87

[Brief research letter by Liu Yupu [0491 3768 3877], Lu Peihua [7120 1014 5478], and Zhang Yinghua [1728 1758 5478] of the CAS Shanghai Institute of Optics and Fine Mechanics (SIOFM) Laser Technology Laboratory, Deng Peizhen [6772 0160 3791], Chai Yue [2693 6460], and Qiao Jingwen [0829 2529 2429] of the CAS SIOFM Laser Crystal Research Laboratory, and Li Qingguo [2621 1987 0948] of the CAS SIOFM Optical Thin Film Laboratory: "Argon-Ion-Laser-Pumped CW Titanium-Gem Laser Developed"; MS received 19 Dec 91]

[Summary] On 18 December 1991, we successfully operated a continuous-wave Ti-gem laser pumped by a domestically made A-240 Ar-ion laser (made by Nanjing Electron Tube Plant). Initial testing reveals that at a wavelength λ = 788 nm, output power is 303 mW. Tunable range is 660-960 nm. The Ti-gem laser medium, grown here at SIOFM, is 3.5 mm x 3.5 mm x 19 mm in size, and has an absorption coefficient α of 1.6 cm^{-1} at a wavelength of 490 nm. Further adjustments and parametric optimization experiments for this laser—which has proven valuable in worldwide research on tunable solid-state laser and ultrashort-pulse (especially femtosecond-pulse) lasers—are now underway.

High-Efficiency Tunable Output Realized With Ti:Gem Laser Pumped by Raman-Shifted Excimer Laser

92P60255B Shanghai ZHONGGUO JIGUANG [CHINESE JOURNAL OF LASERS] in Chinese Vol 19 No 2, Feb 92 p 116

[Brief research letter by Lou Qihong [2869 4388 3163] and Gu Hongping [6581 4767 1627] of the CAS SIOFM Laboratory 1 and Deng Peizhen [6772 0160 3791], Zhang Qiang [1728 1730], and Sun Yang [1327 2543] of the CAS SIOFM Laboratory 8: "High-Efficiency Tunable Output Realized With Ti:Gem Laser Pumped by Raman-Frequency-Shifted Excimer Laser"; MS received 19 Dec 91]

[Summary] We have successfully realized a high-efficiency tunable (668-832 nm) output from a doped titanium-gem (Ti:Al_2O_3) laser pumped by a Raman-shifted XeCl excimer laser. The 308-nm-wavelength XeCl excimer laser is Raman-shifted in high-pressure hydrogen to a three-step Stokes optical wavelength of 499 nm. The Ti:gem crystal, grown by our newly developed induced temperature-field up-shifting method (IFSM), is 5 mm x 5 mm x 24 mm in size, and has peak absorption coefficients α_{490} = 1.98 cm^{-1} and α_{800} = 0.028 cm^{-1}. Our excimer-laser-pumped Ti:gem laser has a threshold oscillation energy of 0.54 mJ, an energy conversion efficiency of 42 percent, a slope efficiency of 59 percent, and a quantum efficiency of 87 percent.

Tunable Forsterite Laser Developed

92P60255C Shanghai ZHONGGUO JIGUANG [CHINESE JOURNAL OF LASERS] in Chinese Vol 19 No 2, Feb 92 p 160

[Brief research letter by Qiu Zhi [8002 3112], Liu Ye [0491 8518], Pan Peicong [3382 0160 5115], and Zhu Hongbin [2612 3163 2430] of the CAS Shanghai Institute of Optics and Fine Mechanics (SIOFM): "Tunable Forsterite Laser Developed"; MS received 26 Dec 91]

[Summary] On 18 December 1991, CAS SIOFM Laser Technology Laboratory researchers, using forsterite (magnesium olivine) crystal grown at SIOFM's Crystal Laboratory, successfully achieved laser output. The pump source was a Nd:YAG laser with a pump light pulse width of 10 ns. The forsterite crystal is 6 mm x 7 mm x 26 mm in size, laser center wavelength is 1.23 μm, spectral width is 24 nm, maximum monopulse energy is 10 mJ, overall energy conversion efficiency is 13.2 percent, and laser pulse width is 5 ns.

A High Power 1079.5 nm Nd:$YAlO_3$ CW Laser

40100035A Shanghai ZHONGGUO JIGUANG [CHINESE JOURNAL OF LASERS] in Chinese Vol 19 No 1, Jan 92 pp 19-21

[Article by Shen Hongyuan, Zhou Yuping, et al., of the Fujian Institute of Material Structure, CAS, Fuzhou, (MS received 25 Feb 91, revised 1 Apr 91) [cf. JPRS-CST-92-006, 20 Mar 92 p 60]]

[Abstract] On the basis of analysis and contrast for the stimulated emission cross section, the fluorescent lifetime, and optomechanical coefficient, as well as the ability to resist the thermal stress, it is shown that similar to the Nd:$Y_3Al_5O_{12}$ crystal, the Nd:$YAlO_3$ crystal is a useful material to develop high power CW solid state lasers. 424W output power with an overall efficiency of 2.54 percent and a slope efficiency of 3.77 percent have been achieved from a φ 7 x 155 mm Nd:$YAlO_3$ rod.

Experimental Frequency Up-Conversion in Yb^{3+}/Er^{3+} Doped Silica Fiber

92P60256B Shanghai ZHONGGUO JIGUANG [CHINESE JOURNAL OF LASERS] in Chinese Vol 19 No 3, Mar 92 pp 219-221

[Article by Hua Yimin [5478 0001 2404], Li Qu [2621 0507], Chen Yingli [7115 5391 4409], and Chen Yixin [7115 4135 2450] of the Department of Applied Physics, Shanghai Jiaotong University, 200030: "Experimental Research on Frequency Up-Conversion in Yb^{3+}/Er^{3+} Doped Silica Optical Fiber," supported by grants from NSFC and Shanghai Jiaotong University; MS received 23 May 91, revised 15 Jul 91]

[Abstract] Frequency up-conversion in Yb^{3+}/Er^{3+} doped silica optical fiber has been experimentally demonstrated. The IR pump source was a 1064-nm-wavelength CW Nd:YAG laser. The fiber, grown via a solution method at the China Institute of Building Materials Science, has a core diameter of 8 μm, a cutoff wavelength of 1.24 μm, a length of 40 cm, a Yb-ion dopant concentration of 2700 ppm, and an Er-ion dopant concentration of 900 ppm. The observed emission spectral lines are at 467 nm (the $^4G_{9/2}$-$^4I_{13/2}$ transition), 546 nm (the $^4S_{3/2}$-$^4I_{15/2}$ transition), and 667 nm (the $^4F_{9/2}$-$^4I_{15/2}$ transition). When intra-fiber CW IR laser power (as measured by a monochromator and an S-20 photomultiplier tube) was increased from 100 mW to 1 W, the power of the 467-nm, 546-nm, and 667-nm visible emission spectral lines measured 4 μW, 100 μW, and 30 μW, respectively, with corresponding conversion efficiencies of 0.0004 percent, 0.01 percent, and 0.003 percent, respectively.

Three figures show the energy level diagram of the Yb^{3+}/Er^{3+} doped system, the emission spectra of the doped silica fiber pumped at 1064 nm, and the power dependence of the emitted radiation at 467, 546, and 667-nm bands on excitation power at 1064 nm.

References

1. T. F. Carruthers, I. N. Duling et al., APPL. PHYS. LETT., 54 (10), 875-877 (1989).

2. A. S. L. Gomes, Cid B. de Araujo, CLEO'90, Anaheim, California, USA, May 1990, paper CME2.

3. D. C. Hanna, R. M. Percival et al., OPT. COMMUN., 78 (2), 187-194 (1990).

4. F. E. Auzel, PROC. OF IEEE, 61 (6), 758-786 (1973).

5. W. L. Barnes, S. B. Poole et al., J. LIGHTWAVE TECH., 7 (10), 1461-1465 (1989).

6. Hua Yimin, Li Qu et al., GUANGXUE XUEBAO [ACTA OPTICA SINICA], 12 (3), 67-70 (1992).

Breakthroughs in Quantum Optics Research Reported

92P60220D Shanghai WEN HUI BAO in Chinese 31 Mar 92 p 3

[Article by Wang Lin [3769 3829]: "Nation's Quantum Optics Research Arouses Attention"]

[Summary] It has been learned from the Shanghai International Quantum Optics Conference convened yesterday that several domestic breakthroughs—some arousing international interest—have been made in the area of quantum optics research, and moreover that research findings have been applied in a number of high-tech areas, including coherent fiber optic communications, new atomic clocks, and high-precision measuring instruments. CAS Shanghai Institute of Optics and Fine Mechanics (SIOFM) scientists recently developed the world's smallest solid-state laser, and were the first in the world to use a semiconductor diode laser to observe 8.5-dB-compressed non-classically correlated twin optical fields, a finding which revises [theory on] the light-emitting characteristics of rubidium glass, and is therefore of major international significance.

The conference was attended by over 100 scientists from 16 nations, including the United States, Britain, Germany, the former Soviet Union, France, Italy, Sweden, and Japan. International Theoretical Physics Center special member and noted Chinese quantum optics specialist Wang Yuzhu [3769 5148 4554] was conference chairman.

Enhancement of Brightness of Laboratory Soft X-Ray Lasers

40100038A Shanghai GUANGXUE XUEBAO [ACTA OPTICA SINICA] in English Vol 12 No 3, Mar 92 (MS received 28 Mar 91, revised 30 Aug 91) pp 284-288

[Article by Wang Zhijiang and Zhang Zhengquan, (Shanghai Institute of Optics and Fine Mechanics, CAS. P.O. Box 800—211, Shanghai 201800, China)]

[Text] Abstract: A large separation "oscillator" source-travelling wave amplifier approach is suggested for attaining high-power fully coherent X-ray source. Using a newly designed aspherical lens combination, a long narrow focal line can be obtained, resulting in a more uniform and narrow laser-produced plasma column. It may be a great help to raise gain-length product.

Key words: soft X-ray laser, brightness.

The past few years have seen enormous progress in the field of generating and amplifying laser radiation in the soft X-ray regime. The development of laboratory soft X-ray lasers leads hope that these devices can serve as an intense source of coherent X-rays. The goal of many of the researchers is to produce a bright, short-pulse, coherent source that would be ideal for the production of holograms of live, wet, biological specimens, affording a unique view into the structures of such live samples at

resolution of about 30 nm. Mathews et al.[1] predict that one will need to produce at least 20 μJ of spatially coherent radiation in a pulse-length of 50 ps and focussed at the sample to a beam of 10 μm diameter. High brightness of soft X-ray source is the most basical requirement for the holography applications. London et al.[2] conclude that wavelengths slightly longer than the 4.37 nm carbon K-edge is an optimal wavelength choice for soft X-ray holography. Considerable attention is also being paid to the study of the coherent characteristics of amplified spontaneous radiation obtained in laboratory systems[3-5].

Current laboratory X-ray lasers function as single-pass amplifiers without the benefit of a feedback mirror and thus behave as amplifiers of incoherent spontaneous emission radiation. As a line-width of order 0.004 nm was assumed (based on a theoretical predication of an ion temperature of 400 eV) for a 20.6 nm-wavelength selenium laser, its longitudinal coherence length, given by $\lambda^2/\Delta\lambda$, is about 100 μm, which may be of great advantage in imaging biological objects more than 1 μm in depth. But for a laser profile size of 100-200 μm and length of 2-4 cm, it gives a lateral coherence length of 1-3 μm, and the laser output end has an estimated 10^3-10^4 transverse modes indicating poor spatial coherence properties[4-6].

For applications that require coherence, such as holography, a laser that radiates in one or a few modes would be much more efficient. As the effective Fresnel number of the laser profile is decreased, the number of transverse modes decreases and so the degree of coherence increases. One way to make such a laser would be to decrease its aperture, but this would also reduce the total output power. Simply increasing the length of laser gain medium to reach gain saturation is also no use for improving its coherence. Since these poor coherence properties are due to the fact that these lasers are highly multimode devices, adding gain saturation only worsens coherence properties. Rosen et al.[6] proposed a two-stage architecture for achieving powerful X-ray beams with high transverse coherence, namely, to produce a small-aperture (25 μm), spatially coherent beam in a first-stage laser, expand the beam with a spatial filter, and then amplify it in a large-aperture power amplifier. But there are many difficulties in both building-up a small-aperture single-mode laser and mode-limiting with a spatial filter in practice. In the case of high-power performance, the spatial filter which consists of multilayer mirrors may be damaged by backward soft X-ray ASE radiation from the amplifier-stage. In addition, it should be noted that because there was no consideration on the time delay between the source and the amplifier, the coupling and interfering between them cannot be avoided.

Based on our experiences in the development of high-brightness, high-energy Nd: glass laser facility, we suggest an approach of large separation "oscillator" source-travelling wave power amplifier to make a bright X-ray source fully coherent. The main idea is to strengthen the amplification of axial fundamental mode and to limit the excess spontaneous emission of off-axial higher modes, by means of properly enlarging the separation between the oscillator source and the power amplifier. Let us discuss how to butt the oscillator source against the power amplifier. For the laboratory X-ray lasers of collisional excitation scheme at present[7, 8], their typical parameters are: output power 20-200μJ/200-250 ps = 10^5-10^6W, wavelength 5-20 nm, output aperture 75-200 μm, length of gain medium 2.5-4 cm, gain coefficient 2.5-4 cm^{-1}, gain-length product 8-16, X-ray beam divergence 10-20 mrad, which is well consistent with the geometric divergence of D/L. According to the well-known formula of lateral coherence length for an incoherent source propagating through free space, the transverse distance d over which a fully incoherent source of transverse size D (at a distance L away) looks like a fully coherent point source (at wavelength λ) is given by

$$d = L\lambda/D, \qquad (1)$$

Using this formula we find, for D = 100 μm and λ = 10 nm, a lateral coherence length d = 100 μm at L = 1 m, which is equal to the aperture size of power amplifier. Assuming the beam divergence of oscillator source is nearly about 10 mrad, the beam will illuminate a $(10mm)^2$ footprint over a 1m distance. That means the $(100\ \mu m)^2$ fully coherent area receiving only 10^{-4} of source signal. In other words, if there is an "oscillator" source which has a gain-length product of about 9, e.g. 3 cm^{-1} x 3 cm, amplifying factor being about 10^4, then we can get a single-mode signal strong enough at 1m distance from amplifier entrance; after propagating through the power amplifier which also has a performance of GL = 9 and D = 100 μm, a diffraction-limited (order of 0.1 mrad divergence) fully coherent radiation output of energy about 20 μJ could be expected. Otherwise, we may still prepare a second amplifier in the same way until we reach gain saturation. On the other hand, there must be a time delay L/c = 3.3 ns, relative to the source, for the amplifier pumping. This delay is quite long compared to the driving laser pulse generally; then there will be a good isolation in time scale between the source and the amplifier. The amplifier can be controlled by an intensive oscillator signal just from the beginning and works in a manner of travelling-wave amplification. Furthermore, a high-reflectivity multilayer mirror placed at a distance may be used in a small-size target chamber to fold the X-ray path and make two laser-produced plasma columns as close together as possible. This is a simple way to attain a single-transverse-mode high-brightness X-ray laser, especially in case of no refraction, i.e. the case of recombination pump scheme. Recently, X-ray laser experiments of two-slab targets set end to end oppositely were reported for the collisional excitation scheme[9, 10], where the refraction effect is rather important. In these experiments, the separation of two targets was only about 1 mm, the time delay was about 90 ps. It is impossible to expect any obvious improvement in their coherence properties. If the separation and the time delay are enlarged enough, the

improvement would be achieved. In this principle, a nuclear-explosion-driven X-ray laser can also get a diffraction-limited output beam.

Another issue in laboratory X-ray laser research is why experiments with a long recombining-plasma column did not attain an estimated high gain-length product, in fact, the gain coefficient of only 0.5 cm^{-1} corresponding to a 6-cm-long plasma[11]. Here the refraction effect in condition of near 10^{19} cm^{-3} electron density is unimportant. The effect of radiation trapping which leads to the reduction of population inversion density may be still serious after using a thinner target. But the uniformity of illumination along the line focus is a problem more worthy to be considered. X-ray laser studies require producing a plasma column as gain medium. This is done by focussing the pump laser beam into a line focus. The usual technique is to use a aplanatic aspherical lens in conjunction with a positive or negative cylindrical lens. The line length may be varied by changing cylindrical lens power. A pair of weak crossed cylindrical lenses with a spherical lens makes it possible to continuously vary the length of the focal line without refocussing. A shortcoming of this method is that the focal line axis maps directly from the near-field beam pattern. For a circular beam of uniform intensity the intensity along the line focus is highest in the center and drops to zero at the ends. The beam may be masked to provide a uniform rectangular beam which can give a uniform intensity distribution, but at the expense of losing energy of the aperture. In any case, realistic beams are never perfectly uniform, so it certainly causes an inhomogeneous intensity distribution along the focal line.

Some new methods have been reported. An array of small cylindrical lenses before a spherical lens or an array of wedges in conjunction with a cylindrical lens were used to provide averaging over many segments of the laser beam resulting in a more uniform intensity distribution along the line focus[1, 13]. But the problem has not been solved thoroughly. The production of a large gain-length product needs a narrow plasma column of several centimeters long. However the existence of astigmatism and field curvature of a practical focussing geometry results in the reduction of the pump laser irradiance, especially in the case of a very long focal line. For a not very thick lens, no matter with spherical or aspherical surfaces, if it meets the aplanatic condition, its astigmatism and field curvature will be constant. Because the spread of light beam along the tangential direction only makes the focal line get somewhat longer, in the sagittal direction it makes the focal line broaden, so that product of sagittal field curvature and numerical aperture does determine the width of the focal line. That is to say, for an optical focussing system generally used in X-Ray laser experiments, when the length of the focal line is 2h and the numerical aperture is 2u, the width w of the focal line at the distance h from the system center is given by

$$w = (1+ 1/n)\, h^2u/f, \qquad (2)$$

where f is the focal length of the lens, n is the refractive index (or an averaging value of the refractive index in case of a lens combination). For example, if f = 400 mm, u = 0.25, n = 1.5, h = 30 mm, then w = 0.9 mm. The broadening of the focal line causes serious decrease of the laser power density on the target. In order to correct sagittal field curvature, a new type of two-element lens combination which consists of one or two aspherical lenses can be designed, and the separation between these two lenses has to be large enough. Generally, a focal line width of less than 20 μm can be satisfied over a focal line length of 6 cm for a lens combination of 20 cm aperture and a focal length of 40 cm. Its circle of confusion on the axis (h = 0) is less than 5 μm at the optimum image plane. For h = 22 mm, the broadening of the focal line is about 10 μm due to the off-axis spherical aberration in the sagittal direction, while the tangential aberration has no contribution to it. A further experiment with this lens combination is being arranged.

References

1. D. L. Mathews, J. E. Trebes, R. A. London, M. D. Rosen, Aug. 89, 15p, GRA, Vol 90, No 7, Apr. 1, 1990, Order No. DE90000784/GEA, NTIS, PC A03.

2. R. A. London, M. D. Rosen, J. E. Trebes, Appl. Opt., 28, 3397-3404 (1989).

3. M. D. Feit and J. A. Fleck, Jr., J. Opt. Soc. Am. B7, 2048-2060 (1990).

4. R. A. London, M. Strauss, M. D. Rosen, Phys. Rev. Lett., 65, 563-566 (1990).

5. M. D. Feit and J. A. Fleck, Jr., Opt. Lett. 16, 76-78 (1991).

6. M. D. Rosen, J. E. Trebes and D. L. Mathews, Comments Plasma Phrs. Controlled Fusion, Vol 10, 245-252 (1987).

7. C. J. Keane, N. M. Ceglio, B. J. MacGowan, D. L. Mathews, D. G. Nilson, J. E. Trebes and D. A. Whelan, J. Phys. B: At. Mol. Opt. Phys., 22, 3343-3362 (1989).

8. B. J. MacGowan, S. Maxon, L. B. DaSilva, D. J. Fields, C. J. Keane, D. L. Mathews, A. L. Osterheld, J. H. Scofield, G. Shimkaveg and G. F. Stone, Phys. Rev. Lett. 65, 420-423 (1990).

9. Wang Shiji, Gu Yuan, Fu Sizu, Ni Yuanlong, Zhou Guanlin, Yu Songyu, Wu Jiang, Zhou Zhenliang, Han Guoqiang, Fandianyuan, Lin Zunqi, Wang Shuseng and Chen Wannian, High Power Laser and Particle Beams (China), Vol. 2, No. 3, 271-279 (1990).

10. D. Neely, C. L. S. Lewis, J. Uhomoibhi, D. O'Neill, S. A. Ramsden, M. H. Key, B. Shiwai, N. Tragin and G. J. Tallents, Annual Report RAL-90-026, 1990. Rutherford Appleton Laboratory. pp. 3-7.

11. P. Jaegle, A. Carillon, P. Dhez, B. Gauthe, F. Gadi, G. Jamelot and A. Klisnick, Europhys. Lett., 7, 337-342 (1988).

12. Wannian Chen, Shusen Wang, Chusheng Mao, Bin Chen and Aifen Xu, Cylindrical lens array line focus system for X-ray laser experiments, in Conference on Lasers and Electro-Optics (1990), p. 282.

13. D. M. Vileneuve, G. D. Enright, H. A. Baldis and J. C. Kieffer, Opt. Comm. 81, 54-58 (1991).

Detailed Descriptions of Newly Developed ICs Provided

Center-Frequency-Tunable BPF Bank

92FE0363A Beijing DIANXIN JISHU [TELECOMMUNICATIONS TECHNOLOGY] in Chinese No 1, Jan 92 pp 42-43

[Article by Chen Zhiliang [7115 1807 5328]: "Center-Frequency-Tunable Bandpass Filter Bank"; See earlier brief report in JPRS-CST-91-006, 5 Mar 91 p 25]

[Text] Based on user requirements, the Institute of Microelectronics of Qinghua University has successfully developed and produced a small batch of a novel bandpass filter (BPF) IC, CFBP3. It is an MOS analog LSI IC using switched capacitor technology. Each chip contains three bandpass filters. Each channel has a six-order Butterworth filter. The center frequency of each filter is independently tunable. This product is compact, lightweight and low-power, and has high accuracy and excellent frequency stability. It does not require external adjustment and has excellent reproducibility and consistency. It has been proven to be stable and reliable after long-term use.

A variable-gain, low-noise input operational amplifier is placed before this three-channel filter to suit different input amplitudes. The center frequency of each BPF, f_0, is determined by its own input clock frequency f_c.

I. Pinout Arrangement and Function

CFBP3 is in a 22-pin DIP (dual in-line package) form and the pinout arrangement is shown in the figure.

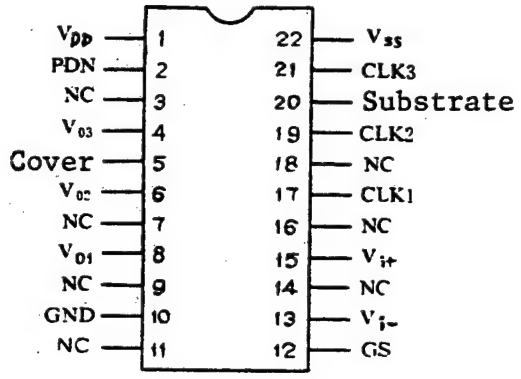

The function of each pin is listed below (using a +/-5 V power supply).

V_{DD}: positive power supply, connects to +5 V.

PDN: power down control terminal. In normal operation, it is connected to + 5 V. If it is connected to -5 V, all operational amplifiers do not function and the circuit is placed in a low-power standby mode.

V_{03}: channel 3 filter output.

COVER: package cover ground.

V_{02}: channel 2 filter output.

V_{01}: channel 1 filter output.

GND: common ground.

GS: low-noise operational amplifier output for gain switching.

V_{i-}: reverse input.

V_{i+}: forward input.

CLK1: clock input for channel 1 filter.

CLK2: clock input for channel 2 filter.

SUBSTRATE: substrate, connected to -5V.

CLK3: clock input for channel 3 filter.

V_{SS}: negative power supply, connected to -5 V.

(Pins 3, 9, 14 and 18 are not used.)

II. Major Technical Specifications

1. Useful frequency range is 0.1 Hz to 7 kHz, center frequency is continuously tunable.

2. Ratio of center frequency f_0 to clock frequency f_c is 1/512 and clock amplitude is +/- 3 to +/- 5 V.

3. Gain at center frequency is 0.2 +/- 0.2 dB and 3-dB bandwidth is 1/sqrt 2 f_0 to sqrt 2 f_0.

4. Out-band attenuation is more than 60 dB at above 8 f_0 and below ⅛ f_0. At above 2 sqrt 2 f_0 and below 1/(2 sqrt 2) f_0, attenuation is over 28 dB.

5. As a frequency-doubling filter, the 3 dB crosspoint detuning of neighboring bands is less than or equal to 0.2 dB. The crosspoint attenuation is 3 +/- 0.1 dB.

6. Input signal range is +/- 10 mV to +/- 2.5 V.

7. Output amplitude is +/- 3.5 V_{p-p} (R_L = 10 kΩ, C_L = 10 pF).

8. Power supply voltage is +/- 5 V and power consumption is less than 180 mW.

9. Operating temperature range is -30 to +85°C. In this range, the mean gain variation is less than 0.001 dB/°C. CFBP3 not only can be used to measure velocity-dependent parameters associated with acoustics, vibration and noise but also can be used as an audio BPF. Based on the application and requirements, either a single +10-V power supply or two +5-V power supplies may be used.

Nine Types of ASICs for S1240 SPC Telephone Switch

92FE0363B Shanghai DIANZI JISHU [ELECTRONIC TECHNOLOGY] in Chinese Vol 19 No 1, Jan 92 pp 26-27

[Article by Ma Xinrong [7456 9515 2837] of Shanghai Bell Telephone Equipment Mfrg., Ltd. and Shanghai Beiling Microelectronics Mfrg., Ltd.: "Domestic Production of LSI-ASICs for S1240 SPC Telephone Switch"; See earlier report in JPRS-CST-91-024, 23 Dec 91 pp 23-24]

[Text] LSI (large scale integration) is one of three leading-edge technologies in the S1240 [digital] SPC (stored-program-controlled) telephone switch (or S12).[1] The domestic production of such ASICs (application specific ICs) includes two aspects:

1. Transfer of manufacturing technology of nine types of ASICs;

2. Supplying users with a large number of highly reliable circuits with at least 25 years of life.

I. Introduction to the Functions of the Nine Types of ASICs

The S12 is a fully distributed modular SPC telephone switch. Its structure primarily consists of three parts:[2] The core is a digital exchange network; peripherals include various functional modules such as analog user module, clock and audio signal module, digital relay module, service circuit module, maintenance and peripheral equipment module, etc.; and terminal controllers between the core and the peripherals.

Table 1 lists the nine ASICs used in the S12.

Table 1

Number	Name	Explanation	Distribution in S12
1	DUSP	Dual switch port	Digital exchange network
2	MBLIC	Modified BiMOS line interface circuit	Analog user module
3	DSP	Digital signal processor	Analog user module
4	DPTC	Dual processor terminal controller	Analog user module
5	TCF	Trans coder filter	Analog user module
6	OBCI	On-board controller interface	Terminal controller Digital relay module
7	QUAP	Quadruple port	Terminal controller
8	POCO	Port controller	Terminal controller
9	IPCU	Integrated processor control unit	Terminal controller

The following is a brief description of the function of every ASIC (in the analog user module).

1. DUSP (dual switch port)[3]

This consists of two pairs of ports to allow intelligent time-space switching of two independent channels of 4.096 Mb/s pulse-code modulated (PCM) signals. It has frame alignment capability and can diagnose loss of synchronization. It can be set for automatic access or guided access and can cancel access. In addition to exchanging digitized voice signals, it can also be used to transmit data and information between microcomputers.

2. MBLIC (modified BiMOS line interface circuit)

This directly connects the S12 telephone switch with the analog user (telephone set). It supplies a constant current or voltage and contains a circuit with both dc resistance and ac impedance. The dc resistance and ac impedance may be selected to meet specific user requirements.

With the exception of coding/decoding (codec) capability, the remaining 6 of the 7 BORSCHT functions of the analog user module, including battery charging (B), over-voltage protection (O), ringing (R), subscriber-line monitoring (S), 2/4 line switching (H) and testing (T), are completed by the MBLIC. Furthermore, a 12 kHz or 16 kHz metering signal is also introduced into the subscriber line by way of the MBLIC.

3. DSP (digital signal processor)

The main function of the DSP is encoding and decoding. It consists of simple analog filters (for A/D and D/A conversion) and digital filters. The latter are used to implement the conversion defined by the PCM system. Digital filter parameters are selected by software to control losses in both transmission and reception, as well as to perform other functions such as echo suppression, transmission of subscriber line monitoring signal and control signals from microcomputers.

4. DPTC (dual processor terminal controller)

This controls user circuits and terminals and serves as an interface between digital exchange networks. It provides two PCM channels; one is connected to the terminal controller of a user module and the other to a terminal controller of a pre-selected user module. If one terminal controller fails or is loading new software, the other terminal will automatically take over all functions to ensure that the telephone calls between these two modules remain uninterrupted.

In addition to implementing terminal control via channel 16, it has other functions such as scanning and driving remote terminals and issuing mismatch reports.

5. TCF (trans coder filter)

The primary function of the TCF is to convert linear pulse code to A-law or μ-law companded code (A-law in

China) and vice versa. Another function of the TCF is to generate and inject a short 12 kHz or 16 kHz sinusoidal metering signal into the telephone set.

6. OBCI (on-board controller interface)

The OBCI is the intelligent interface between the on-board microprocessor (8086/80186) and the terminal controller. It links the serial ports of the two terminal controllers to the parallel port on the on-board controller.

7. QUAP (quadruple port)

The QUAP is comprised of two pairs of ports. Each pair of ports consists of a receiving port and a transmission port. The QUAP is the interface between the serial PCM line and the parallel time-division multiplexing (TDM) bus. The receiving port extracts information from the serial PCM signal and delivers it to the proper address of the TDM bus. The transmission port converts the information sent from the TDM bus into serial PCM signal for output.

8. POCO (port controller)

The POCO is the interface between the TDM bus and the microcomputer. Hence, the POCO is always used with the QUAP. Each POCO can follow the command of a microcomputer to control four QUAPs. Another function of the POCO is to receive tones generated by the DSP (clock and tone module) and transmitted from the PCM line.

9. IPCU (integrated processor control unit)

The IPCU is installed on the CPU board to provide the 80186/80286 microcomputer with a series of serial interface and control capabilities, such as DRAM control, 16-bit error detection and forward-error-correction logic.

II. Characteristics of the Nine ASICs

Special characteristics concerning the manufacturing and packaging of these nine ASICs are tabulated in Table 2.

Table 2

Number	Name	Manufacturing technology	Wafer size (mm x mm)	Degree of integration, package	Analog or digital
1	DUSP	3μ NMOS	6.1 x 6.2	20,000 transistors 68-pin PLCC*	Digital
2	MBLIC	3μ BiMOS	5.0 x 5.4	22 op-amps 10 comparators 200 gates 28-pin CDIP*	A/D hybrid
3	DSP	2.7μ CMOS	5.3 x 5.6	26,000 transistors 24-pin PDIP*	A/D hybrid
4	DPTC	3μ CMOS	6.1 x 6.3	23,000 transistors 28-pin PDIP*	Digital
5	TCF	3μ CMOS	3.0 x 3.3	2,000 transistors 16-pin PDIP*	A/D hybrid
6	OBCI	2.4μ NMOS	7.6 x 6.6	50,000 transistors 68-pin CLCC*	Digital
7	QUAP	3μ NMOS	8.1 x 8.6	39,000 transistors 68-pin PLCC*	Digital
8	POCO	3μ NMOS	7.5 x 7.2	30,000 transistors 132-pin PGA*	Digital
9	IPCU	2.4μ CMOS	6.2 x 6.2	15,000 transistors 84-pin PLCC*	Digital

*PLCC: plastic leaded chip carrier; CDIP: ceramic dual-in-line package; PDIP: plastic dual-in-line package; CLCC: ceramic leaded chip carrier; PGA: pin grid array.

From Table 2, one can see that many of the features listed, including 2.4-3μ NMOS, 2.4-3μ CMOS and BiMOS technology, a high degree of integration (up to 50,000 transistors), large wafer area (up to 70 mm^2) and multi-pin (68, 84, 132) packages, are voids in China's microelectronics industry.

III. Development and Batch Production of the Nine ASICs

Domestic production of these nine ASICs is implemented by Shanghai Beiling Microelectronics Mfrg., Ltd. The first project was to implement the technology transfer of these nine ASICs, i.e., the pilot production of samples. It took Shanghai Beiling a little over a year to produce all nine ASICs. The yield is higher than the original estimate. Hence, the firm rapidly developed the capability to deliver in quantity. The second project of domestic production is also successful. Some products have passed rigorous quality tests performed by foreign companies and end users; they are ready for batch production. Shanghai Beiling has begun shipment of goods to Shanghai Bell.

References

1. Mai Zhiqiang [7796 1807 1730], "Development of S1240 SPC Telephone Switch in China," DIANZI JISHU [ELECTRONIC TECHNOLOGY], Vol 18, No 8, August 1991, p 38.

2. R. Cohen, "System 12 Technological Enhancement," ELECTRICAL COMMUNICATION, Vol 59, No 1/2, 1985, pp 29-34.

3. W. Frank, M. C. Rahier, D. Sallaerts and D. Upp, "System 12 DUAL SWITCH PORT," ELECTRICAL COMMUNICATION, Vol 59, No 1/2, 1985, pp 54-59.

4. J. Danneals and A. Vandevelde, "System 12 ANALOG LINE CIRCUIT," ELECTRICAL COMMUNICATION, Vol 59, No 1/2, 1985, pp 43-47.

GaAs Double Modulation-Doped MIS P-HEMT

92FE0363C Beijing BANDAOTI XUEBAO [CHINESE JOURNAL OF SEMICONDUCTORS] in Chinese Vol 13 No 2, Feb 92 pp 109-115

[Article by Xiang Qi [4161 1142] and Luo Jinsheng [5012 2516 3932] of the Division of Microelectronic Technology, Xian Jiaotong University, Zeng Qingming [2582 1987 2494] of Research Institute 13 of the Ministry of Machine Building and Electronics Industry at Shijiazhuang, Hebei, and Zhou Junming [0719 0971 6900] and Huang Qi [7806 4860] of the Institute of Physics, the Chinese Academy of Sciences, funded by the Doctoral Program Foundation of the State Education Commission: "n-AlGaAs/InGaAs/n-GaAs Double Modulation-Doped Pseudomorphic HEMT With MIS Structure"; MS received 24 Dec 90, revised 8 May 91]

[Text] **Abstract**

An n-AlGaAs/InGaAs/n-GaAs double modulation-doped pseudomorphic HEMT with MIS [metal-insulator-silicon] structure is designed and developed. It combines the advantages of MISFET [metal-insulator-silicon field effect transistor] and double modulation-doped pseudomorphic HEMT (P-HEMT). A 1-μm-gate-length device has a maximum drain current density of 400 mA/mm and a gate reverse breakdown voltage of as high as 15 V. The device also exhibits excellent microwave characteristics.

I. Introduction

In the past decade, the HEMT (high electron-mobility transistor) has been rapidly developed in high-speed and microwave devices. The first AlGaAs/GaAs HEMT[1] was developed in 1980. Shortly afterward, a high-transconductance inverted GaAs/AlGaAs HEMT[2] was developed. A single modulation-doped AlGaAs/InGaAs P-HEMT[3] was developed in 1985. This was followed by the successful development of a double modulation-doped P-HEMT[4] in 1986. The conventional HEMT structure (N_D: 1-2 x 10^{18} cm^{-3}, $n_s < 1 \times 10^{12}$ cm^{-2}) suffers primarily from low drain current density and gate reverse breakdown voltage (typically 100-200 mA/mm and 4-8 V, respectively). Furthermore, there are DX centers. The use of such a device in high-speed IC and microwave power applications is therefore significantly limited. Compared to the conventional HEMT, with a higher ΔE_C, the P-HEMT not only has higher current driving capability because of its larger two-dimensional electron gas (2DEG) density but also can better constrain the 2DEG to lower the output impedance and thus to enhance power efficiency. Furthermore, since the molar fraction of Al is reduced ($x \leq 0.2$), the DX centers are eliminated. The double modulation-doped P-HEMT can further improve the current driving capability. However, the bandgap of AlGaAs is reduced because the molar fraction of Al is decreased. Nevertheless, its doping concentration is still relatively high. Hence, the P-HEMT still has a low gate reverse breakdown voltage. In 1987, a device completely opposite in structure to that of a conventional HEMT, the i-AlGaAs/n-GaAs MISFET, was developed.[5] The MISFET no longer has a high electron mobility; however, it has a high current driving capability. Because of the presence of undoped wide-bandgap $Al_xGa_{1-x}As$ (usually $x > 0.3$) on the surface, it has a very high gate reverse breakdown voltage and a high gate forward voltage tolerance. In addition, there are no DX centers.

A double modulation-doped n-AlGaAs/InGaAs/n-GaAs P-HEMT with MIS structure (MIS P-HEMT) has been designed and developed. The objective is to combine the advantages of the P-HEMT and MISFET in order to develop a device with large current driving capability and high gate reverse breakdown voltage. This is a very rewarding research topic which has bright prospects in development of microwave power and high-speed ICs.

II. Material Structure and Device Fabrication

Figure 1 shows the MIS P-HEMT structure. It includes a 1-μm-thick i-GaAs buffer layer on top of the semi-insulating (S.I.) GaAs substrate, a 100-Angstrom GaAs layer Si doped at 3 x 10^{18} cm^{-3}, a 50-Angstrom-thick i-GaAs isolation layer, a 120-Angstrom i-$In_{0.19}Ga_{0.81}As$ channel layer, a 50-Angstrom i-$Al_{0.4}Ga_{0.6}As$ isolation layer, a 100-Angstrom $Al_{0.2}Ga_{0.8}As$ layer doped with 3 x 10^{18} cm^{-3} of Si, and a 200-Angstrom insulating layer made of i-$Al_{0.4}Ga_{0.6}As$. The surface layer used as source and drain contact includes a 200-Angstrom n^+ variable bandgap layer doped with 4 x 10^{18} cm^{-3} of Si where the molar fraction of Al is varied gradually from 0.25 down to 0 and a 100-Angstrom n^+ GaAs layer doped with 4 x 10^{18} cm^{-3} of Si. In order to further enlarge ΔE_C to raise 2DEG and to strengthen the constraint on 2DEG, the In molar fraction in the InGaAs channel layer is designed to be 0.19 and the Al molar fraction in the AlGaAs isolation layer is set at 0.4. Correspondingly, the thickness of the InGaAs layer is reduced to 120 Angstroms to facilitate elastic absorption of interfacial stress caused by lattice mismatch to form an excellent deformation channel layer. In order to eliminate DX centers and obtain an even larger 2DEG, the Al molar fraction of the n^+ AlGaAs layer is set at 0.2 and its doping concentration is

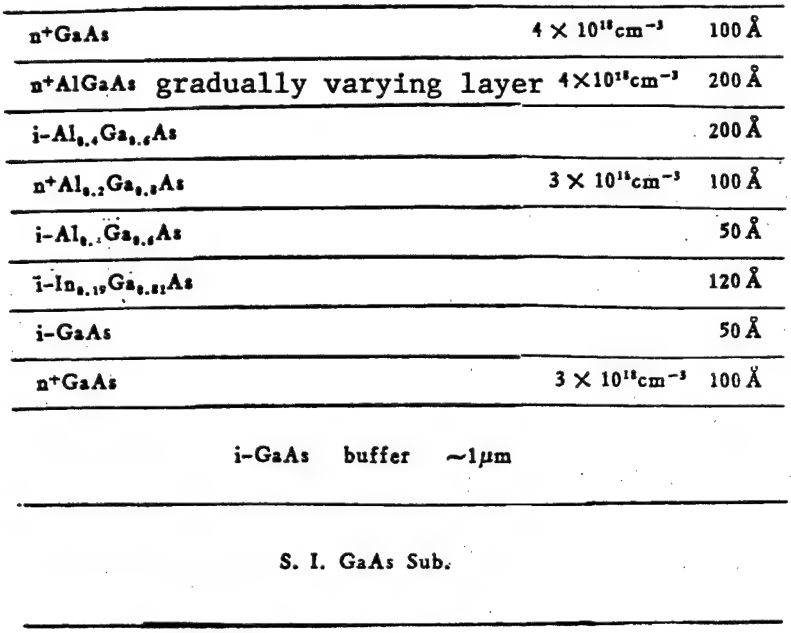

Figure 1. Structure of MIS P-HEMT

increased to 3 x 10^{18} cm^{-3}; correspondingly, layer thickness is reduced to 100 Angstroms to avoid the parallel conductance effect. The Al molar fraction of the undoped AlGaAs insulation layer is set at 0.4 to widen the bandgap in order to raise the gate breakdown voltage and reverse current leakage. Heavy doping of the surface layer at 4 x 10^{18} cm^{-3} and incorporation of the variable-bandgap layer are done to minimize ohmic contact resistance and parasitic series resistance. For such a complicated heterojunction field effect transistor (HFET), there is no simple analytical model for quantitative analysis. A one-dimensional charge-control model for an HFET[6] developed by us is used in our quantitative analysis. The model is based on basic concepts associated with numerical simulation of heterojunction structures and the conventional HEMT charge-control model. It shows that the intrinsic MIS P-HEMT can be expected to have a maximum saturated current of 600 mA/mm and a maximum transconductance of 300 mS/mm.

The materials were grown on a domestically made type-IV MBE machine. The apparent substrate temperature to grow InGaAs is 750°C, and is 820°C for other layers. An abrupt change of Al molar fraction from 0.2 to 0.4 is achieved by using two Al sources.

The fabrication process is similar to that for a GaAs MESFET. A double boron-ion implantation step is implemented to achieve device isolation. Drain-source ohmic contact is realized by alloying AuGeNi/Au in Ar gas for 1 minute at 450°C. The gate is etched chemically. Gate metal is Ti/Pt/Au. Gate and drain-source patterns are formed by an SiO_2 dielectric assisted strip-off technique. A polyimide film is used for passivation and isolation. Figure 2 shows the photo of a typical 1-μm-gate-length device with a 4 x 75-μm gate width and a 5-μm drain-source spacing.

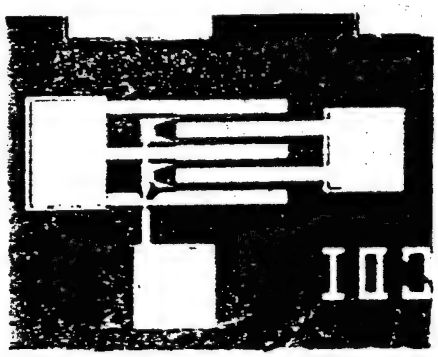

Figure 2. Typical Photograph of P-HEMT With 1-μm-Long, 4 x 75-μm-Wide Gate

III. Device Characteristics

1. DC Characteristics

Figures 3 and 4 show the room-temperature dc I-V characteristics of the MIS P-HEMT at threshold voltages of -0.6 V and -1.8 V, respectively. Both devices have 1-μm-long, 4 x 75-μm-wide gates. The threshold voltage is determined by the depth of the gate slot. As shown in the figures, the devices have excellent saturation and

pinch-off characteristics. Furthermore, they have a very high gate forward bias tolerance. The maximum drain current densities (V_G = 2.5 V) are 300 mA/mm and 400 mA/mm, respectively. This is far greater than the saturation current (100-200 mA/mm) of a conventional single-heterojunction HEMT. The measured maximum transconductance values are 120 mS/mm and 140 mS/mm, respectively. The low transconductance is caused by the high parasitic drain-source series resistance. The high parasitic resistance also causes higher saturation voltage drop (approximately 3 V for both devices). The typical transconductance versus gate bias curve (upper curve in Figure 5) indicates excellent uniformity. Figure 6 [photograph not reproduced] shows the typical gate reverse breakdown behavior. At a gate current of 1 mA/mm, the gate reverse breakdown voltage is approximately 15 V. Table 1 is a summary of the dc characteristics of this MIS P-HEMT in comparison to the measured results of a power HEMT published abroad and to those of a typical conventional HEMT. It shows that, as far as current density and breakdown behavior are concerned, the dc characteristics of the MIS P-HEMT we made have far exceeded those of a conventional HEMT. They even exceed those of a foreign-made power HEMT of comparable channel length. Our device more successfully addresses the dilemma of desiring a high drain current density and high gate reverse breakdown voltage at the same time.

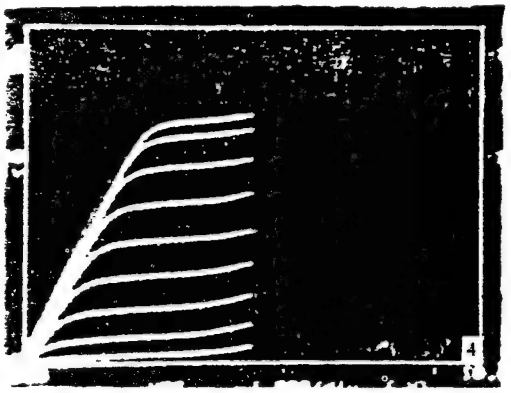

Figure 4. dc I-V Characteristics

V_{th} = -1.8 V, I_D = 15 mA/div, V_{DS}: 1 V/div, V_G = -0.5 V/step, top curve corresponds to V_G = 2.5 V

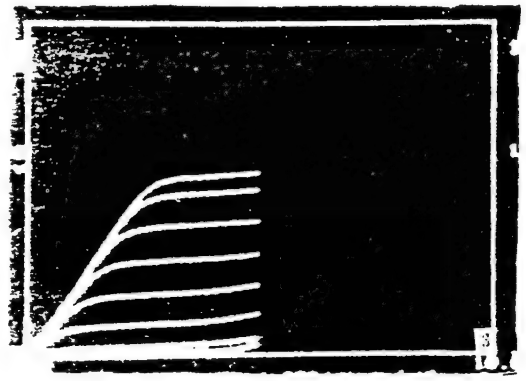

Figure 3. dc I-V Characteristics

V_{th} = -0.6 V, I_D: 15 mA/div, V_{DS}: 1 V/div, V_G: -0.5 V/step, top curve corresponds to V_G = 2.5 V

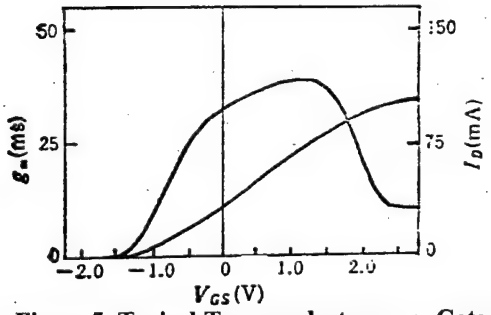

Figure 5. Typical Transconductance vs. Gate Bias for MIS P-HEMT

Table 1. Comparison of dc Characteristics

	MIS P-HEMT		Conventional HEMT	Power DH-HEMT
	Quasi-enhancement mode (Sample 1)	Depletion mode (Sample 2)	Typical parameters from reference 7	Fujitsu, 1986.5 from reference 7
L (μm)	1	1		1
W (μm)	300	300		1200
V_{th} (V)	-0.6	-1.8		-2.5
g_m(max) (ms/mm)	120	140		120
I_D max (mA/mm)	300 (V_G = 2.5 V)	400 (V_G = 2.5 V)	100-200	230
BV_G (V) (I_G = 1 mA/mm)	15	14	4-8	12
BV_{DS} (V) (I_D = 1 mA/mm)	≥20	≥18		17

2. RF Characteristics

Figure 7 shows the typical S-parameter circles of the MIS P-HEMT. The measurement was performed with an HP network analyzer. The device's major features are listed in Table 2. The device exhibits excellent microwave characteristics.

Table 2. Major Microwave Characteristics

Parameter / Frequency	200 MHz	13.1 GHz
S_{21}(MAG)	2.973	1.016
H_{21}(MAG)	18.069	2.980
GU_{max}	64.29 dB	4.96 dB

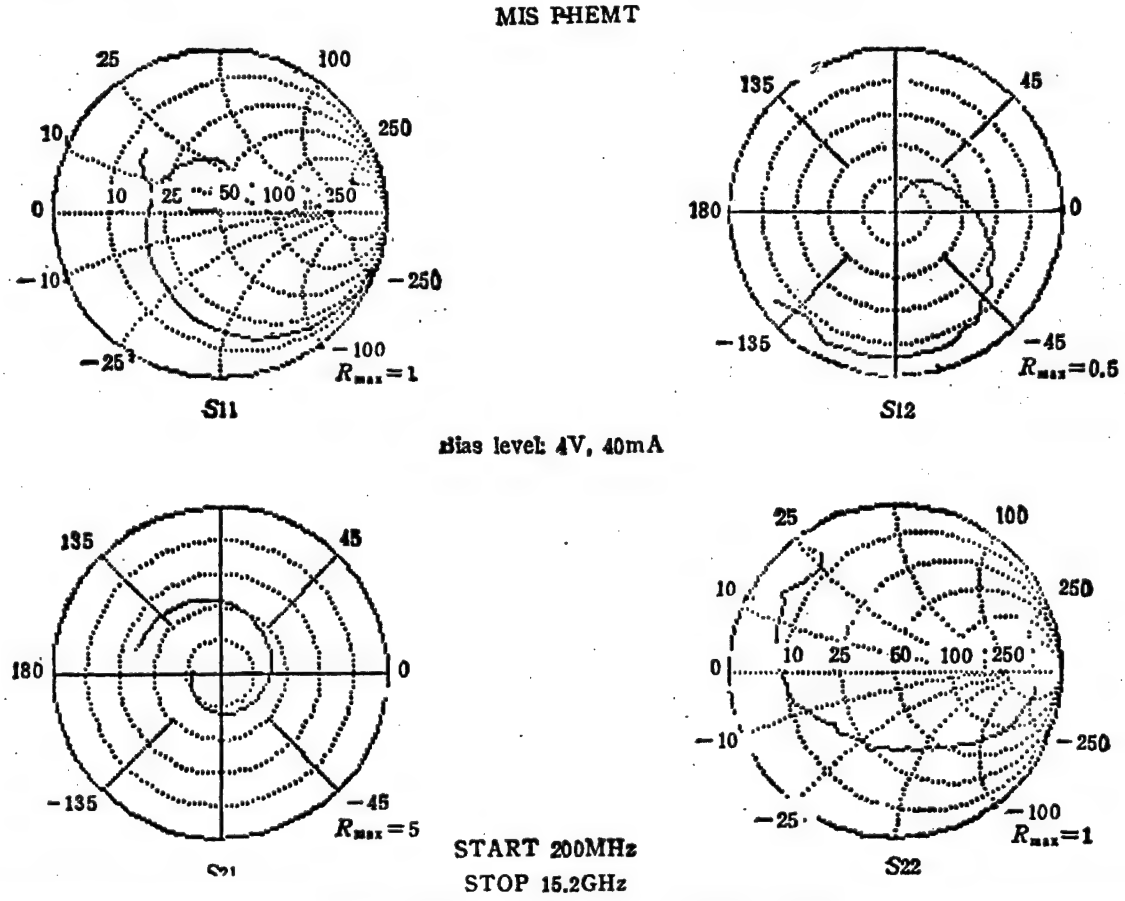

Figure 7. S-Parameter Circles of MIS P-HEMT

3. Discussion

From the standpoint of gate reverse breakdown voltage and maximum current density, the MIS P-HEMT more or less meets our design expectation. The dc transconductance is quite different from the design requirement. This is primarily due to the high parasitic series resistance. There are two causes for the large parasitic resistance. The presence of an insulating layer in the MIS structure causes series resistance to rise. Furthermore, the ohmic contact resistance is high with existing alloying technique. Experimentally, it was found that the alloying conditions could significantly affect saturation voltage drop and current. Further study is required to minimize series parasitic resistance. One way is to adopt an automatic alignment technique to reduce drain-source series resistance. Another is to improve the ohmic contact technique, such as alloying by fast annealing, to minimize ohmic resistance. The third way is to use a heavily In-doped InGaAs surface layer to form a non-alloy ohmic contact.[8]

No apparent photoconductance was observed in dc measurement. This indicates that there are no DX centers. The dc I-V curve also shows no apparent parallel conductance in the range between pinch-off voltage to substantial positive bias. The MIS structure should have even better threshold uniformity than a conventional HEMT. This should be good for batch production and IC fabrication. Since there is a wide-bandgap insulating layer ($Al_{0.4}Ga_{0.6}As$) in the MIS P-HEMT structure, it is very suited for selective etching. Hence, techniques such as RIE selective etching may be used to improve the gate groove-making process to further improve large-area uniformity of the device.

The gate length of the MIS P-HEMT designed is 1 μm. However, the actual gate length after strip-off from photolithography is around 1.2 μm. This increase of effective gate length can lower the microwave performance of the device. Parasitic resistance can also impede the microwave radiation. Despite this, the MIS P-HEMT still exhibited excellent microwave radiation characteristics. The key to further improving its microwave characteristics is to reduce the effective channel length and drain-source spacing. This requires an improvement of the pattern fabrication environment, strengthening the study on fine-pattern fabrication, including replacing photolithographic equipment and photoresist materials. If the characteristic dimension of the device can be reduced to below 0.5 μm, together with pattern refinement, it may be possible to produce a high-performance millimeter-wave device with a reliable gain.

The MIS P-HEMT developed in this work may be used in microwave power and high-speed logic IC applications. The high pinch-off voltage device (Sample 2), as far as dc power is concerned, has far out-performed a conventional HEMT. It has even exceeded the performance of the foreign-made power DH-HEMT of comparable length. The low pinch-off voltage device (Sample 1) can be directly used in SCFLICs (source-coupled field-effect transistor logic ICs). The large positive gate voltage tolerance and high drain current density give the IC high logic amplitude, high noise tolerance and large current capability (large fan-out). Study is being conducted to use this kind of material for an SCFL frequency divider.

IV. Conclusions

The MIS P-HEMT developed in this work combines the advantages of a MISFET and a double modulation-doped P-HEMT. It not only has a high current density but also a high gate reverse breakdown voltage. The maximum drain current density is 400 mA/mm and the highest gate reverse breakdown voltage is 15 V. Furthermore, the device shows excellent microwave characteristics. This MIS P-HEMT is not only suitable for microwave power applications but also for high speed logic circuits.

The authors wish to thank Group 605 of the CAS Institute of Physics for their support in MBE (molecular beam epitaxy); Group 201, Laboratory 2 of MMEI's Research Institute 13 for their cooperation in device fabrication; and Laboratory 13 of MMEI's Research Institute 13 for their assistance in testing the microwave characteristics of the device.

References

1. T. Mimura, S. Hiyamizu, T. Fujii, and K. Nanbu, JPN. J. APPL. PHYS., 19, L225 (1980).

2. Nicholas C. Cirillo and M. S. Shur, IEEE TRANS., ED-7, 71 (1986).

3. J. Rosenberg and M. Benlamri, IEEE ELECTRON DEVICE LETT., EDL-6, 491 (1985).

4. T. Henderson and M. I. Aksan, IEEE ELECTRON DEVICE LETT., EDL-7, 649 (1986).

5. H. Hida, A. Okamoto, H. Toyoshima, and K. Ohata, IEEE TRANS., ED-34, 1448 (1987).

6. Qiang Qi, Ph.D. Thesis, Xian Jiaotong University, 1991.

7. K. Hikosaka, Y. Hirachi, and M. Abe, IEEE TRANS., ED-33, 583 (1986).

8. S. Kuroda, N. Harada, T. Katakami, T. Mimura, and M. Abe, IEEE TRANS., ED-36, 2196 (1989).

Further Details on DSP ASIC for S1240 SPC Switch

92P60215A Shanghai DIANZI JISHU [ELECTRONIC TECHNOLOGY] in Chinese Vol 19 No 3, Mar 92 pp 29-31

[Article by Ren Qi [0117 1505] of Shanghai Beiling Microelectronics Manufacturing Ltd.: "Digital Signal Processor"]

[Summary] The digital signal processor (DSP) LSI ASIC for the analog user module of the 1240 digital stored-program-controlled (SPC) switch is described in detail [see short description of all nine S1240 ASICs (from January 1992 issue) translated in full above]. The circuit's main function is to provide A/D, D/A conversion, and the chip incorporates ΣΔ modulation, programmable gain control, and programmable echo suppression technologies. The DSP is a transmission circuit for control signals passing between the modified BiMOS line interface circuit (MBLIC) and the dual processor terminal controller (DPTC). Fabricated with 2.7 μm N-well CMOS technology, the DSP has the following main parameters: V = 10V +/- 5V, gate oxide layer thickness t_{ox} = 42.5 nm, composition is double-layer polycrystalline silicon, chip area is 33 sq. mm, no. of transistors integrated onto chip is 26,000, and the housing is a 24-pin plastic dual in-line package (PDIP).

The analog user module for the 1240 digital SPC switch is shown schematically in Figure 1. The MBLIC is the interface circuit between the analog user module and the subscriber line, and principally provides these five functions: feeding to the subscriber line, AC/DC loop impedance synthesis, 2-line/4-line conversion, circuit state testing, and overload protection. The voice signal from the MBLIC passes through the DSP, where it is A/D converted, and after gain adjustment the 13-bit linear code is sent to the transcoder filter (TCF). In the TCF, the A-law code is converted into μ-law code. The 8-bit companded code output from the TCF goes via the DPTC into the switching network.

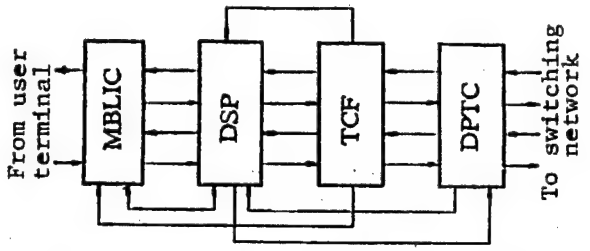

Figure 1. Analog User Module of 1240 SPC Digital Switch

The signal receiving circuit operation is similar.

In addition, the loop state signal detected by the MBLIC is sent via the DSP to the DPTC. At the same time, the DPTC sends control signals to the DSP and the MBLIC to effect programmable gain control, loop impedance synthesis, and other functions.

The DSP circuit structure is shown in Figure 2. At the core of this A/D, D/A converter is the ΣΔ modulator. Unlike a conventional Nyquist A/D converter, the ΣΔ modulator employs several hundred times oversampling; therefore the frequency response requirement for the anti-aliasing filter (AAF) that precedes the A/D conversion is much much lower.

The ΣΔ modulator has a 1 MHz sampling rate and a 1-bit word length; it requires a two-stage RC active filter network (cutoff frequency 50 kHz) serving as the AAF. The two-stage ΣΔ modulator consists of a switched capacitor integrator and a comparator.

The 1 MHz, 1-bit PDM [pulse duration modulation] signal generated by the ΣΔ modulator passes through several digital filter circuits, the first of which is the decimator. Consisting of a 64-stage rectangular FIR [finite impulse response] filter, a 4:1 down converter (1 MHz to 256 kHz), and a 16-stage triangular FIR filter (including a 256 kHz to 32 kHz down converter), the

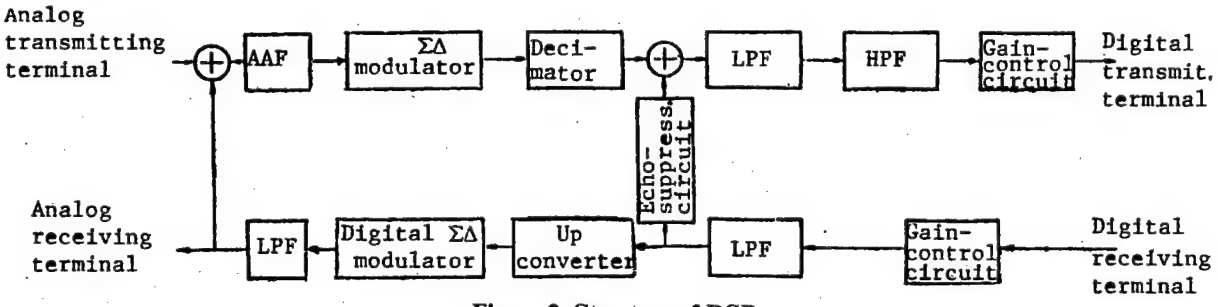

Figure 2. Structure of DSP

decimator filters out a large quantity of out-of-band noise introduced by the ΣΔ modulator (and therefore raises the SNR) and lowers the signal sampling rate. After the decimator, the signal passes through a standard 3.4 kHz low-pass filter (LPF), a 300 Hz high-pass filter (HPF), and a gain-control circuit.

The signal receiving loop structure is similar to that of the transmitting loop. The received digital signal, after passing through a gain-control circuit and LPF, is D/A converted in three steps: (1) the signal passes through a 16-stage triangular up-converting filter and a 4-stage rectangular up-converter filter, which together increase frequency from 32 kHz to 1 MHz; (2) it then passes through a DΣΔ modulator, which decreases signal word length from 13 bits to 1 bit; and (3) the 1 MHz, 1-bit PDM signal is sent through an LPF and thus converted back into the original speech signal.

Figures 3-7 [not reproduced] show the noise-filtering characteristics of a single-stage and two-stage ΣΔ modulator, the structure of a single-stage ΣΔ modulator, the structure and frequency response of the 64-stage rectangular FIR filter, the structure and frequency response of the 4:1 down converter, and the frequency response of the 16-stage triangular FIR filter, respectively.

Sino-Japanese Joint Venture To Make Fuzzy-Control Washing Machines

92P60221A Beijing ZHONGGUO DIANZI BAO [CHINA ELECTRONICS NEWS] in Chinese 23 Mar 92 p 1

[Article by Lu Yuzhou [7120 3022 3166]: "China To Manufacture Fuzzy Home Electrical Products"]

[Summary] Hangzhou Jinyu ["Goldfish"] Electric Appliance Co. and Japan's Matsushita Electric Industry Co. formally reached an agreement the other day in Hangzhou to establish a joint venture—to be called Hangzhou Jinsong [6855 2646] Washing Machine Ltd.—for manufacturing fuzzy-control all-automatic home washing machines to be sold here in China and abroad. The new joint venture will fully utilize the Jinyu Company's existing plant, equipment, and labor force, which will be integrated with Matsushita's advanced (late-eighties/early-nineties-level) technology. Gross investment in this new enterprise is 637 million yen, and plans call for an annual production capacity of 100,000 units. In these sophisticated new machines, sensors and fuzzy-logic-based processors determine the volume of laundry and degree of dirtiness, and then decide the best combination of washing modes, length of cycles, etc. The units come with a 24-hour preset timer and incorporate squelch circuits for lowering noise. Jinsong plans to begin production in the second half of this year. It is understood that this will be China's first fuzzy-control electrical appliance.

29 Analog ASICs Developed by Institute 24 Certified

92P60221B Beijing ZHONGGUO DIANZI BAO [CHINA ELECTRONICS NEWS] in Chinese 27 Mar 92 p 3

[Article by Xu Shiliu [1776 0013 0362] and Liang Shu [2733 2118]: "29 Research Achievements of Institute 24 Pass Appraisal"]

[Summary] Twenty-nine new analog application-specific integrated circuits (ASICs) developed by MMEI's Institute 24 passed the ministry-level product design finalization (part of MMEI's 1991 scientific-research results appraisal) held a few days ago in Yongchuan, Sichuan Province. Over 100 specialists from NDSTIC, the Ministry of Aerospace Industry, MMEI, and other organizations evaluated these new high-tech products, and made the following specific comments: the X0808 ASIC is the first domestically developed CMOS monolithic 8-bit A/D converter which can operate over a full range of temperatures and which can replace the 1980's-era foreign-made ADC0808CCN and ADC0808CJ chips; and six ASICs developed in a short period and fabricated with Institute 24's initially completed experimental 5 μm standard processing line A-group technology indicate a promising new step forward in the nation's development of analog ASICs. These six ASICs include the X1846 pulse-width modulator, the X25 four-terminal adjustable regulated power supply, and the X1526 pulse-width modulator. Other new analog ASICs of note are the S927 ECL 225 MHz divide-by-32/33 frequency divider, the S933 8-bit shift register data output control drive circuit, the X47 phase detector, the X930 phase-shifting pulse detector, and four other ICs independently designed and developed with an IC CAD system to meet specific technical requirements supplied by end users. Applications of these 29 ASICs include radar, communications, instruments and meters, automatic control, data acquisition systems, and frequency synthesis.

Photoluminescence of Silicon Quantum Wire Array Fabricated by Electrolytic Etching

92P60239A Beijing BANDAOTI XUEBAO [CHINESE JOURNAL OF SEMICONDUCTORS] in Chinese Vol 13 No 3, Mar 92 pp 193-197

[Article by Zhang Lizhu [1728 7787 3796], Duan Jiaqi [3008 1367 1800/3045], et al. of the Department of Physics, Beijing University, Beijing 100871: "Photoluminescence of Quantum Wire Array Fabricated by Hydrofluoric Acid Electrolytic Etching of Silicon"; MS received 8 Nov 91]

[Abstract] First, the authors summarize recent research by Canham[7] on the photoluminescence of a several-nanometers-diameter quantum wire array fabricated via electrolytic etching of porous Si and research by Beale et al.[8] on the influence of three factors (resistivity, hydrofluoric acid concentration, and electrolytic current density) on the density of porous Si. Then, based on the

aforementioned research, the authors study the effect of four factors—silicon resistivity, electrolyte composition, electrolytic current density, and electrolysis time—on the room-temperature photoluminescence peaks of a quantum wire array fabricated by hydrofluoric acid electrolytic etching of p-type <111> monocrystalline porous silicon. The optimal parameters are determined to be: volumetric ratio of HF acid to ethyl alcohol = 1:1, current density = 50 mA/cm^2, etching time = 1 hour, and resistivity = 0.74 or 11 or 75 Ω-cm. Based on the observed photoluminescence spectra, the average diameter of the quantum wire in the array is determined to be 2.4-3.1 nanometers. Apparatus and measurement instruments include a 400 mW Ar^+ laser with a 5,145-Angstrom spectral line, an HRD-I dual monochromator, a Ge (77K) detector or S-I photomultiplier tube (-40°C), a lock-in amplifier, and a spectral recorder.

One figure shows a plot of light intensity vs. wavelength for four different values of resistivity. The three strongest peaks are at 8,320 Angstroms (1.49 eV), 8,040 Angstroms (1.54 eV), and 7,880 Angstroms (1.57 eV), corresponding to a resistivity of 0.74 Ω-cm, 11 Ω-cm, and 75 Ω-cm, respectively. Four tables show the relation among resistivity, photoluminescence peak in eV, and average cross-sectional diameter of quantum wire; alcohol-to-HF acid ratio, photoluminescence peak, and quantum wire diameter; current density, photoluminescence peak, and quantum wire diameter; and electrolysis time, photoluminescence peak, and quantum wire diameter, respectively.

References

1. A. Uhlir, BELL SYST. TECHNOL. J., 35, 333 (1956).

2. D. R. Turner, J. ELECTROCHEM. SOC., 105 (7), 402 (1958).

3. Y. Watanabe, Y. Arita, T. Yokohama, and Y. Igarashi, J. ELECTROCHEM. SOC.: SOLID-STATE SCIENCE AND TECHNOLOGY, 1351 (October 1975).

4. T. Mano, T. Baba, H. Sawada, and K. Imai, Symposium on Very Large Scale Integration Technology, Oiso, Japan, September 1982, p 12.

5. K. Imai and H. Unno, IEEE TRANS. ELECTRON DEVICES, ED-31, 297 (1984).

6. T. L. Lin, L. Sadwick, et al., APPL. PHYS. LETT., 51 (11) (1987).

7. L. T. Canham, APPL. PHYS. LETT., 57 (10), 1046 (1990).

8. M. I. J. Beale, N. G. Chew, M. J. Uren, A. G. Cullis, and Benjamin, APPL. PHYS. LETT., 46 (1), 86 (1985).

Deep-Level Studies of GaAlAs/GaAs Single Quantum and Multiple Quantum Well Lasers Fabricated on Si Substrate by MOCVD

40100039A Beijing BANDAOTI XUEBAO [CHINESE JOURNAL OF SEMICONDUCTORS] in Chinese Vol 13 No 3, Mar 92 (MS received 22 Feb 91, revised 22 Apr 91) pp 155-161

[Article by Lu Liwu, Zhou Jie (National Laboratory for Superlattices and Microstructures, Institute of Semiconductors, CAS, Beijing), Zhuang Wanru (Semiconductor Institute Region, Integrated Optoelectronics Laboratories of China, Institute of Semiconductors, CAS, Beijing, 100083), and M. Umeno (Department of Electrical and Computer Engineering, Nagoya Institute of Technology, Nagoya, Japan)]

[Abstract] The deep levels of GaAlAs/GaAs single-quantum-well and multiple-quantum-well lasers fabricated on Si substrate by MOCVD have been studied using DLTS technique. The majority and minority carrier DLTS spectra show that a deep electron trap, having larger capture cross section and concentration, is measured in the quantum well and n-GaAlAs confinement layer of the lasers. This deep electron trap may correlate strongly with MOCVD growth parameters and damage induced by proton bombardment. It may be responsible for the degradation of laser performance. DX center and deep electron trap in quantum well of lasers may spatially localize in interfaces between GaAlAs/GaAs layers.

Orientation Effect in GaAs MESFETs

40100041A Beijing BANDAOTI XUEBAO [CHINESE JOURNAL OF SEMICONDUCTORS] in Chinese Vol 13 No 4, Apr 92 pp 199-208

[English abstract of article by Huang Qingan, Lu Shijie, and Tong Qinyi of the Microelectronics Center, Southeast University, Nanjing, 210018; MS received 11 Mar 91, revised 3 May 91]

[Text] Based on the piezoelectric effect model, the gate orientation dependence in GaAs MESFETs on (100), (011) and (111) substrates is investigated in detail. Expressions for piezoelectric charge are obtained through orthogonal transformation. The dependence of threshold voltage shifts on gate orientation has been analytically obtained by taking into account the depletion layer at the channel-substrate interface. The results predicted by the analytical model are in agreement with those by the two-dimensional numerical model.

Excitation Intensity Dependence of Near-Infrared Photoluminescence in $Ga_{0.5}In_{0.5}P$ Grown on GaAs Substrate

40100041B Beijing BANDAOTI XUEBAO [CHINESE JOURNAL OF SEMIMCONDUCTORS] in Chinese Vol 13 No 4, Apr 92 pp 236-241

[English abstract of article by Zhao Jialong, Gao Ying, Liu Xueyan, and Su Xian of Changchun Institute of Physics,

CAS, Changchun, 130021, Liang Jiachang of College of Civil Aviation of China, Tianjin, 300300, Guan Xingguo and Zhang Qilin of Hebei Institute of Semiconductors, Shijiazhuang, 050051; MS received 23 Mar 91, revised 5 Jun 91]

[Text] The investigation of near-infrared photoluminescence (PL) in ordered $Ga_{0.5}In_{0.5}P$ grown in GaAs substrate by metal-organic chemical vapor deposition (MOCVD) is reported for the first time. Three PL peaks from the deep levels are observed, and their peak energies are 1.17, 0.99 and 0.85 eV, respectively. The relationship between the near-infrared PL spectra and the excitation intensity is further studied. The results demonstrate that three PL peaks originate from donor-acceptor pair recombination (DAP).

Low-Threshold-Current InGaAs-GaAs Strained Layer Quantum Well Laser

40100041C Beijing BANDAOTI XUEBAO [CHINESE JOURNAL OF SEMICONDUCTORS] in Chinese Vol 13 No 4, Apr 92 pp 258-262

[English abstract of article by Xiao Jianwei, Xu Junying, Yang Guowen, Xu Zuntu, Zhang Jingming, and Chen Lianghui of the Institute of Semiconductors, CAS, Beijing, 100083, Zhou Xiaochuan, Jiang Jian, and Zhong Zhantian of the National Laboratory for Surface Physics, CAS, Beijing, 100080; MS received 25 Oct 91]

[Text] Graded-index separated confinement heterostructure strained layer multi-quantum-well (GRINSCH-STL-MQW) buried heterostructure (BH) lasers have been fabricated by a hybrid molecular beam epitaxy (MBE) and liquid phase epitaxy (LPE) technique. Low threshold current—5.6 mA for an uncoated laser (L = 120 μm, CW, 20°C)—was achieved with a MBE wafer threshold current density of 1 KA/cm^2. Lasing wavelength is 9386 Angstroms. External quantum efficiency as high as 0.48 mW/mA and more than 30 mW output power were obtained.

Integrating Amplifier Operating at 77K

92P60254A Hefei DIWEN YU CHAODAO [CRYOGENICS AND SUPERCONDUCTIVITY] in Chinese Vol 20 No 1, Feb 92 pp 54-57

[Article by Qian Zhongyu [6929 1813 6877] of the CAS Beijing Observatory: "An Integrating Amplifier Operating at 77K"; MS received 26 Aug 91]

[Abstract] An integrating amplifier operating at a temperature of 77K and designed to serve as a preamplifier in the readout circuits for multielement high-impedance IR (especially InSb) detectors is introduced. The operating principle is shown in Figure 1 below while waveforms at important points are shown in Figure 2 (not reproduced). In Figure 1, T_1 and T_2 are 2N6483 low-noise J-FETs (junction field-effect transistors), T_3 is a J230, C_{int} is an integrating capacitor (with a 10 pF value under experimental conditions), and C_c is a 1 pF compensating capacitor. Experimentally measured readout noise is about 200 electrons, compared to values of less than 100 electrons for typical CCD devices and of 10-20 electrons for some advanced devices. NEP (noise equivalent power) of this amplifier, when used with a K-band (λ_0 = 2.28 μm) photovoltaic InSb detector, measured 3.7 x 10^{-16} W/(Hz)$^{1/2}$. Also, this amplifier is relatively easy to integrate; the schematic is shown in Figure 4 below. One other figure shows oscilloscope traces of undesired nonlinear performance when t (time) is much less than the time constant τ (= R_d x C_{int}).

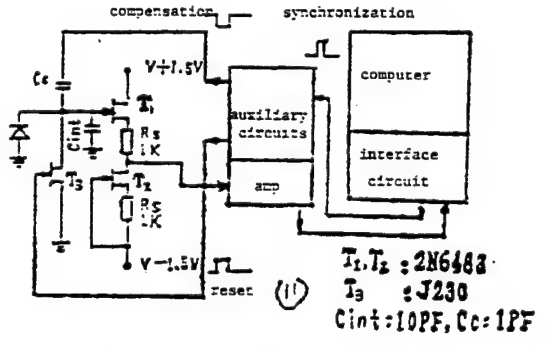

Figure 1 Schematic Diagram of Integrating Amplifier

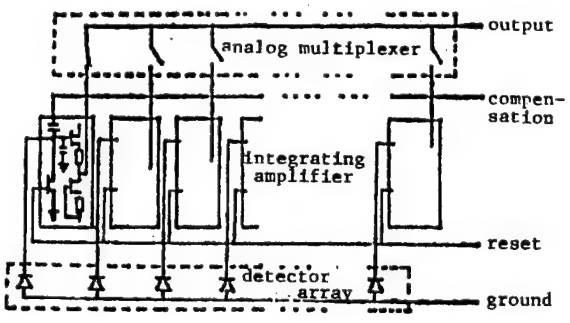

Figure 4 Schematic of Integrated Readout Circuit

References

1. Qian Zhongyu, DIWEN YU CHAODAO, No 1 (1986).

2. A. F. Milton, "Readout Mechanisms for IR Focal Plane Arrays," "SPIE" Vol 443 (1983).

3. Qian Zhongyu, "Trends in Development of Infrared Array Devices, Applications in Astronomy," HONGWAI JISHU [INFRARED TECHNIQUE], to be published.

Superconductivity in $Bi_{1.6}Pb_{0.4}Sr_2Ca_2 Cu_{3-x}Ti_xO_y$ System

40100040A Hefei DIWEN YU CHAODAO [CRYOGENICS AND SUPERCONDUCTIVITY] in Chinese Vol 20 No 1, Feb 92 pp 11-14

[English abstract of article by Lu Yafeng, Wu Xiaozu, and Li Qingyun of Northwest Institute for Nonferrous Research, Baoji, Xin Mianrong and Luo Changxun of the Department of Physics, Shaanxi Normal University, Xian; MS received 3 Jun 91, revised 1 Aug 91]

[Text] A series of samples with nominal composition $Bi_{1.6}Pb_{0.4}Sr_2Ca_2 Cu_{3-x}Ti_xO_y$ (x = 0.0; 0.05; 0.1; 0.2; 0.3) were prepared by solid-state reaction method. The resistivity vs. temperature plots, the a. c. susceptibility vs. temperature plots and XRD spectra were measured; micro-area compositions were examined for the samples. It is found that the zero-resistance temperature of the system is above 100K when x = 0.0-0.2; non-superconducting at LN_2 temperature when x = 0.3. The single phase degree is highest when x = 0.1. EDAX indicates that the micro-area distribution of the element Ti is not very uniform. We believe that Ti is substantially substituted for Ca instead of Cu.

References

1. H. Meada, Y. Tanaka, M. Fukutomi, and T. Asano, JPN. J. APPL. PHYS., 27 (1988), L209.

2. S. M. Green, C. Jiang, et al., PHYS. REV., B38 (1988), 5016.

3. Takayuki, Komatsu, et al., JPN. J. APPL. PHYS., Vol 28, No 7, July 1989; Toranosuke Ashizawa, et al., JPN. J. APPL. PHYS., Vol 28, No 7, July 1989; Ryuji Sato, et al., JPN. J. APPL. PHYS., Vol 28, No 11, November 1989; A. Rojek, et al., SOL. ST. COMMUN., Vol 72, No 1 (1989).

4. Yuping Sun, et al., APPL. PHYS. LETT., 55 (12), 18 September 1989.

5. T. Hatano, et al., CRYOGENICS, Vol 30, 1990.

6. Tarascon, J. M., et al., PHYS. REV., B39 (1989), 4316.

Superconductivity in Tl-Ba-Ca-Cu-K-Al-O System

40100040B Hefei DIWEN YU CHAODAO [CRYOGENICS AND SUPERCONDUCTIVITY] in Chinese Vol 20 No 1, Feb 92 pp 19-24

[English abstract of article by Sun Yuping, Sun Yuchao, Chen Dexing, Lin Yueying, Yang Mingming, Chen Lemin, and Liu Geqing of the Research Department of Electronics R&D Center, CAS; MS received 25 Jun 91]

[Text] Tl-containing septenary oxide with T_{co} above 110K, a TlBaCaCuKAlO system, has been prepared by using a two-step solid-state reaction. The influence of starting cation ratio composition on the superconductivity of the TlBaCaCuKAlO system has been investigated. The experimental results show that decreasing the thallium content in the cation ratio of this system to 0.3 does not adversely affect T_{co}. However, when the content of thallium in it is decreased to 0.2, the superconductivity of the TlBaCaCuKAlO system will be lost. The high-T_c superconductivity of the TlBaCaCuKAl system with lower thallium content can be obtained by doping both potassium and aluminum into the TlBaCaCuO system in a simple synthetic process. The value of T_{co} of $Tl_{0.3}BaCaCu_2K_{0.5}Al_{0.2}O_x$ is up to 114K. There are two high-T_c superconducting phases in it: 2212 and 1112. Both belong to the body-centered tetragonal cell system. Their lattice parameters are a = 5.541 Angstroms, c = 29.081 Angstroms and a = 5.586 Angstroms, c = 19.665 Angstroms, respectively.

References

1. Z. Z. Sheng and A. M. Herman, NATURE, 332 (1988) 138.

2. J. M. Liong, et al., PHYSICA C, 165 (1990) 347.

3. A. W. Hewat, et al., PHYSICA C, 152 (1988) 438.

4. D. S. Ginley, et al., PHYSICA C, 152 (1988) 217.

5. R. M. Hazen, et al., PHYS. REV. LETT., 60 (1988) 1657.

6. Bruno Morosin, et al., PHYSICA C, 165 (1990) 115.

Investigation of TlBaCaCuO RF-SQUID

40100040C Hefei DIWEN YU CHAODAO [CRYOGENICS AND SUPERCONDUCTIVITY] in Chinese Vol 20 No 1, Feb 92 pp 30-34

[English abstract of article by Xue Shouqing and Zhang Jian of the National Institute of Metrology, Wang Chijun and Yang Piyuan of the Institute of Geophysical and Geochemical Exploration, Yang Xiaoming and Huo Yuhua of the Department of Electron Science, Nankai University, and Li Jiazhang of the Department of Physics, Beijing University; MS received 30 Oct 91]

[Text] A single-hole RF-SQUID made from bulk TlBaCaCuO has been fabricated and investigated in liquid nitrogen. The flux-voltage transfer function is 24 $\mu V/\varphi_0$. The corner frequency of 1/f noise was measured around 200-300 Hz. A flux resolution of $2.5 \times 10^{-4}\varphi_0/(Hz)^{1/2}$ and an energy resolution of 6.7×10^{-28} J/Hz were measured at a frequency of 1,000 Hz.

References

1. Z. X. Zhao, L. Q. Chen, et al., KEXUE TONGBAO, 32 (1987) 661.

2. G. J. Cui, X. F. Meng, et al., INTERNATIONAL JOURNAL OF MODERN PHYSICAL B, Vol 1, No 2 (1987) 541.

3. P. H. Wu, Q. H. Cheng, et al., INTERNATIONAL JOURNAL OF MODERN PHYSICAL B, Vol 1, No 2 (1987) 565.

4. J. E. Zimmerman, et al., APPL. PHYS. LETT., 51 (1987) 617.

5. R. H. Koch, et al., APPL. PHYS. LETT., 51 (1987) 200.

6. S. Q. Xue, J. Zhang, et al., CRYOGENICS, Vol 30 (1990) 925.

7. J. W. Qui, L. W. Zhou, et al., CRYOGENICS, Vol 30 (1990) 920.

8. Yan Jie, Yang Xiaoming, et al., NANKAI DAXUE XUEBAO [JOURNAL OF NANKAI UNIVERSITY, NATURAL SCIENCES EDITION], No 2 (1988) 66.

9. Xue Shouqing, Zhang Jian, et al., DIWEN YU CHAODAO.

Growth of $GdBa_2Cu_3O_7$ Superconducting Thin Films on (100) $SrTiO_3$ Single-Crystal Substrates Under Various Substrate Temperature

40100037A Beijing DIWEN WULI XUEBAO [CHINESE JOURNAL OF LOW TEMPERATURE PHYSICS] in Chinese Vol 14 No 2, Mar 92 (MS received 4 Jun 91) pp 86-90

[English abstract of article by Yi Huanren[1,2,3], Wang Ruilan[1], Li Jingwei[1], Li Hongcheng[1], Wang Changan[1], Shi Lei[3], Zhao Zhongxian[1,2] and Li Lin[1]; [1]Institute of Physics, CAS, Beijing 100080; [2]National Laboratory for Superconductivity, Beijing 100080; [3]Structure Analysis Lab., University of Science and Technology of China, Hefei 230026]

[Text] The substrate temperature (T_s) is considered to be one of the most important parameters determining the growth and the properties of the thin films of Y-system high-temperature superconductors. In this work, a series of $GdBa_2Cu_3O_7$ superconducting thin films were grown on (100) $SrTiO_3$ substrates under T_s from 600-850°C, by

using dc magnetron sputtering and rapid annealing method in situ. The results show when T_s = 670°C, thin films with $T_{co} > 88K$ can be obtained.

Oxide Superconductor $Bi_{1.6}Pb_{0.4}Sr_{2-x}M_xCa_2Cu_3O_y$ (M = Mg, Ba)

40100037B Beijing DIWEN WULI XUEBAO [CHINESE JOURNAL OF LOW TEMPERATURE PHYSICS] in Chinese Vol 14 No 2, Mar 92 (MS received 12 Jun 91) pp 97-102

[English abstract of article by Lu Yafeng, Wu Xiaozu, Li Qinyun and Zhou Lian (Northwest Institute for Nonferrous Research, Baoji 721014), Xin Mianrong and Luo Changxun (Department of Physics, Shanxi Normal University, Xi'an 710062)]

[Text] Superconducting samples with nominal composition $Bi_{1.6}Pb_{0.4}Sr_{2-x}M_xCa_2Cu_3O_y$ (M = Mg, Ba) were prepared by solid-state reaction method. The resistivity and a.c. susceptibility as a function of temperature were measured for the samples. It is found that the samples with x = 0.2, 0.4 only display the superconducting transition of the 110K phase above 77K when M = Ba. XRD indicates that the partial substitution of Mg or Ba for Sr promotes the formation ability of 2223 phase, but the samples contain a small amount of the 2201 phase; the 2201 phase is prevented when Mg and Ba are substituted for Sr. XRD and EDXA show that the probability of actual substitution of Ba^{2+} for Sr^{2+} is larger than that of Mg^{2+} for Sr^{2+}.

High-J_c YBaCuO Superconducting Materials Prepared by Zone Melting

40100037C Beijing DIWEN WULI XUEBAO [CHINESE JOURNAL OF LOW TEMPERATURE PHYSICS] in Chinese Vol 14 No 2, Mar 92 (MS received 29 May 91) pp 103-107

[English abstract of article by Fan Zhanguo, Ji Chunlin, and Zhang Guofan (Northeast Institute of Technology, Shenyang 110006), Zhao Zhongxian and Guo Shuquan (Institute of Physics, CAS, Beijing 100080)]

[Text] Zone-melting method for preparing YBaCuO superconductor is proposed. Oriented 90K YBaCuO superconducting materials were made with the zone-melting equipment designed. Critical current density up to $3.75X10^4$ A/cm^2 (77K, OT) and $2X10^4$ A/cm^2 (77K, 1T) has been obtained. Fifty percent of zone melting samples were shown to have J_c over 10^4 A/cm^2. The activity of Y_2BaCuO_5 in zone melting YBaCuO materials is discussed.

Magnetization and Microstructure Studies of Melt-Textured Growth $YBa_2Cu_3O_{7-\delta}$ Irradiated by Fast Neutrons

40100037D Beijing DIWEN WULI XUEBAO [CHINESE JOURNAL OF LOW TEMPERATURE PHYSICS] in Chinese Vol 14 No 2, Mar 92 (MS received 10 Jun 91) pp 108-112

[English abstract of article by Ren Hongtao, Xiao Ling, et al. (General Research Institute for Non-ferrous Metals, Beijing 100088)]

[Text] The effect of fast neutron irradiation on the magnetization properties of Melt-Textured Growth (MTG) $YBa_2Cu_3O_{7-\delta}$ with fluences of $2.3X10^{16}$n/cm^2 and $1.16X10^{17}$n/cm^2, respectively, is studied. The critical current density is found to increase greatly by comparison between the hysteresis loops before and after neutron irradiation. The critical magnetization current density J_c at 77K in a 0.1T field for the irradiated sample with fluence of $1.16X10^{17}$n/cm^2 was estimated to be 4.7 x 10^5A/cm^2, which is tenfold higher than that of the unirradiated sample. The irreversibility lines T* (H) before and after neutron-irradiated sample times show that the activation energy of the flux pinning in the irradiated sample is 1.33 times as high as that of the unirradiated MTG sample.

Preparation of Ag-YBCO Composite Tape With Starting Material Produced by Codecomposition Method

40100037E Beijing DIWEN WULI XUEBAO [CHINESE JOURNAL OF LOW TEMPERATURE PHYSICS] in Chinese Vol 14 No 2, Mar 92 (MS received 10 Oct 91) pp 117-121

[English abstract of article by Wei Wangshui, Gong Shangmin, Luo Le, and Hu Suhui (Shanghai Institute of Metallurgy, CAS, Shanghai 200050]

[Text] Ag-YBCO composite tapes have been prepared with Nitric-salt codecomposition superconducting powders. It was found that the critical current density of these tapes is much higher than that of tapes prepared with the conventional solid-state reaction powders. Apart from the high J_c (77K, OT) value of 5300 A/cm^2 which is about 4 times larger than that of the latter, the former also has a higher stability in water.

Study of Transport Critical Current Density and Magnetization on Ag-Doped Bi-Based Bulk Material

40100037F Beijing DIWEN WULI XUEBAO [CHINESE JOURNAL OF LOW TEMPERATURE PHYSICS] in Chinese Vol 14 No 2, Mar 92 (MS received 20 Apr 91) pp 155-159

[English abstract of article by Wang Shunxi, Wang Yugui, Yuan Songliu, Zhou Xianyi* (Institute of Plasma Physics, CAS, Hefei, 230031); *International Center for

Materials Physics, CAS, Shenyang, 110015, and Department of Modern Physics, University of Science and Technology of China, Hefei, 230026]

[Text] The effect of doping Ag on the transport critical current density and magnetization of Bi-based bulk material with pure 110K phase has been investigated. Through measurement of complex ac susceptibility, transport J_c and magnetic hystereses, we find that the Ag doping improves the connection between the grains, increases the transport J_c from 340A/cm^2 to 1500A/cm^2 (at 77K and zero field), makes the hysteretic area become larger for same-size samples and raises the pinning force density. Our results indicate that improving the grain connection is an effective method for improvement of current-carrying capacity of Bi-based bulk material.

Nanjing Firm, Fujitsu Form Joint Venture To Produce Fiber Optic Communications Equipment

92P60235A Beijing JISUANJI SHIJIE [CHINA COMPUTERWORLD] in Chinese No 14, 8 Apr 92 p 3

[Article by Dai Keqin [2071 0344 0530]: "Sino-Japanese Joint Venture Nanjing Fujitsu Communications Equipment Ltd. Set Up"]

[Summary] On 16 March in the Great Hall of the People, representatives from Nanjing Wired Telecommunications Plant and Japan's Fujitsu Ltd. formally reached an agreement to establish a joint venture to be called "Nanjing Fujitsu Communications Equipment Ltd." Various leaders from the State Planning Commission, the Ministry of Machine-Building and Electronics Industry, the Ministry of Posts and Telecommunications, the CHINATRON Corp., Jiangsu Province, and Nanjing attended the signing ceremony.

The new joint venture's main products will be the most demanded products in modern communications networks: fiber optic communications equipment, including optoelectronic terminals, optical repeaters, monitoring systems, and fiber optic subscriber loop systems (an economical and fast method for solving the problem of an insufficient number of subscriber lines in a particular area). The joint venture's registered capital is US$9 million, and gross investment is US$14.50 million, of which the Chinese side (Nanjing Wired Telecommunications Plant) will put up 60 percent and the Japanese side (Fujitsu Ltd.) 40 percent. The assigned annual output target is 5,500 fiber optic communications equipment systems. In recent years, Fujitsu Ltd. has been one of China's principal suppliers of stored-program-controlled [telephone] switches and fiber optic communications equipment, and a partner in cooperative projects involving software development and LSI ASICs. The formation of this new joint venture—centered around the Nanjing production plant, a backbone enterprise in China's electronics industry—will promote economies of scale in the domestic fiber optic communications and digital communications network industries.

Nation's First Shallow-Sea Fiber Optic Cable Communications System Passes Acceptance Check

92P60222A Beijing ZHONGGUO DIANZI BAO [CHINA ELECTRONICS NEWS] in Chinese 30 Mar 92 p 3

[Article by Zhang Bing [1728 0393]: "Nation's First Shallow-Sea Fiber Optic Cable Communications System Handed Over for Use"]

[Summary] The nation's first shallow-sea fiber optic cable communications system, developed by various plants and institutes under the CHINATRON Corp., formally passed design finalization and acceptance check on 24 February, and was thus formally handed over for use. This 32-km-long, 8.448 Mbps [DS2 standard] system was completed in December 1990, and after that was trial operated for 13 months. The acceptance check followed various tests performed in January and February this year. Throughout, the system uses domestically made shallow-sea fiber optic cable, splice boxes, and optoelectronic equipment. The system was one of the pilot optical communications projects of the State Council's Office for Promotion and Application of Electronic Information Systems. Principal technical indicators meet mid-eighties international standards.

Secure Digital Color TV System Certified

92P60222B Beijing KEJI RIBAO [SCIENCE AND TECHNOLOGY DAILY] in Chinese 5 Apr 92 p 1

[Article by Yu Shenming [0060 5450 2494]: "China Now Has a Secure Digital Color Television System"]

[Summary] The 34 Mbps secure digital color TV system jointly developed for NDSTIC by Beijing Institute of Posts and Telecommunications, the University of Science and Technology for National Defense, and the Luoyang Institute of Tracking and Communications Technology passed appraisal a few days ago. The system has a digital transmission mode, which replaces the traditional analog transmission mode of older systems. This TV system consists of two basic pieces of equipment: the TV compression coder and the digital encryption device, which can transmit highly secure TV images with picture and sound quality improved [over that of an analog system]. The system is compatible with satellite, fiber optic cable, and digital microwave transmission media. At the appraisal, several dozen experts from NDSTIC, MMEI, MPT, and the Ministry of Radio, Film, and Television unanimously judged the new system to be a major breakthrough for the nation's telecommunications modernization, and judged its overall technical performance to be at a late-eighties international level.

Reflection and Transmission of Picosecond Soliton at Interface Separating Two Media in Optical Fiber

40100042A Beijing WULI XUEBAO [ACTA PHYSICA SINICA] in Chinese Vol 41 No 2, Feb 92 pp 244-252

[English abstract of article by Chen Lujun, Liang Changhong, and Wu Hongshi of Xidian University, Xian 710071; MS received 9 Mar 91]

[Text] The governing equations and boundary conditions for reflection and transmission of picosecond solitons at the interface between two media in optical fiber is developed by a radial mode averaging method with slowly varying envelope and quasi-monochromatic approximations. The process of reflection and transmission is numerically simulated by using a beam-propagating method and some numerical examples are given.